Frequency and density dependent radiative recombination processes in III–V semiconductor quantum wells and superlattices

Roberto Cingolani [a] & Klaus Ploog [a]

[a] Max-Planck-Institut für Festkörperforschung, D-7000,
Stuttgart 80, Germany
Version of record first published: 14 Aug 2006.

PLEASE SCROLL DOWN FOR ARTICLE

Frequency and density dependent radiative recombination processes in III–V semiconductor quantum wells and superlattices

By ROBERTO CINGOLANI and KLAUS PLOOG

Max-Planck-Institut für Festkörperforschung,
D-7000 Stuttgart 80, Germany

Abstract

In this paper we review the radiative recombination processes occurring in semiconductor quantum wells and superlattices under different excitation conditions. We consider processes whose radiative efficiency depends on the photogenerated density of elementary excitations and on the frequency of the exciting field, including luminescence induced by multiphoton absorption, exciton and biexciton radiative decay, luminescence arising from inelastic excitonic scattering, and electron–hole plasma recombination.

Semiconductor quantum wells are ideal systems for the investigation of radiative recombination processes at different carrier densities owing to the peculiar wavefunction confinement which enhances the optical non-linearities and the bistable behaviour of the crystal. Radiative recombination processes induced by multi-photon absorption processes can be studied by exciting the crystal in the transparency region under an intense photon flux. The application of this non-linear spectroscopy gives direct access to the excited excitonic states in the quantum wells owing to the symmetry properties and the selection rules for artificially layered semiconductor heterostructures.

Different radiative recombination processes can be selectively tuned at exciting photon energies resonant with real states or in the continuum of the conduction band depending on the actual density of photogenerated carriers. We define three density regimes in which different quasi-particles are responsible for the dominant radiative recombination mechanisms of the crystal: (i) The dilute boson gas regime, in which exciton density is lower than 10^{10} cm^{-2}. Under this condition the decay of free and bound excitons is the main radiative recombination channel in the crystal. (ii) The intermediate density range ($n < 10^{11}$ cm^{-2}) at which excitonic molecules (biexcitons) and inelastic excitonic scattering processes contribute with additional decay mechanisms to the characteristic luminescence spectra. (iii) The high density range ($n \simeq 10^{12}$ cm^{-2}) where screening of the Coulomb interaction leads to exciton ionization. The optical transitions hence originate from the radiative decay of free-carriers in a dense electron–hole plasma.

The fundamental theoretical and experimental aspects of the radiative recombination processes are discussed with special attention to the GaAs/Al$_x$Ga$_{1-x}$As and Ga$_x$In$_{1-x}$As/Al$_y$In$_{1-y}$As materials systems. The experimental investigations of these effects are performed in the limit of intense exciting fields by tuning the density of photogenerated quasi-particles and the frequency of the exciting photons. Under these conditions the optical response of the quantum well strongly deviates from the well-known linear excitonic behaviour. The optical properties of the crystal are then no longer controlled by the transverse dielectric constant or by the first-order dielectric susceptibility. They are strongly affected by many-body interactions between the different species of photogenerated quasi-particles, resulting in dramatic changes of the emission properties of the semiconductor.

The systematic investigation of these radiative recombination processes allows us to selectively monitor the many-body induced changes in the linear and non-linear optical transitions involving quantized states of the quantum wells. The

importance of these effects, belonging to the physics of highly excited semi-conductors, lies in the possibility of achieving population inversion of states associated with different radiative recombination channels and strong optical non-linearities causing laser action and bistable behaviour of two-dimensional hetero-structures, respectively.

Contents   PAGE

1. Introduction

The interaction of electromagnetic radiation with condensed matter is one of the most widely studied fields in solid state physics. This general denomination includes all kinds of quantum mechanical processes involving charged particles in a periodic potential perturbed by an external electromagnetic field. In semiconductor physics the external field has been used as a sensitive and tunable probe to induce electronic transitions between different states of the crystal, thus getting important information on the crystal ground state and on the energy band dispersion. Obviously, the physical processes investigated in this way depend on the type of matter and on the type of interacting electromagnetic field. The most general question to ask is, therefore, *Which phenomena occur when we tune the frequency and the intensity of the radiation exciting a crystal?* This question, which is itself of great fundamental interest, becomes even more important when the excited crystals has unusual physical properties. The advent of atomic layer controlled growth technologies, primarily the well-known molecular

beam epitaxy (MBE), has provided the possibility of tailoring macroscopic quantum mechanical systems, in which the electronic properties are determined by quantum size effects. As a consequence the interaction of radiation with this 'man-made' matter has a fundamental twofold role: first, to study the interaction of photons with different quasi-particles in a material with strong quantization properties, and, second, to provide information on the electronic properties of the material itself.

One way, and probably the simplest, is to study the electronic transitions induced by absorption of photons in semiconductors, and, in particular, to study the radiative recombination processes in quantum wells and superlattices. In this paper we review the radiative recombination processes occurring in semiconductor quantum wells and superlattices under different excitation conditions. We consider processes whose radiative efficiency depends on the photogenerated density of elementary excitations and on the frequency of the exciting field, including luminescence induced by multiphoton absorption, exciton and biexciton radiative decay, luminescence arising from inelastic scattering and electron–hole plasma recombination.

Semiconductor quantum wells and superlattices are ideal systems for the investigation of radiative recombination processes at different carrier densities owing to the high emission efficiency and to the peculiar electronic properties which allow their band structure to be tailored. Different radiative recombination processes can be selectively tuned at exciting photon energies resonant with real states or in the continuum of the conduction band depending on the actual density of photogenerated carriers. As described in the pictorial scheme in figure 1, we can define three carrier
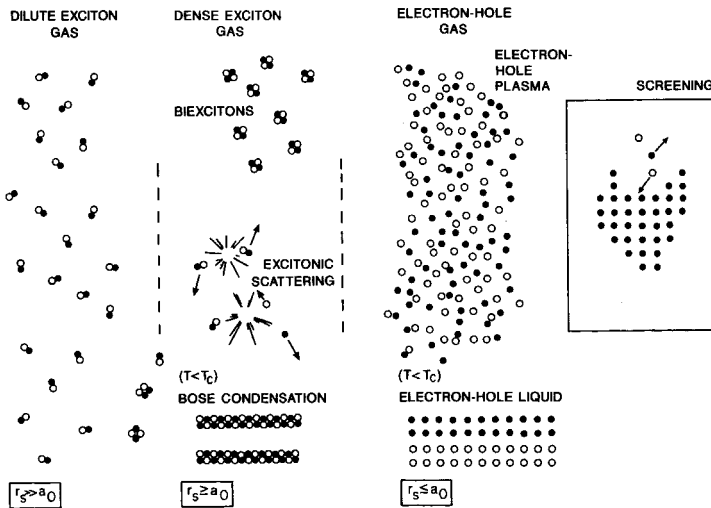
Figure 1. Illustration of the electronic and excitonic processes giving rise to radiative recombination in semiconductors. In the dilute exciton gas, where the mean interparticle distance r_s is much larger than the exciton Bohr radius a_0, spontaneous exciton decay is the main source of luminescence. With increasing densities $(r_s \geqslant a_0)$ excitonic scattering processes and biexciton decay provide new emission channels in the crystal. At high carrier densities $(r_s \leqslant a_0)$ the screening of the Coulomb interaction (right-hand inset) leads to the breakage of excitons. The radiative recombination processes are hence dominated by free-carrier recombination. It is noteworthy that below a certain critical temperature either the dense exciton gas or the dense electron–hole gas can undergo a phase transition, forming a condensed Bose state or an electron–hole liquid, respectively.

density regimes in which different quasi-particles are responsible for the dominant radiative recombination mechanisms of the crystal: (i) the dilute boson gas regime, in which the exciton density is lower than $10^{10}\,\mathrm{cm}^{-2}$. Under this condition the decay of free and bound excitons is the main radiative recombination channel in the crystal. (ii) The intermediate density range ($n \simeq 10^{11}\,\mathrm{cm}^{-2}$) in which excitonic molecules (biexcitons) and inelastic excitonic scattering processes contribute with additional decay mechanisms to the characteristic luminescence spectra. (iii) The high density range ($n \simeq 10^{12}\,\mathrm{cm}^{-2}$) where screening of the Coulomb interaction leads to exciton ionization. In this range all optical transitions originate from the radiative decay of free-carriers in a dense electron–hole plasma. In figure 1 we also show that below a certain critical temperature and under suitable conditions phase transitions may occur, like the Bose condensation of excitons (Snoke, Wolfe and Nysyrowicz 1990) or the transition from electron–hole plasma to electron–hole liquid (Keldysh 1982).

The aim of this work is to give a unified picture of the optical properties of semiconductor quantum wells and superlattices in these different carrier density ranges, providing a guideline for the specific study of the radiative decay of distinct elementary excitations and many-body states in low-dimensional systems. The experimental investigations of these effects are performed in the limit of intense exciting fields, by tuning the density of photogenerated quasi-particles and the frequency of the exciting photons. The energy spectrum of the radiative recombination processes occurring in semiconductors (either bulk or two-dimensional) is represented in figure 2. In the low carrier density range the free-exciton transitions (or interband transitions depending on the temperature) play the dominant role. At intermediate densities, we schematize the formation of biexciton states with a new emission channel developing at lower energy than the exciton emission. The main feature of the collective processes in semiconductors is that they result in a modified ground level for the crystal, and the resulting luminescence always occurs at lower energy than the intrinsic luminescence of the unperturbed crystal. This qualitatively reflects the amount of energy spent by the interaction responsible for the formation of some new quasi-particle in the crystal. With increasing densities the single particle self-energies are strongly renormalized leading to a reduction of the energy of the interband transitions, concomitant to a net increase of the quasi-Fermi levels of the electron and hole population. Under these conditions the optical response of the quantum well strongly deviates from the well-known linear excitonic behaviour. The optical properties of the crystal are then no longer controlled by the transverse dielectric constant or by the first-order dielectric susceptibility. They are strongly affected by many-body interactions between the different species of photogenerated quasi-particles, resulting in dramatic changes of the emission properties.

The second important parameter which varies in the graph of figure 2 is the frequency of the exciting field (arrows on the left hand side), i.e. ultimately the energy of the absorbed photons causing the optical transitions. There are in fact three basic excitation mechanisms: (i) excitation in the transparency region (arrow 1), where only multi-photon absorption can occur, provided the field intensity is large enough; (ii) excitation resonant to some real state of the crystal where electron–hole pairs (or excitons) are resonantly generated without excess energy. This is the domain of the so-called resonant spectroscopy. Finally, (iii) excitation in the continuum of the absorption, obtained with photons of energy larger than the crystal energy gap. In this case electron–hole pairs are generated with some excess energy which relax through different non-radiative decay mechanisms. It is noteworthy that under this condition
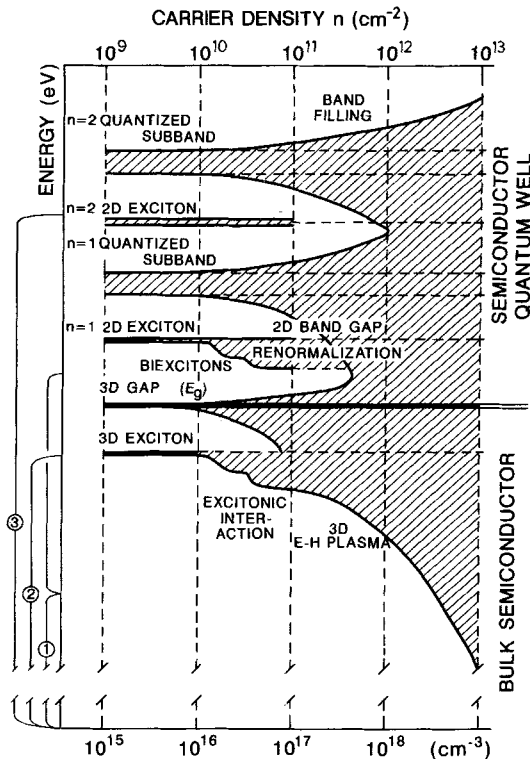
Figure 2.   Schematic energy spectrum of radiative recombination processes occurring in two-
and three-dimensional semiconductors at different carrier densities. The vertical arrows
indicate different photogeneration mechanisms, namely, excitation in the transparency
region (arrow 1), resonant to some excitonic state (arrow 2) or in the absorption continuum
(arrow 3).

there is a transient non-equilibrium phase in which the photoexcited carriers loose their
excess energy and relax to the bottom of the band. During this short transient there are
several interactions, like intercarrier scattering, LO phonon interaction and intravalley
scattering, which also depend on the carrier density and on the initial excess energy of
the particle. These processes characterize the early ps lifetime of the particle.
Subsequently, the carriers can be considered to be at quasi-equilibrium and they
populate the lowest-energy crystal states. In this work we will mainly discuss this quasi-
equilibrium situation, assuming that the relaxation processes of the thermalized
carriers have already occurred on a time scale much shorter than the radiative decay
times of the processes we are going to discuss.

    This review is organized as follows. First we give a brief outline of the basic
theoretical concepts concerning the electronic states and the optical transitions in
quantum wells (QW). Throughout the paper we mostly treat III–V semiconductor
quantum wells and superlattices formed by the GaAs/AlGaAs and InGaAs/InAlAs
material systems. In the second section we discuss the radiative recombination
processes induced by multi-photon absorption procsses, which are obtained when the
crystal is excited in the transparency region with an intense photon flux. The
application of this non-linear spectroscopy gives direct access to probe the excited
excitonic states in the quantum wells owing to the symmetry properties and the

selection rules for artificially layered semiconductor heterostructures. In the third section we briefly address the optical properties of quantum wells and superlattices in the low density regime, i.e. when excitonic luminescence dominates the optical spectra. We describe different experiments performed on type I and type II superlattices, and discuss the kind of information on the excitonic states that one can get by the application of resonant optical spectroscopy. In the fourth section we discuss the optical properties of quantum wells with increasing carrier density and under different photogeneration mechanisms. The physics of the biexciton formation and of the inelastic excitonic collision will be described based on the peculiar changes of the emission spectra of the quantum wells. Finally, in the last section, we extensively discuss the high-density regime and the electron–hole plasma recombination in confined systems.

The systematic investigation of the radiative recombination processes associated to these different states allows us to selectively monitor the many-body induced changes in the linear and non-linear optical transitions involving quantized states of the quantum wells and superlattices. The importance of these effects, belonging to the physics of highly excited semiconductors, lies in the possibility of achieving population inversion of states associated with different radiative recombination channels and strong optical non-linearities causing laser action and bistable behaviour of quasi two-dimensional (2D) systems, respectively.

2. Basic theoretical concepts of electronic states and optical transitions in quantum wells and superlattices

In two-dimensional (2D) heterostructures and quantum wells the confinement of the electron and hole wavefunctions in the growth direction (z-axis) causes strong changes in the dispersion relation of the density of states. Electronic states along the basal plane of the quantum well (x–y plane) are described by plane-waves, while along the z-axis they are characterized by wavefunctions with the same periodicity of the superlattice. The density of states assumes the well known step-like shape. This is shown in figure 3 for the case of an isolated quantum well and for a superlattice. In short-period superlattices the increased delocalization of the wavefunctions results in the formation of minibands dispersed along the k_z momentum direction and consequently in a smoothing of the 2D density of state step-edges.

There are different methods to calculate the electronic states confined in a quantum well, which are based on very different conceptual approaches. A first method is the so-called envelope function approach, in which the compositional superlattice is treated like a homogeneous crystal with a superimposed periodicity along the confinement direction. The envelope function varies slowly on the length scale of the lattice constant (a_0) and the crystal potential is taken into account by means of the effective mass approximation. The accuracy of the envelope function model is quite good in superlattices where the total period $d = L_z + L_b \gg a_0$. In this case the interface plane is really a minor perturbation on the slowly varying envelope function. The disadvantage of the envelope function approach in its simplest form lies in the applicability to energy states very close to the band gap edge of the constituent bulk materials. In addition, the accuracy of the model drops in ultrathin layer heterostructures, where the superimposed periodicity approaches the bulk crystal period ($d \simeq a_0$). In these cases microscopic models are needed which treat the superlattice period as the unit cell of a new crystal and take into account the actual atomic nature of the constituent materials.
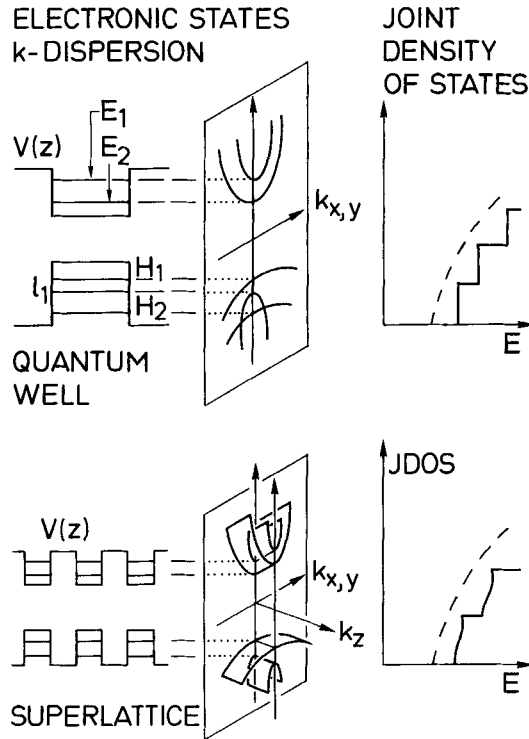
Figure 3.   Electronic states and joint density of states in quantum wells and super-lattices. In superlattices the well coupling results in an additional dispersion along the confinement direction. The dashed lines represent the three-dimensional density of states.

At the cost of considerable computational complexity, these *ab initio* methods provide a deeper insight into the electronic properties of the superlattice. A comprehensive survey of the different theoretical methods to calculate the superlattice electronic states is given in the specific review papers of Smith and Mailhiot (1990) and of Giannozzo, Grosso and Pastori Parravicini (1990). However, for most cases of practical interest the envelope function approximation is found to work very well. A large part of the experimental work on the optical properties of semiconductor quantum wells has in fact been analysed on the basis of this intuitive theoretical method.

Throughout the discussion we will consider a general superlattice consisting of two different materials (A for the well and B for the barrier) of respective thicknesses L_z and L_b. The band structure of the layered heterostructure is calculated by matching the envelope functions at each interface. It is supposed that the wavefunctions of the constituent materials take the form

$$\psi_{A,B}(\mathbf{r}) = F_j^{A,B}(\mathbf{r}) U_j^{A,B}(\mathbf{r}). \tag{2.1}$$

In equation (2.1) $U_j(\mathbf{r})$ is the Block function at $k=0$ and $F_j(\mathbf{r}) = S^{-1/2} \exp(i\mathbf{k}_\perp \cdot \mathbf{r}_\perp) \chi_j(z)$ where $\chi_j(z)$ is the slowly varying envelope function and S the quantum well surface. In doing so the following assumptions are explicitly made: (i) the materials A and B are lattice matched and the interfaces are perfectly abrupt, i.e. $U^A(\mathbf{r}) = U^B(\mathbf{r})$; (ii) only superlattice states close to the Γ point of the host materials are involved in the optical transitions. In the case of III–V heterostructures, only the usual Γ_6, Γ_7 and Γ_8 band

edges contribute to the superlattice wavefunction; (iii) the electron dynamics of the superlattice is described by the envelope functions which are eigen-states of the superlattice Hamiltonian. All the details on the physical properties of the material are included in the band structure parameters of the constituent bulk crystals, namely, the band gaps, the effective masses and the Kane matrix elements. Finally (iv), the lack of inversion symmetry of the Zincblende materials is neglected in order to define parity of the superlattice Bloch functions and derive selection rules for the optical transitions. The latter approximation, although rather crude, has been demonstrated to work very well in III–V and II–VI compounds (see also section 3.2).

In the realistic case of potential wells of finite depth, the calculation of the quantized sub-bands is performed by using a square well potential for uncoupled quantum wells (i.e. with wavefunctions totally confined in the well), or a periodic Kronig–Penney potential for superlattice structures with coupled wells (Bastard 1981, Bastard 1982, Huang-Sik Cho and Prucnal 1987). In the former case, by applying the boundary conditions (Bastard 1981)

$$\frac{1}{m_A}\frac{dF^A}{dz} = \frac{1}{m_B}\frac{dF^B}{dz}, \tag{2.2}$$

which ensures the probability current conservation across the interfaces, the following dispersion relations can be found

$$\frac{m_B}{m_A} K_A \tan\left(\frac{K_A L_z}{2}\right) = K_B, \tag{2.3}$$

for even states confined in the well, and

$$\frac{m_B}{m_A} K_A \cotan\left(\frac{K_A L_z}{2}\right) = -K_B, \tag{2.4}$$

for odd states confined in the well. For superlattices consisting of thin barriers, i.e. with strong coupling of the wavefunctions in different wells, the confined states merge into superlattice minibands. The use of a Kronig–Penney potential for these minibands results in the dispersion relation

$$\cos kd = \cos K_A L_z \cosh K_B L_b + \frac{1}{2}\left[\frac{m_A K_B}{m_B K_A} - \frac{m_B K_A}{m_A K_B}\right] \sin K_A L_z \sinh K_B L_b. \tag{2.5}$$

In equations (2.3)–(2.5)

$$K_A = \left(\frac{2m_A E}{\hbar^2}\right)^{1/2},$$

and

$$K_B = \left(\frac{2m_B(V-E)}{\hbar^2}\right)^{1/2},$$

where V is the potential barrier at the interface.

The key quantity for the optical processes between different sub-bands is the transition matrix element. Using the time dependent perturbation theory, we can write the interband absorption coefficient of the quantum well near the band gap edge as

$$\alpha(\hbar\omega) \approx \sum_{i,f} |\boldsymbol{\varepsilon} \cdot \boldsymbol{p}_{if}|^2 \delta(E_f - E_i - \hbar\omega)[f(E_i) - f(E_f)], \tag{2.6}$$

where the indices i and f indicate the initial and final states of energy E_i and E_f, respectively, and the $f(E_{i,f})$ are the statistical population factors of the two levels. The matrix element appearing in equation (2.6), can be factorized into an integral dependent on the $U_j(r)$ functions and in a summation at different lattice points of the slowly varying envelope functions. After some calculations one can obtain (Bastard 1988)

$$\boldsymbol{\varepsilon} \cdot \boldsymbol{p}_{if} \simeq \boldsymbol{\varepsilon} \cdot \langle U_i | \boldsymbol{p} | U_f \rangle \int_{\text{vol}} F_i^* F_f \mathrm{d}^3 r + \delta_{if} \boldsymbol{\varepsilon} \int_{\text{vol}} F_i^* \boldsymbol{p} F_f \mathrm{d}^3 r. \tag{2.7}$$

Equation (2.7) gives rise to the peculiar selection rules governing the interband absorption in quantum wells. The overlap integral between envelope functions selects the quantum number of the sub-bands involved in the transition. According to equation (2.1) we have

$$\int_{\text{vol}} F_i^* F_f \mathrm{d}^3 r \simeq \int \mathrm{d}z \chi_{n,i}^*(z) \chi_{m,f}(z) * 1/S \int \mathrm{d}^2 r_\perp \exp\left[\mathrm{i}(k'_\perp - k_\perp) r_\perp\right],$$

where S is the quantum well surface, n and m the quantum numbers of the initial and final state, respectively, and $r_\perp$ and $k_\perp$ are the components of the position and momentum vectors perpendicular to the carrier confinement direction. For a type I quantum well, in which both the electron and hole wavefunctions are confined in the same well and the envelope functions have a defined parity with respect to the centre of the well, the integral $\langle \chi_n | \chi_m \rangle$ is non-zero only for transitions with $n+m$ even. Conversely, in type II heterostructures, where electrons and holes are spatially separated, the above integral depends on the overlap of the exponential tails of the electron and hole wavefunctions confined in the barrier (B) and in the well (A) respectively. As a result, the type II absorption strength is reduced by about two orders of magnitude as compared to the type I absorption. Furthermore, the atomic-like dipole matrix element $\langle U_i | \boldsymbol{p} | U_f \rangle$ determines the dependence of absorption selection rules on the polarization of the exciting light wave. In particular in III–V quantum wells, the heavy-hole to electron transition has a strength three times larger than the light-hole to electron one, and both transitions are allowed for electric fields parallel to the basal plane of the quantum well. On the contrary, only light-hole to electron transitions are allowed when the electric field is parallel to the carrier confinement direction. We finally note that equation (2.7) indicates that the absorption coefficient for a given resonance is independent of the well thickness. As the Kane matrix element $\langle U_i | \boldsymbol{p} | U_f \rangle \simeq 23\,\text{eV}$ is almost the same for all semiconductors, the transition rate per layer is almost constant (Weisbusch 1987).

Large deviations from the behaviour predicted by the independent particle theory is found owing to the enhancement of the Coulomb interaction between electrons and holes in the heterostructures. For the ideal 2D case this leads to the formation of excitons with energy eigenvalues (Shinada and Sugano 1966)

$$E_n^{2\text{D}} = E_g - \frac{E_b}{(n - \frac{1}{2})^2}, \tag{2.8}$$

where E_g is the semiconductor gap and E_b is the three-dimensional exciton binding energy

$$E_b = \frac{e^4 \mu}{2\varepsilon_0^2 \hbar^2}, \tag{2.9}$$

μ being the exciton reduced mass and ε_0 the static dielectric constant. In the limit of perfectly 2D system it results in $E_b^{2D} = 4E_b^{3D}$. Therefore the 2D exciton is more strongly bound and much more stable than the corresponding 3D quasi-particle. In real quantum wells there is a strong dependence of the exciton binding energy on the well width, i.e. on the degree of confinement of the electron and hole wavefunctions. In particular the relevant exciton parameters, like binding energy, oscillator strength and Bohr radius, are found to monotonically vary between the extreme 2D and 3D values in the range $4\,\mathrm{nm} < L_z < 50\,\mathrm{nm}$. Many theoretical papers have been published on the physical properties of excitons in quantum wells (Bastard, Mendez, Chang and Esaki 1982b, Shinozuka and Matsuura 1983, Greene, Bajai and Phelps 1984, Ekemberg and Altarelli 1987, Duggan and Ralph 1987, Andreani and Pasquarello 1988, Wu 1989b, Dignam and Sipe 1990, Whittaker 1990). In figure 4 we show the results of recent calculations on the well width's dependence of these parameters in GaAs quantum wells. For large L_z values the quantities depicted in figure 4 converge to the well known bulk values.

The strong binding energy and the high oscillator strength of the quasi-two dimensional exciton result in the dominant excitonic character of optical transitions in quantum wells. This is depicted in figure 5 where we compare the absorption spectra of
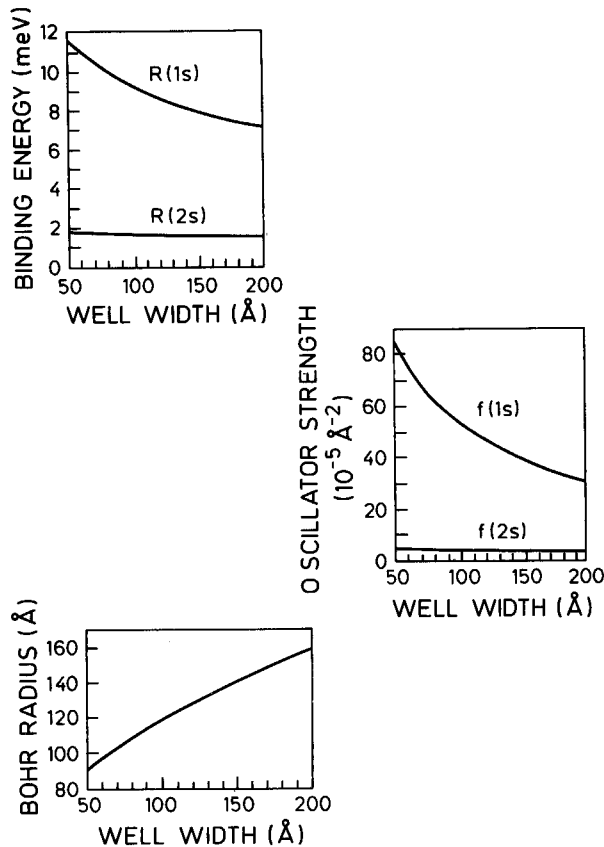

Figure 4.   Binding energy, oscillator strength and Bohr radius versus the well width for a GaAs/Al$_{0.4}$Ga$_{0.6}$As quantum well (after Andreani and Pasquarello 1988).
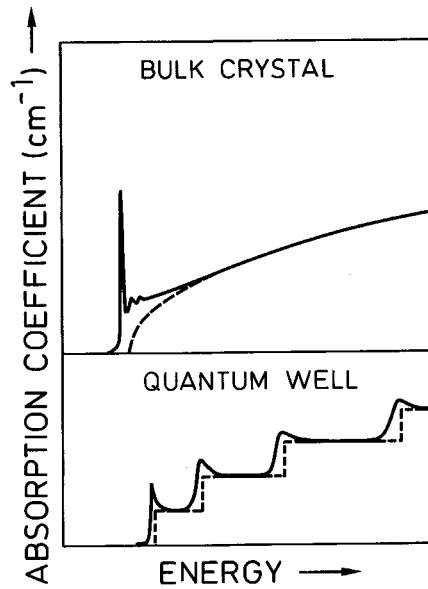
Figure 5. Absorption line shapes in bulk semiconductors and quantum wells with (continuous lines) and without (dashed lines) inclusion of excitonic effects.

3D and 2D semiconductors. The absorption coefficient for excitonic transitions can be expressed as

$$\alpha(\hbar\omega) \simeq |\langle U_{\mathrm{e}}(\boldsymbol{r})|\boldsymbol{\varepsilon}\cdot\boldsymbol{p}|U_{\mathrm{h}}(\boldsymbol{r})\rangle|^2 |\langle\chi_{n,\,\mathrm{h}}|\chi_{n,\,\mathrm{e}}\rangle|^2 |\Phi^l|^2 \delta_{K_\perp,\,0}\delta(E_{\mathrm{exc}}-\hbar\omega), \qquad (2.10)$$

where the first term is the transition matrix element for the Bloch functions, $\chi_{n,\,\mathrm{e(h)}}$ is the envelope function of the electron (hole) state of quantum number n, Φ^l is the exciton envelope function with angular momentum of quantum number l (usually s-states), and the delta functions give the momentum and energy conservation in the transition (E_{exc} is the energy of the exciton state). The following properties of the 2D exciton should be pointed out: (i) the presence of the $|\Phi^l|^2$ term in equation (2.10) introduces a specific dependence of the excitonic absorption on the well width, as the exciton envelope function depends on L_z. (ii) The narrow exciton peaks appearing in the absorption spectra reflect the momentum conservation of the excitonic transition. The k-conservation is relaxed in the presence of disorder, alloy fluctuation, interface roughness or carrier localization, resulting in broadened excitonic absorption structures. (iii) In III–V semiconductor quantum wells the LO phonon interaction is reduced as compared to other strongly ionic materials (like the II–VI) semiconductors. Therefore, unlike the wide gap materials where excitons are ionized at room temperature, the increase of the exciton binding energy due to the wavefunction confinement in III–V quantum wells is sufficient to keep excitons bound at room temperature. (iv) The exciton oscillator strength in quantum wells increases proportionally to the shrinkage of the exciton wavefunction. This results in a strong enhancement of the excitonic features superimposed to the intraband continuum, as compared to the corresponding bulk material. In the next sections we will apply the theoretical concepts outlined here to the interpretation of the optical spectra of semiconductor quantum wells and superlattices in the different carrier density regimes schematized in figures 1 and 2.

3.   Luminescence induced by multiphoton absorption processes

In recent years a great deal of interest has been devoted to the experimental and theoretical study of the non-linear optical properties of semiconductor quantum wells and superlattices, and several interesting articles have been published on this topic (see Chemla, Miller, Smith, Gossard and Wiegmann 1984, Haug and Schmitt-Rink 1985, Peyghambarian and Gibbs 1985, Chemla and Miller 1985, Schmitt-Rink, Chemla and Miller 1989). Most of the attention has been attracted by the strong exciton non-linearities caused by the wavefunction confinement in the heterostructures (Hanamura 1989). This phenomenon results in a huge enhancement of the third order non-linear susceptibility [$\chi^{(3)} = 10^{-2}$ esu in GaAs quantum wells to be compared with $\chi^{(3)} = 10^{-8}$ esu in bulk Si (Chemla et $al.$ 1984)] which is responsible for the macroscopic room temperature saturation of the exciton absorption and for the bistable operation observed under continuous-wave low-power excitation in GaAs (D. A. B. Miller, Chemla, Eilenberger, Smith, Gossard and Tsang 1982, Gibbs, Tarng, Jewell, Weinberger, Tai, Gossard, McCall, Passner and Wiegmann 1982) and In$_x$Ga$_{1-x}$As (Weiner, Pearson, D. A. B. Miller, Chemla, Sivco and Cho 1986) quantum wells. However, there are other interesting non-linear optical processes manifesting themselves under off-resonant excitation in the transparency region of the crystal, namely, multi-photon absorption and second and third harmonic generation.

In this section we discuss the theoretical and experimental aspects of the two-photon absorption (TPA) processes in quantum wells, with special attention to the radiative recombination processes induced by the non-linear absorption process in quantum confined systems.

3.1. Theoretical aspects of multiphoton absorption processes

Following the scheme of figure 2, the TPA process can be considered as the fundamental absorption mechanism for excitation in the transparency region of the crystal (arrow no. 1). The simultaneous absorption of two photons of energies $\hbar\omega_1 \leqslant E_g$ and $\hbar\omega_2 \leqslant E_g$ produces an excited state of energy $\hbar\omega = \hbar\omega_1 + \hbar\omega_2$, whose luminescence depends quadratically on the intensity of the exciting radiation. The calculation of the TPA transition rate (W_{cv}) is performed in the frame of the perturbation theory, assuming that the absorption transition involves a $virtual$ intermediate state. Two basic approximations are used to calculate the two-photon transition rate in bulk crystals: namely the two-band (Mahan 1968) and the three-band (Loudon 1962) schemes. In both models the summation over all the intermediate states is replaced by a suitable choice of a single intermediate state. In the three-band model the TPA transition consists of two interband transitions involving a higher-energy virtual intermediate state (lying either in the conduction or in the valence sub-band). In the two-band model the TPA transition involves an interband and an intraband transition in which the final state itself serves as intermediate level. The assumption of different transition mechanisms results in different dependences of the TPA transition rates on the photon energies, namely $W_{cv} \approx (2\hbar\omega - E_g)^{1/2}$ for the three-band model and $W_{cv} \approx (2\hbar\omega - E_g)^{3/2}$ for the two-band model, which have been experimentally demonstrated in several II–VI and III–VI and III–V semiconductors (Van der Ziel 1976, Catalano, Cingolani and Lepore 1986, Catalano, Cingolani, A., Cingolani, R., Lepore 1988).

The calculation of the TPA transitions in semiconductor quantum wells has been performed in a similar manner (Spector 1987, Pasquarello and Quattropani 1988, Shimizu 1989). In figure 6 we show a typical real space energy-band scheme adopted for the calculation of the TPA transition probability in quantum wells. The calculation is
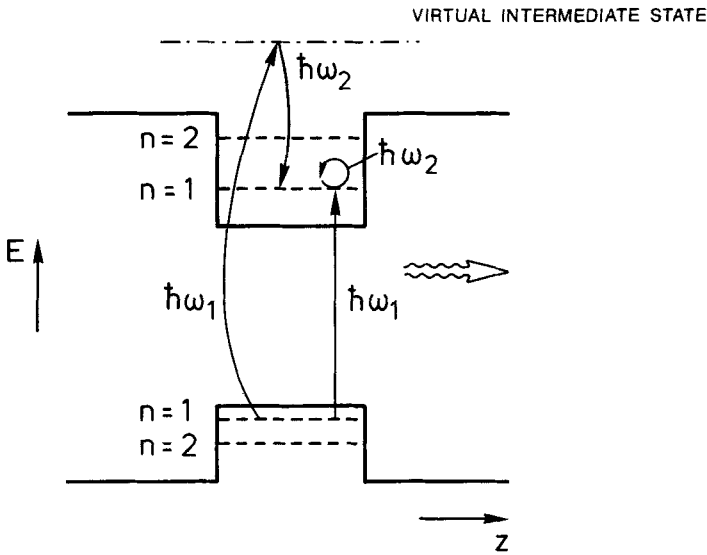
VIRTUAL INTERMEDIATE STATE

Figure 6. Two-photon absorption processes in quantum wells. The first photon ($\hbar\omega_1$) can be absorbed either on a virtual intermediate state (three-band model) or on the same initial or final state of the transition (two-band model).

performed by using several simplifying assumptions. First, the TPA transition is calculated in a two-band scheme in which the summation over all the intermediate states are replaced by a single virtual state. Second, excitonic effects are neglected in a first approximation. The intermediate virtual state is assumed to be coincident with either the initial or the final state and the total TPA process occurs via an intra-valence or intra-conduction sub-band transition (circular arrow in figure 3). It should be mentioned that, within the perturbation theory, the TPA transition probability per unit time is expressed as (Bassani and Pastori Parravicini 1975)

$$W_{c,v} = \frac{2\pi}{\hbar} \left| \sum_i \frac{\langle \psi^c|H|\psi^i\rangle\langle \psi^i|H|\psi^v\rangle}{(E_i - E_v - \hbar\omega)} \right|^2 \delta(E_c - E_v - 2\hbar\omega). \tag{3.1}$$

Therefore, the latter assumption is reasonable because the energy difference between the intermediate ψ^i and the initial ψ^v states occurs in the denominator of W_{cv}. The TPA rate will thus be larger for processes involving an intraband intermediate transition. Nevertheless, in GaAs quantum wells care must be taken since the interband matrix elements for transitions involving the top of the valence band and the Γ_{15} and Γ_8 conduction bands are of comparable magnitude (Cardona, Christensen and Fasol 1988). The above approximation is then reliable only near resonant conditions ($2\hbar\omega \simeq E_g$), and it must be considered as a simplifying approximation in the evaluation of the TPA transition rate near the band gap edge (see also Pasquarello and Quattropani 1990a, b).

In the two-band model of Pasquarello and Quattropani (1988) the interband matrix element of W_{cv} has the form

$$\langle \psi^c(n, k)|\varepsilon \cdot p|\psi^v(n', k')\rangle = \varepsilon \cdot p_{cv}\delta_{nn'}\delta_{kk'}, \tag{3.2}$$

while the intraband matrix element is

$$\langle \psi^c(n, k) | \varepsilon \cdot p | \psi^c(n', k) \rangle = \frac{\varepsilon B(n, n')}{m_c}, \tag{3.3}$$

where

$$\varepsilon \cdot B(n, n') = \frac{\varepsilon_z 2i\hbar}{L_z} [1 - (-1)^{n+n'}] \frac{nn'}{[n^2 - n'^2]} (1 - \delta_{nn'}) + \hbar k \cdot \varepsilon_{xy} \delta_{nn'}, \tag{3.4}$$

and where ε_z and ε_{xy} are the polarization vectors of the exciting electromagnetic field parallel and perpendicular to the carrier confinement directions, n and n' are the sub-band indexes and the superscript c and v indicate conduction and valence band states, respectively. Additional selection rules for the TPA absorption processes are derived from these matrix elements which depend on the polarization direction of the exciting field. When the light is polarized perpendicular to the confinement direction the matrix elements of the momentum operator are non-vanishing only for transitions involving states with the same principal quantum number n. The selection rule $\Delta n = 0$ is therefore expected to be valid for the case $\varepsilon \perp z$ (ε_{xy} geometry). Conversely, TPA transitions for the polarization $\varepsilon \| z(\varepsilon_z)$ can only involve sub-bands whose quantum numbers differ by an odd integer ($\Delta n \neq 0$ selection rule) and light-hole valence sub-bands. This is exemplified in figure 7 where the TPA transition rates calculated by means of equations (3.2) and (3.3) are depicted for a 10 nm wide GaAs/Al$_{0.4}$Ga$_{0.6}$As quantum well in the ε_z and ε_{xy} polarization conditions. We note that the two-photon absorption onset is raised in energy as compared to the bulk GaAs gap owing to the additional carrier confinement energy. The ε_{xy} curve exhibits an almost featureless spectrum with weak changes of slope corresponding to the transitions with $\Delta n = 0$. The ε_z spectrum presents marked onsets at the main interband transitions with $\Delta n \neq 0$, and only transitions involving light-hole valence band states are allowed by symmetry. In both cases the total TPA transition rate is found to grow with increasing photon energies. Furthermore, the two photon absorption coefficient ($\alpha^{(2)}$) in the ε_z configuration is expected to be larger than the one-photon absorption coefficient (α) (Spector 1987).
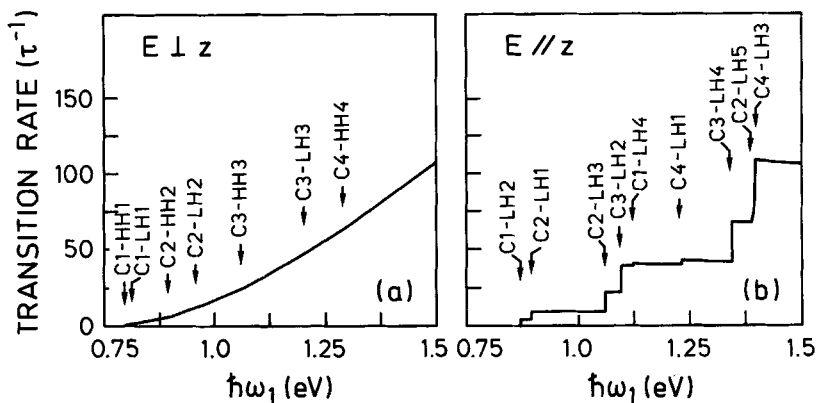

Figure 7. Theoretical two-photon absorption transition rates calculated for a GaAs/Al$_{0.4}$Ga$_{0.6}$As quantum well with $L_z = 10$ nm and infinite barrier height. $E\|z$ and $E\perp z$ indicate the polarization configurations parallel and perpendicular to the confinement direction, respectively. (After Pasquarello and Quattropani 1988.)

Up to now we have been dealing with the band-to-band TPA processes, neglecting the contribution of excitonic states as final states of the non-linear absorption process. An extension of the previously discussed model including exciton states has recently been made by Shimizu (1989) and Pasquarello and Quattropani (1990b). The basic result of these works is that different final excitonic states are involved in the TPA process depending on the polarization of the exciting field. Before discussing the quantum well case, we recall that selection rules complementary to the ones usually assumed for the linear excitonic absorption are found to be valid in crystal having inversion symmetry. For crystals with dipole allowed one photon absorption (OPA) transitions, only excited 2p excitonic states are allowed as final states of the TPA process. This can easily be understood in the frame of the two-band model, assuming that the first transition creates a 1s exciton state, as in the usual OPA process, while the second transition scatters this 1s state into a 2p state to allow parity conservation in the overall process. Analogously, in the three-band model the TPA transition occurs through an intermediate state having opposite parity to the initial and final states, thus resulting in a final 2p exciton level. These rules are strictly valid in crystals having inversion symmetry, in which parity is a good quantum number. The lack of inversion symmetry in non-centro-symmetric crystals makes these selection rules less stringent, and care must be taken in comparing the OPA and the TPA spectra. In the next section we present a simplified group analysis of GaAs quantum wells in order to derive approximated parity selection rules for the TPA and OPA processes. The limitations of these selection rules due to the lack of inversion symmetry are also discussed.

3.2. *Symmetry properties of the electronic and excitonic states in GaAs quantum wells*

In crystals having inversion symmetry, parity selection rules can be derived for optical transitions by a group theoretical analysis of the electronic and excitonic states (Andreani, Bassani and Pasquarello 1989). For zincblende crystals like GaAs (non-centro-symmetric lattice) the lack of inversion symmetry prevents parity selection rules to be defined. In GaAs/Al$_x$Ga$_{1-x}$As quantum wells grown along the (001) direction the point group of the layered structure can be derived from the original T_d point group of the zincblende GaAs by considering the set of operations of T_d which transforms the z-axis into itself. The quantum well point group at $k=0$ is then found to be D_{2d}. In this symmetry the original fourfold degenerate Γ_8 valence band states split into the twofold degenerate Γ_6 and Γ_7 states due to the removal of the heavy- and light-hole degeneracy. However, although the T_d and D_{2d} groups have no inversion symmetry, in most phenomenological models the effective mass Hamiltonian of the GaAs quantum wells is assumed to have the full cubic symmetry of the O_h group. This is possible by neglecting the terms which depend on the antisymmetric part of the crystal potential (Andreani *et al.* 1989). Following this approximation the point group of the GaAs quantum wells at $k=0$ reduces to the centro-symmetric D_{4h} group. The irreducible representations of the lowest conduction and valence band states in the T_d, D_{2d}, D_{4h} and O_h groups are summarized in figure 8. The approximated D_{4h} symmetry is obtained by neglecting the terms which remove the spin degeneracy at $k \neq 0$ in the Luttinger Hamiltonian which describes the valence band states of the quantum well. In this approximation the effective mass equation has the same symmetry as if the crystal structure were diamond-like (O_h group). It should be noted that in figure 8 the irreducible representation of the D_{4h} and O_h groups (labelled Γ_i^+ and Γ_i^-) have parity
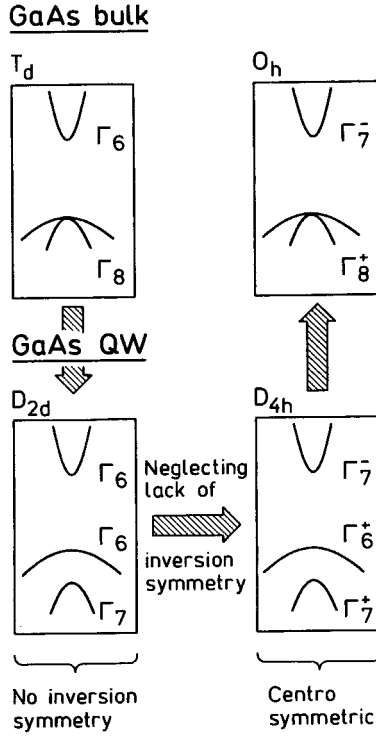
R. Cingolani and K. Ploog

GaAs bulk

Figure 8. Schematic group symmetry analysis for GaAs quantum wells (see text for explanations).

Table 1. Irreducible representation of the first two conduction (CB) and valence sub-bands (VB) in the D_{2d} and D_{4h} groups. Note that in the D_{4h} group the electronic states have definite parity $P_{c,v} = P_U \cdot P_F$ under spatial inversion (see text).

	CB1	CB2	HH1	HH2	LH1	LH2
D_{2d}	Γ_6	Γ_7	Γ_6	Γ_7	Γ_7	Γ_6
D_{4h}	Γ_7^-	Γ_7^+	Γ_6^+	Γ_6^-	Γ_7^+	Γ_7^-
P_U	$-$	$-$	$+$	$+$	$+$	$+$
P_F	$+$	$-$	$+$	$-$	$+$	$-$
$P_{c,v}$	$-$	$+$	$+$	$-$	$+$	$-$

under spatial inversion. This allows us to derive approximate selection rules for the electronic and excitonic transitions in GaAs quantum wells. The detailed classification of the quantum well states for both the D_{2d} and the D_{4h} symmetries is shown in table 1.

Provided the above approximation is valid, the parity of the electronic states in the quantum well can be studied by considering the irreducible representations of the wavefunctions $\Psi(r) = F(z)U(r)$. The envelope function $F(z)$ of the quantized state has even parity (P_F) for odd sub-bands and odd parity for even sub-bands, while the Bloch function $U(r)$ has a definite parity (P_U) in the approximated D_{4h} symmetry, as discussed before (table 1). Parities for the conduction and valence band states can therefore be calculated as $P_{c,v} = P_U P_F$, as shown in table 2. We emphasize that the parity of the

Table 2. Parity selection rules for one-photon (OPA) and two-photon (TPA) absorption transitions (see text). (a) and (f) indicate allowed and forbidden processes, respectively.

Transition	P_c	P_v	P_χ	P_{exc}	OPA	TPA
E_{11h}^{1s}	+	−	+	−	a	f
E_{11h}^{2p}	+	−	−	+	f	a
E_{111}^{1s}	+	−	+	−	a	f
E_{111}^{2p}	+	−	−	+	f	a
E_{12h}^{1s}	−	−	+	+	f	a
E_{12h}^{2p}	−	−	−	−	a	f
E_{22h}^{1s}	−	+	+	−	a	f
E_{22h}^{2p}	−	+	−	+	f	a
E_{221}^{1s}	−	+	+	−	a	f
E_{221}^{2p}	−	+	−	+	f	a
E_{13h}^{1s}	+	−	+	−	a	f
E_{13h}^{2p}	+	−	−	+	f	a
E_{211}^{1s}	+	+	+	+	f	a
E_{211}^{2p}	+	+	−	−	a	f

Bloch functions defined in tables 1 and 2 results from the higher symmetry (D_{4h} instead of D_{2d}) obtained by neglecting the lack of inversion symmetry of the zincblende lattice. In a similar way the parity of the excitonic states can be calculated as $P_{exc} = P_c P_v P_\chi$, where P_χ is the parity of the excitonic envelope function (even for s-states and odd for p-states). These are given in the fourth column of table 2. The parity selection rules for the linear and non-linear excitonic transitions are reported in the last two columns of table 2. In the one-photon transition processes the final P_{exc} parity is multiplied by the odd contribution of the absorbed photon, while in TPA processes the parity of the final state does not change (since the two-photons give even parity contribution). Transitions in which the total parity is not conserved with respect to the parity of the initial state are forbidden. These selection rules, although approximate, provide a reliable means for predicting the strength of the linear and non-linear absorption processes in quantum wells. Deviations from the selection rules mainly originate from: (i) terms in the effective mass approximation which describe the lack of inversion symmetry in the zincblende lattice; and (ii) terms in the $k \cdot p$ expansion which go beyond the effective mass approximation (Andreani *et al.* 1989).

3.3. *Experiments on two-photon-absorption spectroscopy*

Two-photon absorption in solids has been the subject of extensive investigations in recent years (for a recent review in bulk semiconductors see V. Nathan *et al.* 1985). The method has the advantage of producing a uniform concentration of electrons throughout the excited volume of the crystal rather than in the thin penetration depth usually achieved in linear absorption experiments. In addition, the relevance of the specific intermediate state provides information on the band structure of the crystal not easily achievable with linear absorption techniques (Inoue and Toyozawa 1965). In the last few years several experimental studies have been reported on TPA spectroscopy in GaAs/Al$_x$Ga$_{1-x}$As multiple quantum wells (Van der Ziel and Gossard 1978, Tai, Mysyrowicz, Slusher and Cho 1989, Catalano, Cingolani, A., Cingolani, R., Lepore and Ploog 1989a, Catalano, Cingolani, A., Cingolani, R., Lepore and Ploog 1989b, Nithisoontorn, Unterrainer, Michaelis, Sawaki, Gornik and Kano 1989) and on ternary alloy Al$_x$Ga$_{1-x}$As/AlAs MQW (Catalano, Cingolani, A., Cingolani, R., Lepore

and Ploog 1990). The basic purpose of these experiments was the investigation of the TPA absorption processes in resonance with quantized sub-bands in the well. It should be mentioned that in contrast to the case of bulk crystals the experimental investigation of TPA processes in quantum wells is difficult because very small absorption changes through the ultrathin epitaxial layers have to be detected (typically 1 μm of total quantum wells or superlattice thickness). Therefore, two-photon induced photo-luminescence excitation spectroscopy (TPA–PLE) (Tai *et al.* 1989, Catalano *et al.* 1989) or photocurrent spectroscopy (Nithisoontorn *et al.* 1989) have been adopted to study this non-linear absorption process. Non-linear transmittance in magnetic field around the fundamental exciton state in GaAs multiple quantum wells has also been performed (Fröhlich, Wille, Schlapp and Weimann 1988). The authors used a suitable two-beam technique in which a dye laser beam almost resonantly excites the exciton while a CO_2 laser completes the TPA transition.

In figure 9 we show the TPA spectrum of a $GaAs/Al_{0.38}Ga_{0.62}As$ superlattice consisting of a 60 periods of 4·7 nm GaAs sandwiched between 5·7 nm $Al_{0.38}Ga_{0.62}As$. The two-photon absorption has been measured by detecting the luminescence of the fundamental heavy-hole exciton E_{11h} as a function of the exciting photon energies $2\hbar\omega$ in the ε_{xy} polarization. The spectrum exhibits a step-like line-shape which follows the 2D density of states, and a strong exciton peak related to the light-hole exciton E_{11l}. This E_{11l} peak is blue-shifted by about 9 meV with respect to the exciton resonance observed in the linear absorption or reflectance spectrum. Similar results are obtained for a 10 period multiple quantum well consisting of 10 nm GaAs sandwiched between 11 nm $Al_{0.36}Ga_{0.64}As$ (figure 10). In this case the TPA spectrum exhibits two excitonic features associated with the second sub-bands in the well (E_{22h} and E_{22l}). These structures are blue-shifted by about 7 meV with respect to the corresponding excitonic resonances in the linear spectra. The observed shift in the excitonic energies can be
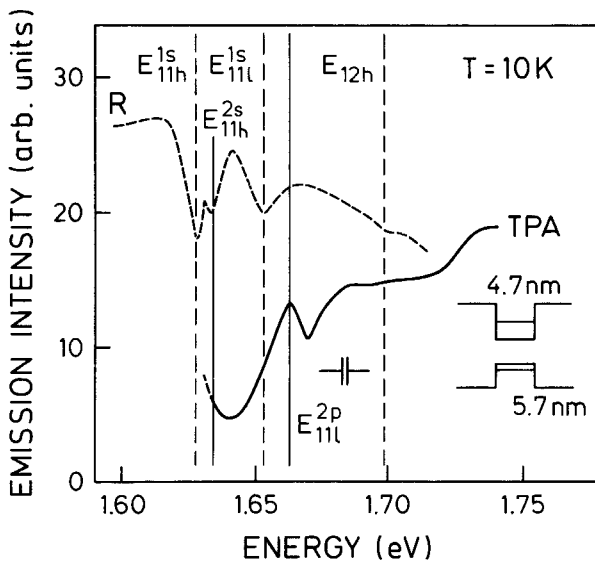

Figure 9.   TPA luminescence excitation spectrum versus $2\hbar\omega$ of a $GaAs/Al_{0.38}Ga_{0.62}As$ superlattice. The solid curve is compared with the reflectance spectrum (dashed line labelled R). The vertical continuous and dashed lines indicate excitonic transitions allowed and forbidden in the TPA process, respectively.
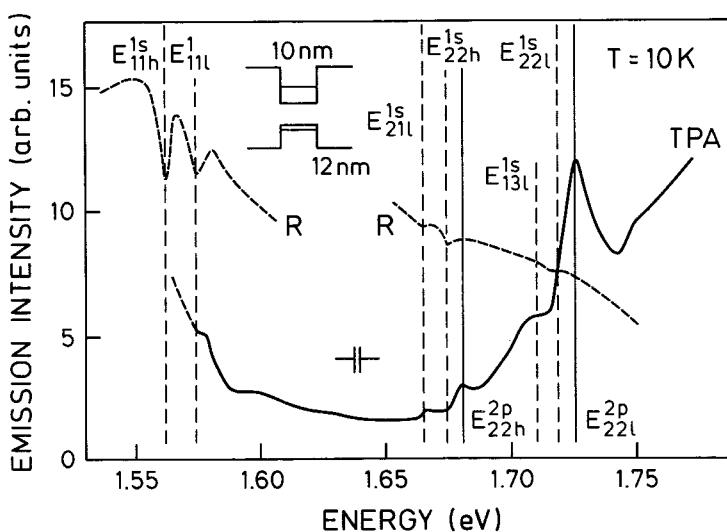
Figure 10. As in figure 9, for a GaAs/$Al_{0.36}Ga_{0.64}As$ multiple quantum well of different structural parameters. The high energy part of the reflectance spectrum has been magnified for a better comparison.

explained by the different parity selection rules of the TPA process, as summarized in table 2. TPA transitions with $\Delta n = 0$ (ε_{xy} configuration) involve final excited 2p excitonic states, while 1s states, allowed in the linear absorption processes, become forbidden in the TPA processes. These results account well for the observed blue-shift of the excitonic peaks in the experimental spectra of figures 9 and 10. Such a shift is in fact coincident with the 1s–2p splitting measured in luminescence experiments under electric field (Vina, Collins, Mendez and Wang 1988) and calculated with variational techniques (Greene *et al.* 1984, Matsuura and Shinozuka 1984). On the basis of these data the binding energy of the 2p excitonic state can be estimated to be about 2 meV for the E_{11l} in the 4·7 nm well and about 1·5 meV and 1 meV for the E_{22l} and the E_{22h} excitons in the 10 nm well, respectively. The latter measurement also accounts for the observed thermal ionization of the TPA E_{22h} peak occurring around 14 K. It is worth noting that similar experiments performed by Tai *et al.* (1989) evidence a pronounced absorption tail corresponding to the E_{11l}^{2p} state, instead of the above discussed peak. The strong reduction of the strength of the 2p exciton peak compares well with the theoretical predictions of Shimizu (1989) and Pasquarello and Quattropani (1990b). The oscillator strength of the excited exciton states scales as l^{-3} (where *l* is the quantum number of the angular momentum) resulting in the reduction of the strength of the 2p states by a factor of 8. However, such a decrease should not prevent the observation of the 2p states in high sensitivity TPA–PLE experiments. A possible reason for the discrepancy between the results of Catalano *et al.* (1989) and Tai *et al.* (1988a, b) can be the difficulty to obtain the necessary excitation power density for the direct observation of the 2p exciton states in TPA experiments (about 30 MW cm^{-2} in the experiments of Catalano *et al.* 1989a, b), although further work is necessary to quantitatively measure the strength of the 2p exciton absorption in TPA experiments.

Another interesting feature of the spectra of figures 9 and 10 is the presence of weak structures corresponding to the 1s state of $\Delta n \neq 0$ exciton. As discussed before, these transitions are allowed in the ε_z polarization. A possible origin for the observed peaks is

the absorption of a weak ε_z component of the polarization vector projected by the laser beam impinging on the crystal surface at $45°$ angle. It should be mentioned that Nithisoontorn *et al.* (1989, 1990) did observe both 1s and 2p exciton states in their TPA photocurrent spectra. The authors interpret their finding as due to the linear absorption of the second-harmonic beam produced by the intense exciting field in their asymmetric GaAs multiple quantum wells. At present, it is difficult to discriminate which of the two effects can be responsible for the appearance of the 1s states in the TPA spectra. In fact, the selection rules derived in the previous section, treating the GaAs quantum well as a diamond-like crystal having an inversion centre, cannot be considered as strictly valid. Therefore, the observation of weak $\Delta n = 0$ transitions with the final 1s exciton state in the TPA spectra might be related to the deviations from these selection rules due to the lack of inversion symmetry of the GaAs lattice. However, these selection rules are also observed in the two-photon magnetoabsorption experiments of Fröhlich *et al.* (1988), who first demonstrated that inter-Landau level TPA transitions follow the modified $\Delta n = 1$ selection rule (where n is the quantum number of the level). This controversy, not yet fully resolved, also persists in different polarization configurations. In the next section we describe the results of the polarization dependent TPA photoluminescence measurements, and we discuss the possible deviations from the above selection rules.

3.4. *Measurements of the polarization dependence of the two-photon absorption in quantum wells*

In section 3.2 we have discussed that for light polarized perpendicular to the direction of carrier confinement (ε_{xy}), the matrix elements of the momentum operator are non-vanishing only for $\Delta n = 0$ transitions. Conversely, transitions induced by light polarized parallel to the carrier confinement direction (ε_z) involve states with different quantum numbers ($\Delta n \neq 0$). Polarization dependent studies of TPA have been performed by Tai *et al.* (1989) and Catalano *et al.* (1989b). In these experiments either a wave-guide configuration in which the multiple quantum well is sandwiched between two thick cladding layers, or a $5\,\mu m$ thick multiple quantum well have been used to allow propagation of the exciting beam along the basal plane of the heterostructure in the ε_z configuration. The polarization dependent TPA–PLE spectra of a multiple quantum well structure with 10 nm GaAs wells are shown in figure 11. The attribution of the observed spectral features has been made by comparing the TPA–PLE spectrum with the one-photon absorption (OPA–PLE) spectrum measured in the same sample. The OPA–PLE curve exhibits the heavy- and light-hole exciton peaks associated with the $n = 2$ sub-band in the well and two weaker parity allowed transitions (E_{13h} and E_{24h}). In addition, a sharp E_{21l} transition is observed at $1·664\,eV$, which will be discussed later (details on this OPA–PLE spectrum and on the calculations of the main excitonic transitions will be given in the next section). On the basis of these assignments we can analyse the TPA–PLE spectra of figure 11 (*a*), measured for the two polarization configurations in the energy range $1·61 < 2\hbar\omega < 1·76\,eV$ (we have not extended the investigation range to lower energies because the E_{11l} line is very close to the detection wavelength and cannot be well resolved in the PLE spectrum). As discussed in the previous section, the spectrum recorded in the ε_{xy} geometry exhibits $\Delta n = 0$ excitonic peaks. The structures labelled E_{22h}^{2p} and E_{22l}^{2p} are blue shifted by about 8 meV with respect to the corresponding 1s states observed in the linear spectrum. This is consistent with the expected 2p–1s splitting of the heavy- and light-hole excitons associated with the $n = 2$ sub-band in a 10 nm GaAs QW (Matsuura and Shinozuka 1984).
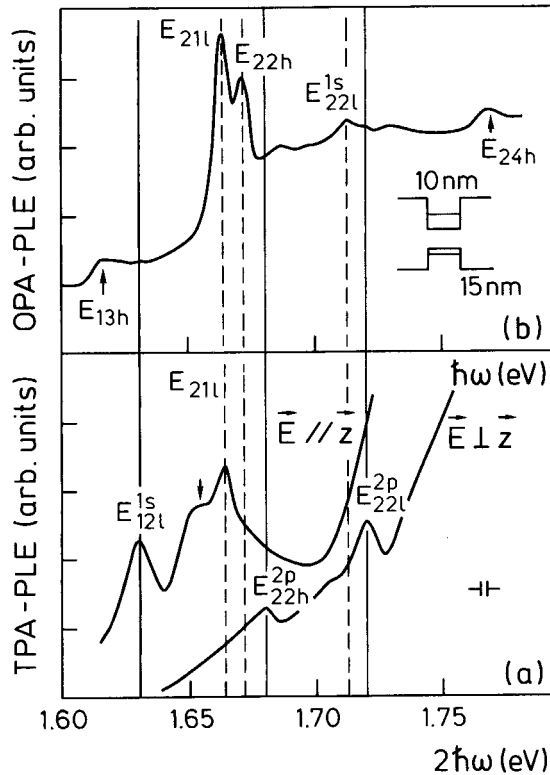
Figure 11. (*a*) TPA–PLE spectra of a GaAs/Al$_{0.36}$Ga$_{0.64}$As multiple quantum well structure in the polarization configurations parallel ($E/\!/z$) and perpendicular ($E\perp z$) to the confinement direction. (*b*) OPA–PLE for the same sample. The continuous and dashed lines have the same meaning as in figures 9 and 10.

Dramatic changes in the TPA–PLE spectrum occur in the ε_z configuration. This curve exhibits sharp $\Delta n = 1$ excitonic resonances labelled E_{121} and E_{211} (at 1·631 and 1·644 eV, respectively) and a broad structure around 1·652 eV. The E_{121} and E_{211} transitions are forbidden in the OPA process, and can only be observed in TPA spectroscopy applying the ε_z configuration. In addition, the E_{22h}^{2p} and E_{221}^{2p} transitions observed in the ε_{xy} configuration disappear in the ε_z spectrum, indicating a large on/off ratio of the observed non-linearity. According to the parity selection rules given in table 2, the E_{121}^{1s} peak is related to the 1s exciton associated with the $n = 1$ electron sub-band and the $n = 2$ light-hole sub-band.

The attribution of the E_{211} transition observed at the same energy in both the linear and non-linear spectra of figure 11 is not straightforward. In contrast to the early interpretation of Miller *et al.* (1985a, b), Andreani and Pasquarello (1989) have recently demonstrated that the 1s state of the E_{211} exciton is forbidden in linear absorption, even if valence band mixing is taken into account. Conversely, in GaAs quantum wells of well width around 10 nm (as in our experiment), Coulomb coupling between excitons belonging to different sub-bands enhances the oscillator strength of the 2p state of the E_{211} exciton. In this case the E_{211}^{2p} line can be resolved in the linear PLE spectra. According to the results of this theoretical treatment, we conclude that both the OPA and TPA spectra of figure 11 exhibit the 2p state of the E_{211} exciton, in contrast to the

selection rules of table 2. An appealing feature of this interpretation is that the broad structure in the low energy side of the E_{211} peak lies at the expected energy of the 1s state of the E_{211} exciton, which is allowed in the ε_z polarization. However, we have no clear explanation yet for the simultaneous occurrence of both transitions in the TPA spectrum. The effect of the valence band mixing as well as the deviation from the predicted selection rules due to the non-centro symmetric part of the Bloch function can be invoked to qualitatively explain the observed effect. Further work is necessary to fully understand the TPA selection rules and to quantitatively measure the TPA rate in both polarization configurations. This will also be helpful to determine the importance of the higher energy intermediate states in the strength of the TPA transitions, and to clarify the reliability of the approximate selection rules derived by neglecting the lack of inversion symmetry in GaAs.

3.5. Multiphoton absorption processes in ternary alloy $Al_xGa_{1-x}As$ quantum wells

Following the investigation on GaAs quantum wells, TPA spectroscopy has been successfully applied to ternary alloy $Al_xGa_{1-x}As$/AlAs quantum wells to study high-index excitonic states associated to heavy- and light-hole sub-bands (Catalano *et al.* 1990). In these ternary alloy quantum wells most of the important excitonic features are obscured in the linear absorption spectra (Scamarcio, Cingolani, A., Cingolani, R., and Ploog 1989) owing to the phenomena of alloy broadening (Schubert, Göbel, Horikoshi, Ploog and Queisser 1984) and interface roughness (J. L. de Miguel, Fujiwara, Briones and Ploog 1986). The former effect is dominant in ternary alloy materials due to the random distribution of Al and Ga on the group III sites of the lattice. The broadening of the excitonic lines is found to scale as $a_0^{-3/2}$ (Schubert *et al.* 1984), where a_0 is the exciton Bohr radius. However, 2p exciton states are expected to have a reduced sensitivity to the fluctuations of the crystal potential owing to the larger spatial extent of this wavefunction. This is clearly demonstrated by comparing the linear (OPA) and non-linear (TPA) absorption spectra of the $Al_{0.37}Ga_{0.63}As$/AlAs multiple quantum wells structure shown in figure 12. The sample consists of 30 wells with $L_z = 19.3$ nm sandwiched between 9·8 nm wide AlAs barriers. The low temperature OPA spectrum (upper curve) exhibits several structures related to the heavy- and ligh-hole excitons associated with the first four sub-bands. The energy position of the observed transitions is consistent with the results of envelope function calculations (details on the linear absorption and luminescence of these ternary alloy quantum wells are given in the next section). The excitonic peaks are rather broad (FWHM of about 16 meV) and the light-hole exciton peaks are not well resolved.

A different situation is observed in the TPA spectrum (lower curve), which exhibits sharp 2p exciton features blue-shifted with respect to the corresponding 1s-states in the linear spectrum. The measured 2p–1s splitting amounts to 12·5 meV for the E_{22h} exciton, indicating an exciton binding energy of the order of 13 meV in these 19 nm wide $Al_{0.37}Ga_{0.63}As$ quantum wells. In addition, we can clearly resolve the light-hole exciton peaks up to the $n=4$ sub-band. From the measured energy splitting between the 2p states of the heavy- and light-hole states of the same principal quantum number we have determined the valence band-offset of the heterostructure. The observed splittings of 24, 52 and 91 meV for the $n=2$, 3 and 4 sub-bands, respectively, are compared with the splittings calculated in the usual square well model as a function of the valence band discontinuity. Our experimental data are consistent with a valence band offset of 340 ± 15 meV, in good agreement with the determination made earlier on
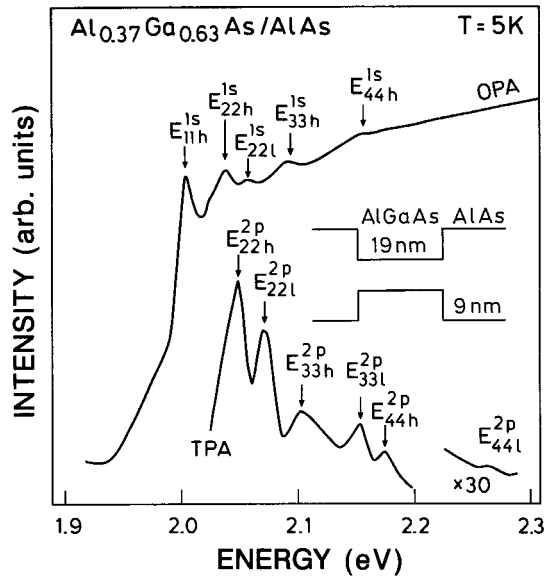
Figure 12. Linear absorption spectrum (OPA) and two-photon absorption luminescence excitation spectrum (TPA) of a ternary alloy $AlAs/Al_{0.37}Ga_{0.63}As$ multiple quantum well heterostructure.

type II $Al_xGa_{1-x}As/AlAs$ quantum wells (Dawson *et al.* 1986a, b). It is worth noting that our determination does not depend on the actual value of the ternary alloy gap E_g. Assuming $E_g = 1.99$ eV (at 5 K) for $x = 0.37$ (Lee, Juravel, Wolley and Spring Thorpe 1980), a 70:30 conduction to valence band-offset ratio is obtained. A detailed discussion of the ternary alloy properties is given in the next section.

We finally outline the determination of the absolute TPA coefficient β by means of the quantitative non-linear luminescence technique. This method allows the determination of the β coefficient by comparing the intensities of the one- and two-photon excited luminescence signals (L_1 and L_2 respectively) and assuming the quantum efficiency to be independent of the pumping mechanism (this condition is fulfilled for $\hbar\omega_1 = 2\hbar\omega_2$, where $\hbar\omega_1$ and $\hbar\omega_2$ are the photons absorbed in the linear and non-linear process, respectively). In this case the TPA coefficient results (Catalano, Cingolani, Ferrara and Lugara 1980):

$$\beta(E) = \frac{L_2}{L_1}\frac{I_1}{I_2^2}\frac{\alpha(E)\alpha_e}{\alpha(E)-\alpha_e}\frac{1-\exp(-(\alpha(E)-\alpha_e)l)}{[\exp(\alpha_e \cdot l)-1]}, \qquad (3.5)$$

where I_1 and I_2 are the exciting photon fluxes at the energies $\hbar\omega_1$ and $\hbar\omega_2$, respectively, $\alpha(E)$ is the linear absorption coefficient, α_e is the linear absorption coefficient at the energy $E = \hbar\omega_1 + \hbar\omega_2$, and l is the active thickness of the sample. The application of this model is possible provided the OPA coefficient is negligible at the $\hbar\omega_1$ and $\hbar\omega_2$ frequencies. In single beam experiments, as in the present case, this condition is always fulfilled as $\hbar\omega_1 = \hbar\omega_2 \simeq E_g/2$ and $\alpha(E_g/2) \simeq 0$. The absolute β coefficient is evaluated at the energy of the E_{33h}^{2p} transition, lying at 2.101 eV in the TPA spectrum of figure 12. Using the measured value of $\alpha_e = 2.097\ 10^4\ cm^{-1}$ at this energy, the resulting TPA coefficient at the E_{33h}^{2p} frequency is $\beta = (1.2 \pm 0.3) \times 10^{-1}\ cm\ MW^{-1}$. Using the same procedure, we evaluate $\beta = (2.2 \pm 0.55) \times 10^{-1}\ cm\ MW^{-1}$ at the frequency of the E_{33l}^{2p}

exciton (2·153 eV in figure 12). The obtained β values are quite comparable to those already measured in bulk GaAs (Nathan, Guenter and Mitra 1985). In addition, the observed increase of the TPA coefficient by a factor of two in the spetral range of the E_{33h}^{2p} and E_{33l}^{2p} excitons is consistent with the TPA photoconductivity and TPA photoluminescence excitation experiments of Nithisoontorn et al. (1989) and Catalano et al. (1989a, b), respectively, performed on GaAs quantum wells and with the theoretical predictions of Spector (1987).

4. Radiative recombination of excitons in the low density regime

In this section we discuss the optical properties of excitons in semiconductor quantum wells under weak optical excitation conditions. In the schemes of figures 1 and 2 this corresponds to the regime of low density of elementary excitations, directly produced by resonant excitation (arrow 2) or by photogeneration of free electron–hole pairs in the absorption continuum (arrow 3). In recent years, an impressive amount of work has been devoted to the study of the effects of wavefunction confinement and energy quantization on the electronic properties of low dimensional semiconducting systems, and the fundamental optical properties of excitons in quantum wells and superlattices are now well understood. Most of the results on the linear and non-linear optical properties of confined excitons are summarized in several comprehensive review papers and books treating the topic from both the theoretical and experimental aspect (see, for example, Dingle 1975, Miller and Kleinman 1985, Weisbuch and Nagle 1987, Bastard 1988, Schmitt-Rink et al. 1989). We therefore restrict ourselves to a brief survey of some selected recent experimental and theoretical results on the excitonic properties of quantum wells. In section 4.1 we discuss the radiative recombination processes of free-excitons and how to extract the fundamental free exciton parameters from the analysis of the optical spectra. We then consider exciton states localized around two-dimensional potential perturbations in the proximity of the quantum well interfaces. An extensive treatment of the linear and non-linear optical properties of excitons in quantum wells is beyond the scope of this section. Instead, we discuss a few crucial experimental results to evidence the main physical properties of the dilute exciton gas in two-dimensional semiconductors. For more extensive discussions on these topics the reader is referred to the recent review paper of Schmitt-Rink et al. (1989). In addition, we will not enter in details of different material systems, like the II–VI semiconductor heterostructures, or the many interesting optical experiments performed in magnetic fields. For the latter topics we refer to the general review papers by Maan (1987 and references therein) and Vina (1989 and references therein).

4.1. *Optical spectroscopy of the electronic and excitonic states in quantum wells*

Optical spectroscopy is a fundamental tool to study the linear and non-linear properties of excitons confined in potential wells. We discuss some important properties of the ground state excitons in quantum wells, studied by luminescence, and the higher energy states studied by absorption and photoluminescence excitation measurements. Photoluminescence (PL) and photoluminescence excitation (PLE) are the fundamental experimental tools for the investigation of excitonic radiative recombination processes in quantum wells. In the low density regime (left-hand column of figures 1 and 2) excitons can be considered as non-interacting elementary excitations which couple to the external radiation field (photons), thus providing important information on the ground-state of the crystal. The combination of PL and PLE gives a reliable description of the energy states in the quantum wells, thus allowing important

parameters to be found such as the potential discontinuity at the interface and the exciton binding energy.

As discussed in the previous section, one of the most interesting characteristics of semiconducting quantum wells is the persistence of the excitonic states up to room temperature. Clear observation of room temperature excitons have been reported in the luminescence spectra of a GaAs *single* quantum well (Fujiwara, Tsukada and Nakayama 1988), of GaSb/AlGaSb (Miyazawa, Tarucha, Ohmori, Suzuki and Okamoto 1986) and InGaAs/InAlAs (Chemla and Miller 1985) multiple quantum wells, and in the photocurrent spectra of strained InGaAs/GaAs multiple quantum wells (Gershoni, Temkin, Panish and Hamm 1989). These results have stimulated a great technological interest in view of the fabrication of electro-optic devices based on room temperature exciton non-linearities (Chemla and Miller 1985, Schmitt-Rink *et al.* 1985a b, Peyghambarian and Gibbs 1985). Typitcal high and low temperature photoluminescence spectra of GaAs/AlGaAs multiple quantum wells of different well widths are shown in figure 13. The exciton luminescence is still rather sharp even at room temperature and shows the expected red shift with increasing well width and temperature. The excitonic origin of this luminescence in the wide temperature range investigated is confirmed by the coincidence of the luminescence peaks with the excitonic resonances in the reflectance spectra (Cingolani, Chen and Ploog 1988). The effect of the intersub-band transitions becomes dominant at higher temperatures. The emission line shape changes dramatically due to thermal population of higher energy sub-bands, and broad emission bands evolve in the high energy tail of the spectra (figure 14).
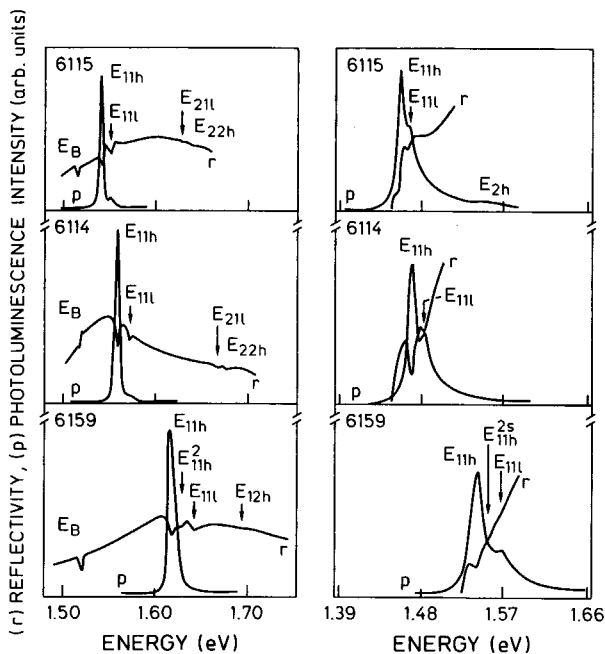

Figure 13.   Photoluminescence (PL) and reflectance (R) spectra of three GaAs/Al$_x$Ga$_{1-x}$As multiple quantum well heterostructures at 10 K (left) and 300 K (right). The sample parameters are the following: $x=0.36$, $L_z=10$ nm and $L_b=11$ nm for sample 6114, $x=0.32$, $L_z=12$ nm and $L_b=13$ nm for sample 6115, and $x=0.36$, $L_z=4.7$ nm and $L_b=5.7$ nm for sample 6159.
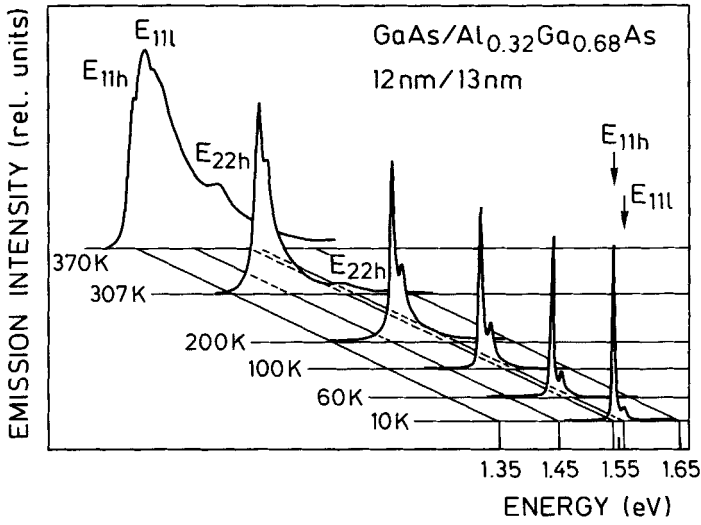
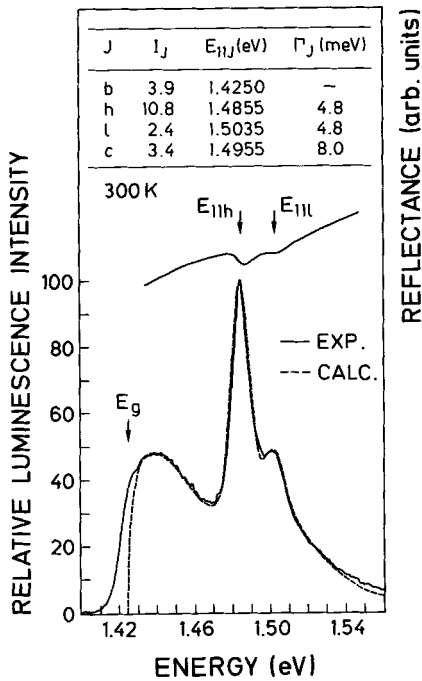Figure 14. Temperature dependence of the luminescence taken from sample 6115 of figure 13.

Figure 15. Experimental (continuous line) and calculated (dashed line) room temperature luminescence spectra of a 9 nm wide $GaAs/Al_{0.3}Ga_{0.7}As$ multiple quantum well heterostructure (see text for explanations).

Information on the fundamental $n = 1$ exciton state can be obtained by means of a statistical line-shape fitting of the luminescence spectra (Chemla and Miller 1985, Chen, Cingolani, Andreani, Bassani and Massies 1988). In figure 15 we show the measured and calculated line shape of the room temperature luminescence of a 9 nm GaAs/Al$_{0.3}$Ga$_{0.7}$As multiple quantum well. At room temperature both the heavy and the light-hole exciton states are thermally populated, thus allowing the observation of two excitonic peaks. The exciton character of the recombination is established by considering the reflectance spectrum in which the excitonic resonances, although broadened, still persist at 300 K. In addition, a broad emission band around 1·44 eV is observed due to the underlying GaAs buffer layer. The experimental spectrum $I(\hbar\omega)$ is fitted taking into account four different contributions:

$$I(\hbar\omega) = I_1(\hbar\omega) + I_2(\hbar\omega) + I_3(\hbar\omega) + I_4(\hbar\omega), \tag{4.1}$$

where

$$I_1(\hbar\omega) = I_b\omega^2 \exp\left(-\frac{\hbar\omega - E_g}{kT}\right)(\hbar\omega - E_g)^{1/2}, \tag{4.2}$$

is the contribution of the band to band recombination from the bulk GaAs

$$I_2(\hbar\omega) = I_h\omega^2 \exp\left(-\frac{\hbar\omega - E_{11h}}{kT}\right)\exp\left(-\frac{\hbar\omega - E_{11h}}{\Gamma_h^2}\right), \tag{4.3a}$$

and

$$I_3(\hbar\omega) = I_l\omega^2 \exp\left(-\frac{\hbar\omega - E_{11l}}{kT}\right)\exp\left(-\frac{\hbar\omega - E_{11l}}{\Gamma_l^2}\right), \tag{4.3b}$$

are the emissions of the fundamental heavy- and light-hole excitons expressed at room temperature by two Gaussians (see, for example, Bebbs and Williams 1972) multiplied by the corresponding distribution functions. The last term

$$I_4(\hbar\omega) = I_c\omega^2 \exp\left(-\frac{\hbar\omega - E_c}{kT}\right) \cdot \frac{1}{1 + \exp\left(-\frac{\hbar\omega - E_c}{\Gamma_c}\right)} \cdot \frac{2}{1 + \exp\left(-2\pi\left(\frac{E_b}{|\hbar\omega - E_g|}\right)\right)^{1/2}}, \tag{4.4}$$

represents the convolution of the two-dimensional step-like density of states with the two-dimensional Sommerfeld factor, which accounts for the Coulomb interaction of the electrons and holes in the continuum (Shinada and Sugano 1966, Chemla and Miller 1985). The symbols I_j, E_j and Γ_j in equations (4.1)–(4.4) indicate the intensity parameters, the eigenstate energies and the broadening factors, respectively, and are assumed as free parameters in the calculations. The sub-indexes b, h, l and c relate the above quantities to the contributions of the bulk, heavy-hole, light-hole and 2D continuum emission, respectively. As shown in figure 15, this simple statistical model well accounts for the measured luminescence spectrum, with the best fit parameters reported in the figure. We deduce an exciton binding energy of 10 meV for a 9 nm GaAs well from these data, in good agreement with the theoretical expectations (see figure 4).

Information on higher energy states can hardly be obtained from photo-luminescence measurements since this technique only probes the lowest energy state of the crystal. For such investigations absorption or photoluminescence excitation measurements are more powerful. In particular PLE spectroscopy is most suitable for

studying the absorption processes in heterostructures grown on non-transparent substrates. In this case the absorption under resonant excitation of different electronic states is probed through the relaxation into the fundamental $n = 1$ heavy-hole exciton. Typical examples of PLE and absorption spectra of GaAs/Al_xGa_{1-x}As, $Ga_{0.47}In_{0.53}$As/$Al_{0.48}In_{0.52}$As and GaSb/AlSb and $Al_{0.37}Ga_{0.63}$As/AlAs multiple quantum wells are shown in figures 16 and 17. In all these spectra sharp exciton peaks associated with different sub-band levels can be clearly resolved. We emphasize that, unlike the case of bulk materials, the PLE spectra of quantum wells give almost identical results as the absorption spectra, indicating that in semiconductor QW the quantum efficiency of the radiative processes is almost constant over a large energy range and approaches the value of unity (Weisbuch 1987). The attribution of the fundamental excitonic transitions in the spectra of figures 16 and 17 is made by calculating the confinement energies of the conduction and valence sub-bands as explained in section 1.

The observation of distinct excitonic absorption peaks in the optical spectra of semiconductor quantum wells has been used to determine the band gap discontinuity at the interface (Miller, Gossard and Kleinman 1985b, Menendez, Pinkzuk, Werder, Gossard and English 1986, Cohen and Fang 1989). The energies of optical transitions involving higher energy sub-bands are in fact much more sensitive to the conduction-to-valence band offset ratio than the fundamental $n = 1$ transition. The experimental
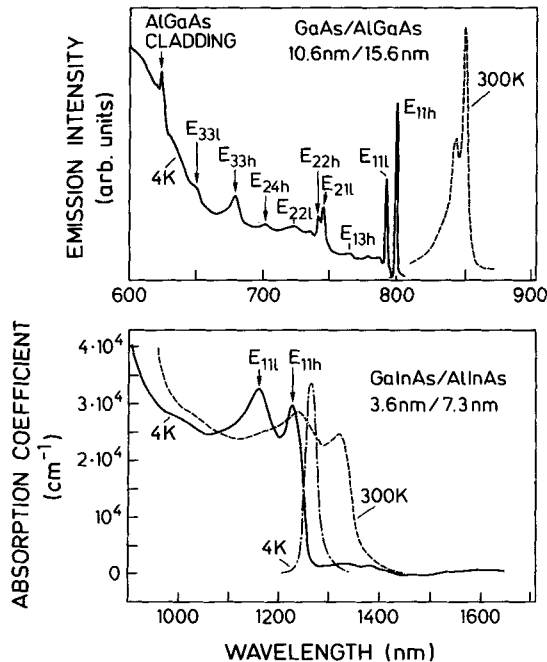

Figure 16. Upper curve: photoluminescence excitation spectra (PLE) of a GaAs/$Al_{0.36}Ga_{0.64}$As multiple quantum well grown on a 1 µm thick $Al_{0.36}Ga_{0.64}$As cladding layer taken at 4 K. The dashed curve is the room temperature luminescence. The low temperature luminescence coincides with the E_{11h} peak in the PLE spectrum (i.e. no Stokes shift). Lower curve: absorption spectra of a $Ga_{0.47}In_{0.53}$As/$Al_{0.48}Al_{0.52}$As multiple quantum well structure taken at different temperatures. The Stokes shift between the low temperature absorption and luminescence (dash-dotted line) amounts to less than 6 meV at 4 K.
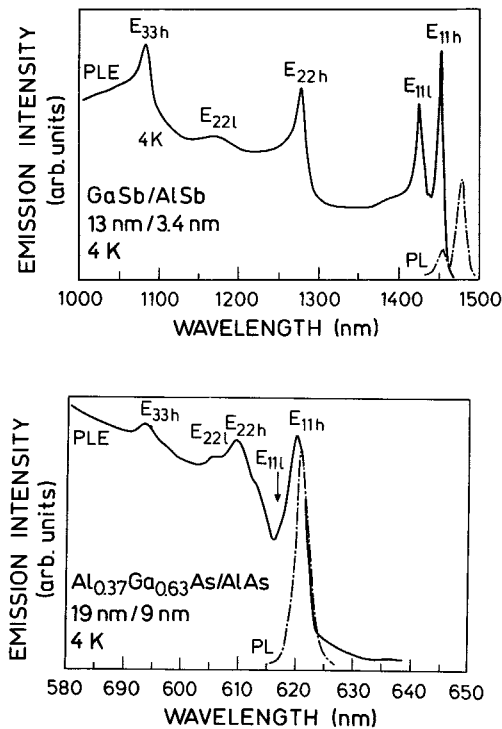
Figure 17. As in figure 15 but for GaSb/AlSb and $Al_{0.37}Ga_{0.63}As$/AlAs multiple quantum well heterostructures. The low temperature GaSb/AlSb luminescence (dash-dotted line) exhibits a slightly Stokes shifted exciton peak and a stronger impurity related emission around 1475 nm. The luminescence from the ternary $Ga_xAl_{1-x}As$ alloy quantum wells is Stokes-shifted by about 6 meV and has a bandwidth of about 9 meV, due to the alloy broadening effects on the optical spectra.

data can therefore be fitted to the theoretically predicted transition energies, within the envelope function approximation, as a function of the offset value. This has given the now commonly accepted conduction-to-valence band offset ratio values between 60:40 and 70:30, which are routinely used to fit the optical spectra of different III–V heterostructures. The small spread in these values depends on the degree of accuracy of the experimental method and on the possible uncertainty of the effective mass parameters of the bulk crystals (Rössler 1988).

There are other important properties of confined excitons which can be deduced from the photoluminescence excitation spectra. Laurelle and Etienne (1988) and Koteles, Owens, Bertolet and Lau (1988) have studied the saturation of the light-hole and heavy-hole exciton splitting in the PLE spectra of GaAs quantum wells with $L_z < 3$ nm. Their results have been interpreted in terms of the increased penetration of the hole wave function in the barrier as the well width is reduced. PLE experiments have been used to study the miniband dispersion in $Ga_xIn_{1-x}As$/GaAs strained layer superlattices (Moore *et al.* 1990) and to evidence excitonic effects associated to saddle points of the density of states dispersion in GaAs/AlAs multiple quantum wells (Song, Jung, Yoon, Chu, Chang and Tu 1989) and to the split-off band transitions in GaAs/AlGaAs superlattices (Duggan, Ralph, Dawson, Moore, Foxon, Nicholas, Singleton and Rogers 1987b). It is important to note that the increase of the exciton

oscillator strength with decreasing well width has been demonstrated experimentally by measuring the integrated area of the exciton absorption spectrum as a function of L_z in GaAs quantum wells (Masumoto, Matsuura, Tarucha and Okamoto 1985). In addition Feldmann et al. (1987) elucidated the fundamental relation between radiative lifetime and spectral linewidth of quantum well excitons by temperature dependent time-resolved spectroscopy. More recently the contribution of the localized and bound exciton states to this free exciton time dynamics has been questioned by Colocci, Gurioli, Vinattieri, Fermi, Deparis, Massies and Neu (1990b), who have shown that the intrinsic radiative recombination of free-excitons is strongly affected by other extrinsic recombination mechanisms in the wide temperature range investigated (5–300 K).

An important parameter concerning the effect of spatial confinement on quantum well excitons is the free-exciton binding energy. Despite the large number of theoretical studies on this subject (see section 2) there are only few experimental investigations of the well width dependence of the exciton binding energy. A reliable value of E_b can be deduced from the 2s–1s splitting of the fundamental $n = 1$ heavy- and light-hole excitons measured in PLE experiments. Assuming a simple hydrogenic series for the excited states of the 2D exciton (Shinada and Sugano 1966) the 2s exciton state is almost coincident with the sub-band edge. Therefore the 2s–1s splitting gives the exciton binding energy with an accuracy better than 1 meV. This method has been used by Miller, Kleinman, Tsang and Gossard (1981), Dawson, Moore, Duggan, Ralph, and Foxon (1986b) and more recently by Koteles and Chi (1988) for high quality GaAs/Al$_x$Ga$_{1-x}$As multiple quantum wells and by Moore, Duggan, Woodbridge and Roberts (1990b) for strained Ga$_x$In$_{1-x}$As/GaAs heterostructures. Magnetolumines- cence spectroscopy has also been used to measure the exciton binding energy. In this case the E_b value is deduced from the non-linear extrapolation at zero magnetic field of the spectral position of the magnetoluminescence of the excited exciton states. Measurements have been reported for several materials, including GaAs/Al$_x$Ga$_{1-x}$As (Maan, Belle, Fasolino, Altarelli and Ploog 1984, Tarucha, Okamoto, Iwasa and Miura 1984, Ossau, Jakel Bangert, Landwehr and Weimann 1986, Rogers, Singleton, Nicholas, Foxon and Woodbridge 1986, Petrou, Waytena, Liu, Ralston and Wicks 1986), Al$_x$Ga$_{1-x}$As/AlAs (Tarucha, Iwamura, Saku, Okamoto, Iwasa and Miura 1986), Ga$_{0.48}$In$_{0.52}$As/Al$_{0.47}$In$_{0.53}$As (Stolz, Maan, Altarelli, Tapfer and Ploog 1987) multi- ple quantum wells and strained Ga$_x$In$_{1-x}$As/GaAs heterostructures (Hou, Segawa, Aoyagi, Namba and Zhou 1990). A survey of the experimentally determined exciton binding energies is given in figure 18 for GaAs/Al$_x$Ga$_{1-x}$As quantum wells with well widths ranging between 3·8 and 21·8 nm. Unlike the earlier data, a general agreement is now observed for the most recent results, independent of the experimental method, indicating the achievement of a good standard quality of the investigated samples in recent years. The experimental values compare favourably with the results of recent theoretical calculations discussed before. It is worth noting that the Ga$_x$In$_{1-x}$As/Al$_x$In$_{1-x}$As quantum wells exhibit E_b values about 20% smaller than those of the GaAs material system (Stolz et al. 1987), reflecting the intrinsically weaker exciton binding energy in the bulk ternary alloy Ga$_x$In$_{1-x}$As.

Another interesting example for the application of optical spectroscopy to the fundamental study of the electronic and excitonic states in quantum wells concerns the determination of the type I–type II cross-over in (GaAs)$_m$/(AlAs)$_n$ ultra-short-period superlattices (USPS, where m and n indicate the number of monolayers [lattice planes] constituting the well and barrier slabs) performed by means of PLE spectroscopy. The electronic properties of the type II heterostructures have been the subject of
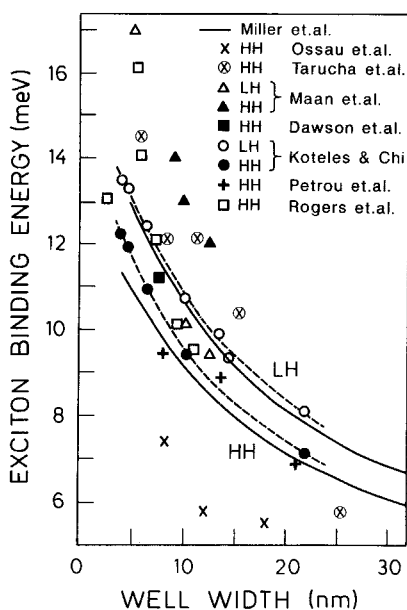
Figure 18.   Exciton binding energies in GaAs/Al$_x$Ga$_{1-x}$As quantum wells versus the well width. The symbols represent a collection of recent experimental data from different groups (see text). The solid lines are the theoretically calculated curves for heavy- and light-hole excitons. The dashed lines are the empirical fits to the data (after Koteles and Chi 1988).

tremendous research efforts in the last years. A more comprehensive survey on the optical investigation of these superlattices can be found in several recently published review articles (Wilson 1988, Cingolani, Ploog, Scamarcio and Tapfer 1990, Dawson 1990). Here we briefly discuss the specific influence of the staggered band alignment on the optical properties of type II USPS. In figure 19 we schematically show the real space energy band alignment of a type II superlattice. Due to the indirect nature of the AlAs barrier and the strong confinement energy in the ultra-thin GaAs well, the X-point of the AlAs barrier can lie at lower energy than the GaAs Γ-point. As a consequence, electrons at the AlAs X-point are confined in the barrier by the higher energy Γ-point of the GaAs layer. This results in a staggered band alignment in which the lowest conduction band state of the superlattice is located in the AlAs barrier and has the symmetry properties of the AlAs X-point, while the top of the valence band is still located at the GaAs Γ-point. The effects of these peculiar electronic properties on the emission and absorption processes of the USPS are shown on the right-hand side of figure 19. The luminescence arises from the lowest energy levels of the superlattice, i.e. from the X–Γ or type II transition, while the absorption has a considerable strength only above the direct type I (Γ–Γ) edge. Therefore, the comparison of PL and PLE provides complementary information on the type I and type II gaps in the USPS. Furthermore, we note that the type II transitions are indirect in real space, while their direct or indirect character in k-space is determined by the folding of the X-states onto the Γ-state, i.e. ultimately on the symmetry properties of the superlattice minizone (Lu and Sham 1989). According to equation (2.7), the transition matrix element for type II processes depends on the overlap integral of the electron wavefunctions at the AlAs X-point and the hole wavefunctions at the GaAs Γ-point. The calculated overlap integral
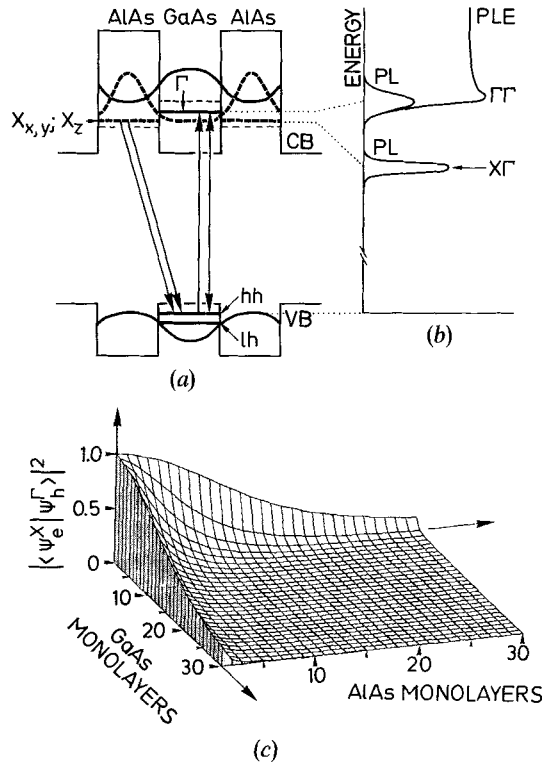
Figure 19. (a) Schematic illustration of a real space energy band diagram of a type II
GaAs/AlAs short-period superlattice and (b) impact of the staggered band alignment on
the optical properties of the superlattice. The continuous lines in (a) indicate the Γ-
symmetry states while the dashed lines refer to X-symmetry states. The bold lines indicate
the confined electronic states in the GaAs well (type I) and in the AlAs barrier (type II) and
the respective wavefunctions. The absorption onset in the photoluminescence excitation
spectrum (PLE in the right-hand side graph) is blue-shifted to the type I Γ–Γ transition,
while the luminescence appears at the lowest type II gap (Γ–X). In the plot (c) we indicate
the overlap of the electron wavefunctions confined to the AlAs layer and the hole
wavefunctions confined to the GaAs layer as a function of the number of monolayers
constituting the superlattice slabs.

$\langle \chi_e^{AlAs} | \chi_h^{GaAs} \rangle$ assuming superlattice wavefunctions in the Kronig–Penney approxi-
mation (Cho and Prucnal 1987) is depicted in the bottom diagram of figure 19 versus
the well and the barrier width. The efficiency of the real space indirect emission is
therefore strongly affected by the superlattice configuration and drops when increasing
the layer thickness. Conversely, the direct luminescence, though conserving the usual
high transition probability, is not easily observable because of the presence of the low
lying type II gap. Thermal band filling through high carrier injection rates must be used
in order to populate the electron Γ states and to observe both type I and the type II
radiative recombinations (to be discussed in section 5.2).

Typical PL and PLE spectra measured in a set of symmetric (i.e. $m = n$)
$(GaAs)_m/(AlAs)_n$ USPS with an increasing number of monolayers are shown in figure
20. When the well width is increased, the confinement energies of the GaAs Γ-states and
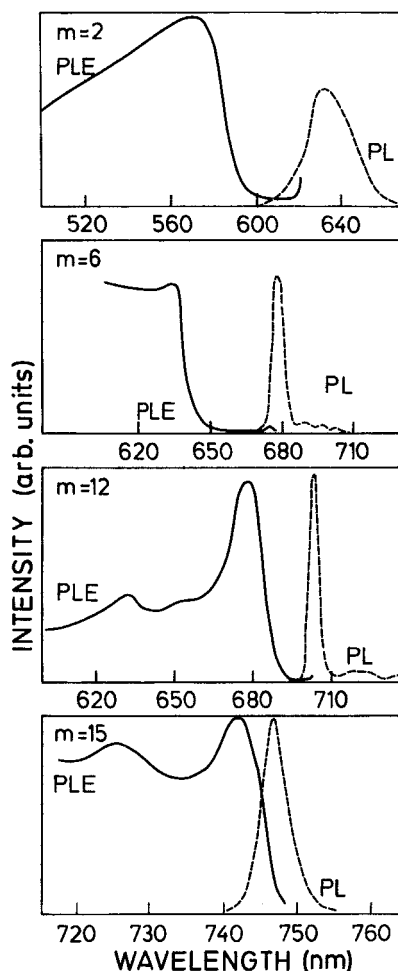AlAs X-states reduces and both the PLE and PL spectra shift to the red. However, due

Figure 20. Low temperature photoluminescence excitation (PLE) and photoluminescence (PL) in a set of symmetric short-period $(GaAs)_m/(AlAs)_m$ superlattices with increasing m.

to the larger electron mass at the AlAs X-point, the red shift of the PLE spectra is more pronounced. As a consequence, the PL peak (type II gap) and the PLE onset (type I gap) approach each other in energy when increasing the number of monolayers, and finally merge for $(m=n)>12$ monolayers. Above this critical thickness the $(GaAs)_m/(AlAs)_n$ USPS recover the direct character and the energy splitting between PL and PLE reduces to the usual Stokes shift. The thickness-induced type II–type I cross-over has been determined in this way for different USPS configurations by several groups (see, for example, Danan, Etienne, Mollot, Planel, Jean-Louis, Alexandre, Jusserand, Le Roux, Marzin, Savary and Sarmage 1987, Moore, Duggan, Raukema and Woodbridge 1988). Additional information on this size-induced change of the band alignment come from luminescence measurements in electric fields (Meynadier, Nahory, Worlock, Tamargo, de Miguel and Sturge 1988), under hydrostatic pressure (Li, Jiang, Han, Wang and Ploog, 1989, Holtz, Cingolani, Reimann, Muralidharan, Syassen and Ploog 1989) and by photoacoustic and high
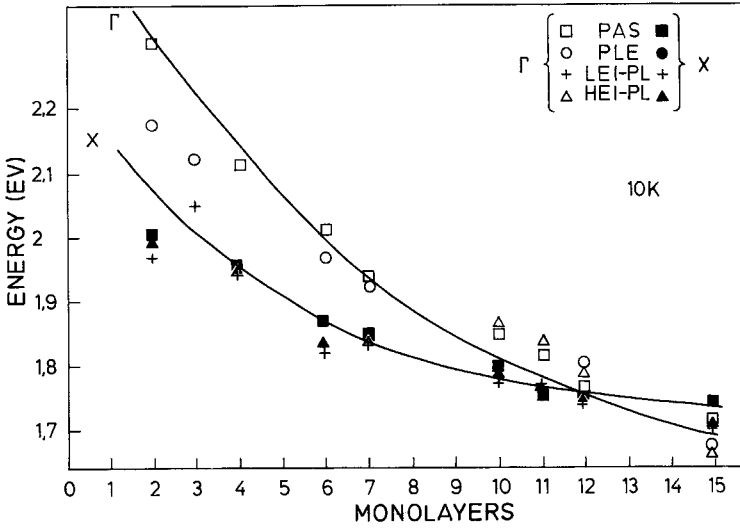
Figure 21.   Experimental (symbols) and theoretical (continuous lines) size induced type I–type
II cross-over in symmetric short-period $(GaAs)_m/(AlAs)_n$ superlattices versus the number
of monolayers, m. The type I (Γ curve) and type II (X curve) transitions have been
calculated assuming a Kronig–Penney potential for the superlattice. The symbols
represent the results of photoacoustic spectroscopy measurements (PAS), photolumines-
cence excitation (PLE) and low- and high-excitation intensity luminescence measurements
(LEI–PL and HEI–PL, respectively).

excitation intensity spectroscopy (Cingolani et al. 1989). In figure 21, we show the
comparison of a collection of optical data obtained from a set of symmetric
$(GaAs)_m/(AlAs)_n$ USPS with the well width dependences of the type I and type II gaps
calculated in the frame of the envelope function approximation and assuming a
Kronig–Penney potential. As mentioned before, the type II–type I cross-over occurs
around 12 monolayers, in excellent agreement with recent theoretical calculations (Xia
and Chang 1990).

4.2. Excitonic properties in the presence of localizing potentials

In the previous section we have discussed the radiative recombination of free-
excitons confined in the potential well of semiconducting heterostructures. A few basic
approximations have been made in modelling the quantum well exciton: first, the
interfaces in the heterostructure were assumed to be perfectly abrupt and to extend over
large flat areas (this means that the quantum well thickness L_z is established with a
precision of less than one monolayer fluctuation of L_z). Second, the quantum well had
to be virtually infinite along the x and y directions. These assumptions should result in
delta-like exciton peaks in the absorption and luminescence spectra of semiconductor
quantum wells. However, in real quantum wells and superlattices the interfaces
between semiconductors are never perfectly abrupt, thus causing a homogeneous
broadening of the emission lines. The actual structure and morphology of the interfaces
strongly affect the line-shape of the excitonic transitions. The important physical
process related to the potential perturbations of the interface manifests itself in the
localization of excitons. In this section we discuss the exciton localization at interfaces
of a quantum wells induced by L_z fluctuations, with special attention to the radiative

transitions. The enhancement of the recombination rate due to carrier localization has been first described for $GaAs/Al_xGa_{1-x}As$ quantum wells by Göbel, Jung, Kuhl and Ploog (1983) who measured a reduction in the carrier lifetime with decreasing well widths.

In recent years there has been a growing interest in investigating the relations between the microscopic interface structure and the optical properties of quantum wells. This topic has two distinct aspects: first, to refine optical techniques to reliably characterize semiconductor quantum wells, and second, to study the quantum mechanical aspects of exciton localization in semiconductors. Tapfer *et al.* (1989) have evidenced the important correlation between the structural configuration of the interface and the optical properties of excitons in quantum wells. In their experiment the interfaces of a $Ga_xIn_{1-x}As/Al_yIn_{1-y}As$ multiple quantum wells were intentionally perturbed by inserting an InAs plane during growth. This causes large fluctuations of the constituent materials at the interface, as clearly shown by the broad superlattice satellite peaks appearing in the high-resolution X-ray diffraction spectrum of this sample shown in figure 22. The identical sample grown under optimized growth conditions and without insertion of the InAs planes at the interfaces exhibits a very sharp X-ray spectrum showing the distinct diffraction peaks of well-resolved interfaces. In this case the interface region is constrained to the one monolayer transition region usually expected for the best ternary–ternary alloy interfaces. The impact of these
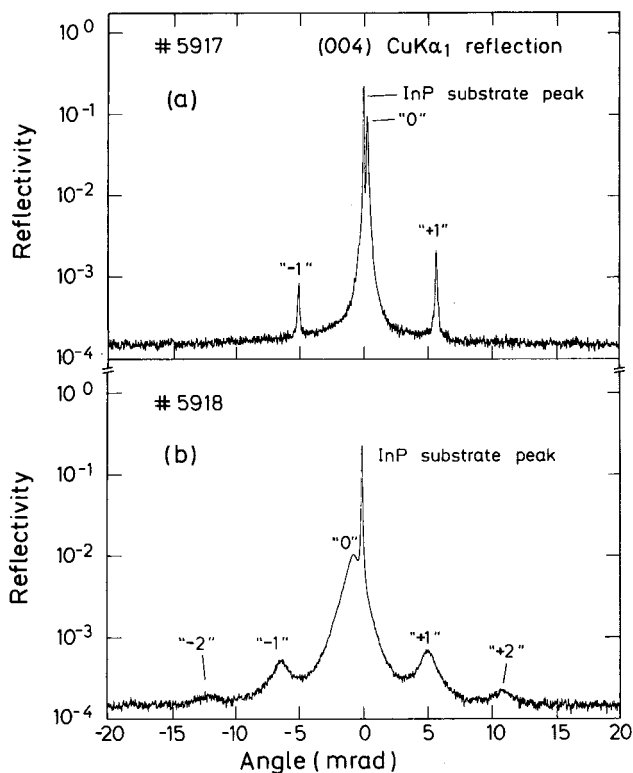

Figure 22.   High-resolution double-crystal X-ray diffraction spectra taken from a high quality $Ga_xIn_{1-x}As/Al_yIn_{1-y}As$ multiple quantum well sample lattice matched to InP (*a*) and from the same heterostructure grown with intentionally degraded interfaces (*b*).
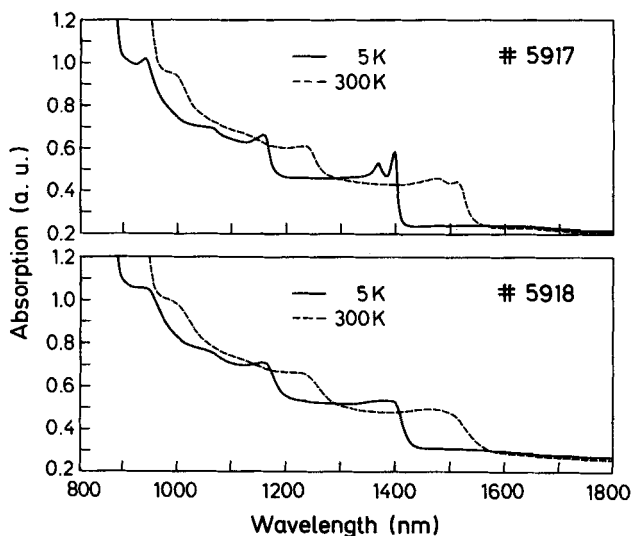
Figure 23.   Absorption spectra taken at 5 K and 300 K, from the two heterostructures of figure 22.

tailored interfaces on the optical absorption spectra of the quantum well is shown in figure 23. The nominally perfect sample exhibits sharp excitonic absorption peaks up to room temperature, while the intentionally perturbed sample clearly shows a degradation of the optical properties.

The microscopic structure of the interfaces is therefore extremely important in determining the optical properties of excitons in quantum wells. This phenomenon has been intensively studied by different groups (Goldstein, Horikoshi, Tarucha and Okamoto 1983, Deveaud, Emery, Chomette, Lambert and Baudet 1984, Miller, Tu, Sputz and Kopf 1986, Bimberg, Mars, Miller, Bauer and Oertel 1986, Sauer, Harris and Tsang 1987, Fuijwara *et al.* 1989a, b, Kohl, Heitmann, Tarucha, Leo and Ploog 1989, Zhou, Jiang, Bannwart, Solin and Bai 1989). The major effects of the interface structure on the excitonic luminescence established by these authors are schematically depicted in figure 24. Samples prepared without growth interruption during epitaxial growth (left-hand side) exhibit intermixed interfaces over a few monolayers producing a statistical compositional disorder around the interface region. This results in a well width fluctuation ΔL_z and hence in a broadening of the eigenenergy of the confined state given by $\Delta E \simeq \Delta L_z (h^2 \pi^2 / m L_z^3)$ (Bimberg *et al.* 1986). The resulting luminescence is a broad line centred around the energy of the exciton corresponding to the nominal L_z and with a linewidth proportional to the spread of the continuous distribution of well widths around L_z. When growth is interrupted for several tens of seconds at the interface, the chemisorbed atoms have time to diffuse along the x–y plane before the next monolayer is deposited. In this case a more ordered interface region is obtained consisting of large islands of one-monolayer height and extending over several tens of μm along the x–y plane (right-hand side of figure 24). Therefore a discrete set of quantum wells of widths L_z ($L_z + 1$ monolayer) and ($L_z - 1$ monolayer) is obtained. Localization of excitons can be very efficient in these one-monolayer height islands, provided their extension is larger than the exciton Bohr radius along the x–y plane. In this case distinct luminescence peaks originate from excitons localized in the different
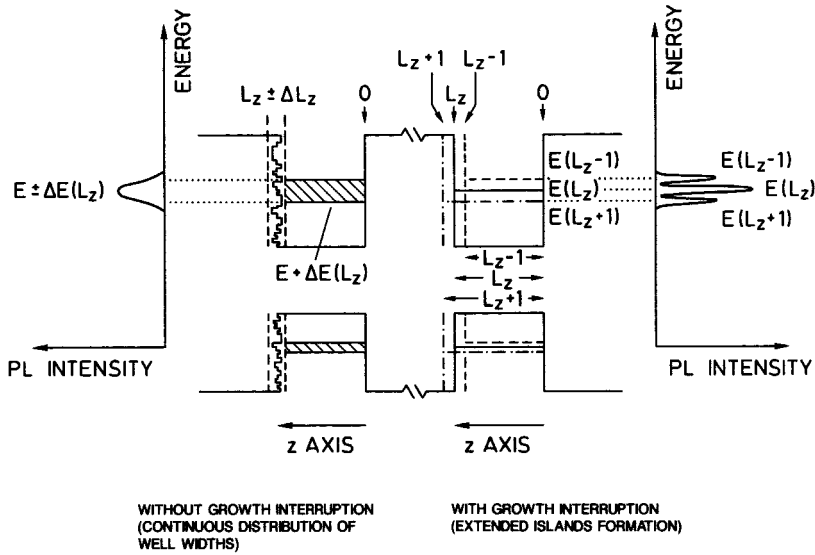
Figure 24. Effect of the interface quality on the excitonic luminescence of quantum wells. Heterostructures grown with growth interruption (right-hand side) exhibit rather sharp interfaces with extended monolayer height islands forming distinct quantum wells of size $(L_z \pm 1$ monolayer). This results in a set of sharp luminescence lines corresponding to the different quantization energies in the different well regions. Conversely, heterostructures grown without growth interruption exhibit a continuous distribution of well-widths ΔL_z around the nominal L_z value, resulting in a broadened luminescence spectrum.

islands. The energy position of these lines reflects the increase $(L_z - 1$ monolayer) or the decrease $(L_z + 1$ monolayer) of the confinement energy with respect to the main exciton line (corresponding to the nominal well width L_z). Typical luminescence and photoluminescence excitation spectra from excitons localized at the one-monolayer height extended islands in GaAs quantum wells are shown in figure 25. The exciton corresponding to the nominal L_z well width clearly dominates the PLE spectra independent of the detection wavelength, owing to the large density of states. Conversely, absorption due to excitons localized at the $(L_z + 1$ monolayer) well can be selectively observed by adjusting the detection wavelength at the peak of the corresponding luminescence line. In this case a weak shoulder can be observed in the PLE spectrum, indicating the small density of states of these localized particles.

In addition to the importance of the localization mechanisms for the optical characterization and the investigation of the quantum well interface structures in different material systems, these phenomena provide a unique possibility to study the dynamics of localized excitons and their time and temperature dependence. Recently Fuijwara, Kanamoto and Tsukada (1989b) and Kohl *et al.* (1989) demonstrated that the exciton population of the $(L_z \pm 1)$ quantum wells strongly depends on the temperature and the excitation intensity. At low temperature, the wider well $(L_z + 1)$ is more populated, resulting in a high intensity of the lowest energy emission. With increasing temperature (or excitation intensity) band filling effects become dominant and higher energy states [from the $(L_z - 1)$ well] are populated. The relaxation into different quantum wells also depends on resonant or non-resonant excitation conditions (Kohl *et al.* 1989). The luminescence from different well width regions is only
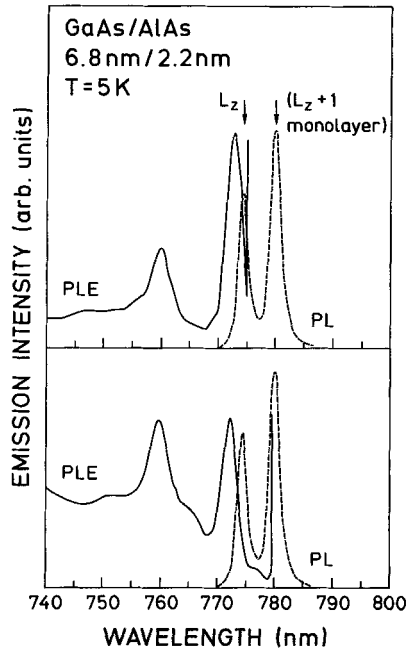
Figure 25.   Photoluminescence (PL—dashed line) and photoluminescence excitation spectra (PLE—continuous line) of a GaAs/AlAs superlattice with extended monolayer height islands. In the upper spectra the PLE is measured fixing the detection wavelength at the nominal well-width exciton line (L_z). In the lower panel, the PLE is measured setting the detection wavelength at the wavelength of the luminescence arising from the exciton localized in the ($L_z + 1$ monolayer) well. In this case a weaker absorption is observed, due to the low density of localized states.

really proportional to the extension of the extended island along the x–y plane under suitable excitation conditions. Fujiawara *et al.* (1989b) demonstrated that the ($L_z - 1$) well occupies about 30% of total available area on the x–y plane while about 14% is occupied by the wider ($L_z + 1$) well, by studying the temperature dependence of the luminescence of excitons in GaAs/$Al_x Ga_{1-x}$As quantum wells localized in one-monolayer height islands. Similar investigations have been reported by Deveaud *et al.* (1987) who studied the exciton transfer between different extended islands by time resolved spectroscopy.

A striking evidence of the strong oscillator strength of two-dimensional localized excitons has recently been reported in sub-monolayer InAs/GaAs quantum wells (Cingolani, Brandt, Tapfer, Scamarcio, La Rocca and Ploog 1990b). The insertion of nominally one monolayer thick InAs quantum wells in a bulk GaAs matrix has been used to study the formation of excitons associated with the electronic states localized around the strained InAs planes. In figure 26 we compare the photoreflectance (PR), photoluminescence excitation (PLE) and luminescence (PL) spectra measured on a sample consisting of 10 InAs wells of 0·8 monolayer width separated by 10 monolayers of GaAs. The non-integer well width, accurately determined by X-ray diffraction, indicates that the InAs well consists of extended islands, whose average size along the x–y plane is of the order of 20 nm [measured by electron microscopy (Brandt, Tapfer, Cingolani, Ploog, Hohenstein and Phillips 1990)]. The optical spectra exhibit sharp
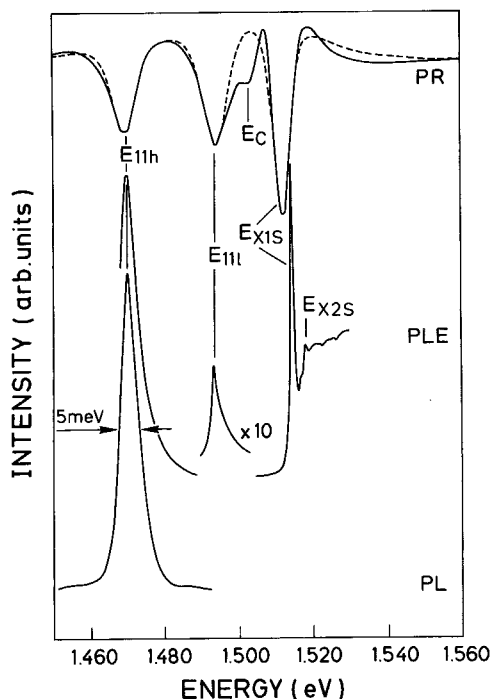
Figure 26.   Photoreflectance (PR), photoluminescence excitation (PLE) and photolumines-
cence (PL) taken at 4 K from a strained InAs/GaAs multiple quantum well structure with
about 3 Å wide InAs wells. The dashed line is the theoretically calculated two-dimensional
excitonic PR spectrum (the E_c feature not included in the fit originates from extrinsic
transitions). E_{11h} and E_{11l} indicate the heavy- and light-hole excitons localized at the InAs
layers, while the E_{x1s} and E_{x2s} peaks are related to the 1s and 2s states of the bulk GaAs
exciton, respectively.

excitonic features associated with the heavy-hole and light-hole exciton states in the
InAs well. The PR spectrum, fitted by the conventional 2D exciton line-shape model,
exhibits sharp resonances at the energy of the PLE and PL peaks.

These results raise the interesting question about the actual nature of the potential
responsible for the exciton formation in sub-monolayer InAs wells. The intuitive
picture of the particle in a box breaks down in the limit of ultra-narrow wells, in which
the interface region has an extension comparable to the quantum well itself. A more
realistic calculation has been performed similar to the case of localization of carriers in
an isoelectronic sheet of impurity in GaAs (Hajalmarson 1982). We have used a
simplified one-dimensional linear-chain model to describe a superlattice with N-1
GaAs sites and 1 InAs site. Despite the simplicity of our tight binding approach the
results are quite consistent with the experimental findings. In particular we find that the
InAs layer induces electron and hole levels in the GaAs gap, with a total localization
energy of about 53 meV. The carrier wavefunctions are localized within a few
monolayers around this spike perturbation, thus accounting for the observed strong
recombination efficiency. A strong confirmation of our conclusion comes from the very
recent self-consistent pseudopotential calculation of the electronic states in InAs/GaAs
quantum wells, performed by Shiraishi and Yamaguchi (1990). A very good qualitative
and quantitative agreement is found between our results and the results of the *ab initio*

calculations of these authors. It is interesting to note that Marzin and Gerard (1989) have successfully evidenced the spatial variation of the probability density of the electronic states in multiple quantum wells. The authors determined the energy of the bound states by optical spectroscopy as a function of the position of a highly localized perturbation potential given by an isoelectronic substituted impurity plane in GaAs/AlGaAs quantum wells. Another interesting evidence of exciton localization has recently been reported by Moore et al. (1990a, b) who observed a distinct splitting of the exciton peaks in the PL and PLE spectra of strained InGaAs/InAs multiple quantum wells. They demonstrated that this effect is due to a small degree of randomness in the potential periodicity which localizes holes within a few monolayers.

We conclude that the refinement of the epitaxial growth procedures down to the atomic monolayer regime not only provides a helpful tool to understand the relations between structural and optical properties of quantum wells and superlattices, but it also allows for the direct access to study localization phenomena around intentionally inserted short-range potential spikes.

5. Radiative recombination processes based on interacting excitonic states

In this section we discuss the spontaneous radiative decay of biexcitons and the radiative recombination of excitons and biexcitons induced by inelastic scattering between quasi-particles. These phenomena become important in dense exciton systems ($n \simeq 10^{10}$ cm^{-2}), in which the average distance between excitons is of the order of a few Bohr radii but still below the exciton screening threshold (central column of figures 1 and 2). Under these conditions van der Waals-like interactions between excitons form excitonic molecules or biexcitons. The process is somewhat similar to the formation of H_2 molecules from a dense gas of hydrogen atoms, which are similar to the exciton particle. The stability of the biexciton state depends on the masses of the constituent particles and on the polarizability of the crystal, and it is therefore not possible to predict a priori whether biexcitons can exist in a given semiconductor or not (Hanamura 1975, Ueta, Kanzaki, Kobayashi, Toyozawa and Hanamura 1986). However, in crystals where biexcitons can exist as stable particles a mixed phase of excitons and biexcitons can be established at suitable photogeneration rates and temperatures. This particular phase is studied in this section. We first survey the experimental and theoretical results concerning biexcitons in quantum wells. There are only limited experimental evidence of the existence of 2D biexcitons in GaAs quantum wells, owing to the very small binding energy of this quasi-particle in III–V semiconductors. The observation of biexciton states is more favourable in II–VI semiconductors, due to their larger binding energy. However, the difficulties with the fabrication of high quality II–VI semiconductor quantum wells has up to now also limited the number of investigations on biexcitons in this material systems. We then discuss the radiative recombination processes competing with the biexciton recombination, i.e. the radiative decay of excitons induced by inelastic scattering with free electrons or free excitons. Also for these phenomena, there are a very limited number of theoretical and experimental studies, mainly concerning the GaAs/Al$_x$Ga$_{1-x}$As material system.

5.1. Biexcitons in quantum wells

The first evidence of biexciton luminescence in GaAs/Al$_x$Ga$_{1-x}$As QW has been provided by Miller, Kleinman, Gossard and Montenau (1982). In recent years more distinct observations have been reported by Charbonneau, Steiner, Thewalt, Koteles,
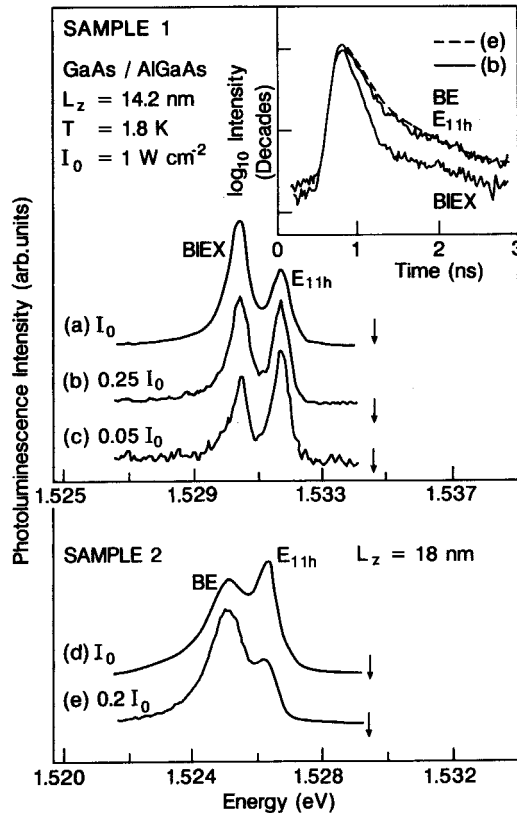
Figure 27. Exciton (E_{11h}), biexciton (BIEX) and bound exciton (BE) luminescence spectra obtained from different GaAs/Al$_x$Ga$_{1-x}$As multiple quantum well samples of different structural configurations at low temperature and at different excitation intensities ($I_0 = 1$ W cm^{-2}). Inset: temporal decay of the E_{11h}, BIEX and BE luminescence peaks of curves e and b (after Charbonneau *et al.* 1988).

Chi and Elman (1988), Cingolani, Chen and Ploog (1988b) and Reynolds, Bajaj, Stutz, Jones, Theis, Yu and Evans (1989). In all these experimental studies the characteristic biexciton luminescence appears as a more or less sharp peak (BIEX) in the low energy tail of the fundamental $n = 1$ heavy-hole exciton line (E_{11h}) as shown in figure 27. The spectral position of the biexciton luminescence is $\hbar\omega \simeq E_{11h} - E_b^{BIEX}$ (where E_b^{BIEX} is the biexciton binding energy), as deduced from the energy conservation of the radiative decay of biexcitons into a free exciton and an electron–hole pair. The observed biexciton emission grows superlinearly with the excitation intensity ($I_{PL} \simeq I_{Laser}^{1.4-1.7}$), it does not exhibit any polarization dependence and drops in intensity with increasing temperatures or by applying a magnetic field. The BIEX line arises about 1 meV below the E_{11h} line, i.e. at an energy position very close to the bound exciton line (BE) frequently detected in the luminescence spectra.

The observation of the biexciton luminescence gives rise to the important question about the stability of this quasi-particle in GaAs quantum wells. In GaAs crystals, for instance, the expected biexciton binding energy is of the order of 0·1 meV (Ueta *et al.* 1986), thus preventing the spectroscopic observation of biexciton luminescence. The experimental results of Miller *et al.* (1982), Charbonneau *et al.* (1988) and Reynolds

et al. (1989) demonstrated, however, that the splitting between the $n=1$ exciton luminescence and the BIEX emission depends on the well width and varies between 1·5 and 0·6 meV. This finding indicates that confinement effects in quantum wells cause a considerable enhancement of the biexciton binding energy (Miller *et al.* 1982). Strong support to this assumption comes from the variational calculations of Kleinmann (1983), who calculated the biexciton binding energy by using the six parameters wavefunction of Brinkmann *et al.* (1973) as a function of the well width. The results of the Kleinmann theory are shown in figure 28 and compared with a selection of recent experimental data from different authors. The measured biexciton binding energy deduced from the E_{11h}–BIEX splitting decreases with increasing well width and varies between 1·5 and 0·6 meV in the range $5\,\text{nm} < L_z < 30\,\text{nm}$. This result is in very good agreement with the theory despite the difficulty of clearly resolving the biexciton luminescence feature. In particular, the bound exciton luminescence occurs in the same energy region of the biexciton line, thus complicating the interpretation of the experimental data (see figure 27). In the early paper of Miller *et al.* (1982) a deviation from the trend of the decreasing biexciton binding energy was observed for $L_z > 20\,\text{nm}$ (open dots for $L_z > 20\,\text{nm}$ in figure 28). Recently Reynolds *et al.* (1989) made clear that this deviation was probably caused by the slightly larger splitting between the bound exciton and the free exciton luminescence, and they found a much better agreement between theory and experiments also in this well width range (black dots in figure 28).

The ambiguity in the interpretation of the biexciton luminescence can be removed by measuring the time decay of the biexciton luminescence. Charbonneau *et al.* (1988) found that the biexciton luminescence decays with a time constant a factor two shorter
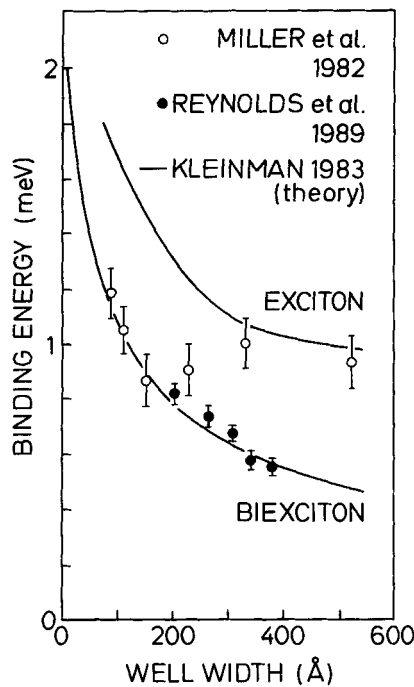

Figure 28.   Experimental (points) and theoretical (continuous line) biexciton and bound exciton binding energies in GaAs quantum wells versus the well width. The experimental points are collected from different works (after Reynolds *et al.* 1989).

than the exciton luminescence, while the bound exciton luminescence has the same decay rate as that of the free exciton (inset of figure 27). Similar results have also been obtained from $ZnSe/Zn_{0.77}Mn_{0.28}Se$ quantum wells (Fu, Lee, Mysyrowicz, Nurmikko, Ghunshor and Kolodziejsky 1988), where a sharp biexciton luminescence is observed in the low energy tail about 35 meV below the E_{11h} line. Also in this case the observed splitting between the two lines indicates a biexciton binding energy about one order of magnitude larger than in the corresponding bulk crystal.

An important aspect of the biexciton luminescence is the strong optical-non-linearity associated with this quasi-particle (for a review on the non-linear optical properties of biexcitons in bulk materials see, for example, Klingshirn and Haug 1981, Ueta *et al.* 1986 and Levy, Hönerlage and Grün 1988). The low transition probability for the spontaneous radiative decay of biexcitons reflects the low probability of direct biexciton formation by means of photogeneration experiments. However, giant oscillator strength processes can be stimulated by two-photon excitation resonant to the biexciton state (Golovin and Rashba 1973). Under this condition the transition probability for the biexciton recombination increases in bulk crystals by up to five orders of magnitude. In the inset of figure 29 we show the typical energy level scheme for a multi-step biexciton generation process. We consider two possible mechanisms: (i) the
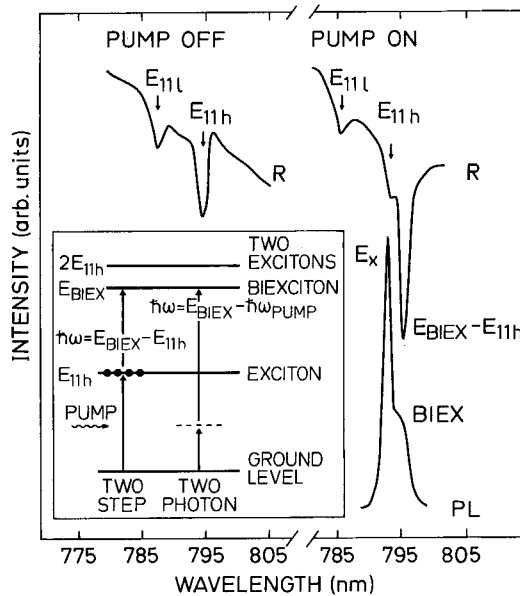

Figure 29. Optical conversion of exciton into biexciton measured in a 10 nm GaAs quantum well structure at low temperature by pump and probe reflectivity spectroscopy. The reflectance spectrum (left-hand side) exhibits the usual light- and heavy-hole exciton resonances. Switching on the pump (right-hand side spectra) a new resonance-like structure appears at the energy of the biexciton luminescence. The inset shows a scheme of the exciton–biexciton conversion induced by the absorption of two photons. The biexciton level (E_{BIEX}) can be reached either via an intermediate transition through a virtual intermediate state, indicated by the dashed line (two-photon process), or via the intermediate real transition from the real exciton state (E_{11h}) two step process). In the former process the energy of the second absorbed photon depends on the energy of the first photon ($\hbar\omega_{pump}$), while in the latter process it has the energy $\hbar\omega = E_{BIEX} - E_{11h}$, coincident with the spectral position of the new resonance in the reflectance spectrum.

biexciton is generated by two-photon absorption through a virtual intermediate state (analogous to the TPA process discussed in section 3); or (ii) the biexciton can be formed by two-photon absorption processes in which the exciton level plays the role of real intermediate state (two-step process in figure 29). In this case the first transition forms an exciton and the second transition resonantly produces the biexciton through the absorption of a photon of energy $\hbar\omega = E_{BIEX} - E_{11h}$. This process, also called optical conversion of excitons into biexcitons, is expected to have a larger transition probability (giant oscillator strength) since the intermediate transition involves a real state. The multiphoton formation of biexcitons has been widely documented for bulk II–VI semiconductors (Duy Pach, Bivas, Hönerlage and Grün 1977, Hönerlage, Levy, Grün, Klingshirn and Bohnert 1985, Nagasawa, Kuwata, Hanamura, Itho and Mysyrowicz 1989, Levy *et al.* 1988) by using two-beam experimental techniques in which a first source (pump) populates the real intermediate excitonic state and a second broad band source (probe) completes the optical conversion of excitons into biexcitons. The data of figure 29 show the evidence of optical conversion of excitons into biexcitons in GaAs quantum wells (Cingolani *et al.* 1988b). In this experiment the pump beam is provided by a cw Argon laser and the completion of the two-step process is monitored through the induced changes in the reflectivity spectrum of the broad band probe. When the pump is off, the reflectivity spectrum exhibits the expected heavy- and light-hole exciton resonances (E_{11h} and E_{11l}, respectively). When switching on the pump a new dip appears in the reflectivity spectrum about 1·5 meV below the E_{11h} resonance, indicating that photons of energy resonant to the transition $E_{BIEX} - E_{11h}$ have been absorbed to complete the two-step process for the biexciton formation. It is worth noting that the additional structure in the reflectivity spectrum appears together with the biexciton luminescence located about 1·5 meV below the E_{11h} line. The observed non-linear process supports the idea of an enhanced oscillator strength for the two-step biexciton formation in quantum confined systems, and confirms the order of magnitude increase of the biexciton binding energy in these systems.

5.2. *Radiative recombination processes induced by excitonic scattering processes*

Inelastic excitonic scattering phenomena are competing with the radiative recombination of biexcitons. In the dense exciton gas produced by external photogeneration a dynamical equilibrium is established between the rate of formation of stable particles (excitons and biexcitons) and the rate of dissociation of bound states due to collisional processes. The luminescence induced by these scattering processes has been widely studied in bulk II–VI semiconductors (Klingshirn and Haug 1981 and references therein). The large binding energy of excitons in these crystals strongly favours the direct observation of the luminescence induced by different collisional events. This is not the case for III–V semiconductors, where only a few experimental studies on the exciton–electron (Göbel, Shaklee and Epworth 1975) and exciton–exciton (Moriya and Kushida 1976) interactions have been performed for bulk-like GaAs. In quantum wells, the observation of these phenomena should be favoured by the enhanced exciton binding energy and hence by the larger stability of the exciton states. However, in contrast to this expectation, the radiative decay induced by inelastic scattering processes is strongly quenched in quantum wells by the extremely efficient electron–hole plasma recombination, which is easily established in high excitation intensity luminescence experiments. As for the case of biexciton luminescence, emission due to interacting excitonic states is hardly observed in conventional luminescence experiments.

Evidence for exciton–electron scattering was recently reported by Cingolani R., Ploog, Peter, Hahn, Göbel, Moro and Cingolani A. (1990c), who used spatially- and time-resolved luminescence measurements. In figure 30 we show the spatially resolved time-integrated luminescence spectra taken under picosecond excitation from a 10 nm wide GaAs multi-quantum well heterostructure. Strong changes are observed in the PL spectra taken at different distances d from the centre of the excited spot on the crystal surface (in these spectra the lateral spatial resolution of about 20 μm was obtained by scanning an enlarged image of the excited spot onto the 20 μm wide entrance slit of the monochromator). The integrated PL spectrum at $d = 0$ exhibits the characteristic $n = 1$ heavy-hole exciton peak (E_{11h}) and a weak shoulder arising by less than 2 meV at low energy (B band). When spatially resolving the luminescence far away from the spot centre we observe an overall decrease of the emission intensity and the rising of new emission bands on the low energy side of the E_{11h} line. In particular we detect the BB band 3·5 meV below the exciton line at intermediate displacements ($80 < d < 180$ μm) and an additional line (EE) arising 7·5 meV below the E_{11h} band for $d > 160$ μm. It is worth noting that both the BB and EE bands disappear when the excitation intensity is reduced, thus excluding the possibility that they might be due to extrinsic emissions. In addition, they can only be resolved under picosecond excitation. Under stationary excitation conditions using ns pulses of comparable intensity (around $0.5\,\mathrm{MW\,cm^{-2}}$) only electron–hole plasma luminescence is observed. The origin of these remarkable changes in the spatially resolved PL spectra derives from the formation process of different quasi-particles under ps excitation conditions. During the short pulse transient a dense electron–hole plasma is formed which relaxes to the bottom of the sub-band and forms excitons on a time scale of the order of a few hundreds ps [the
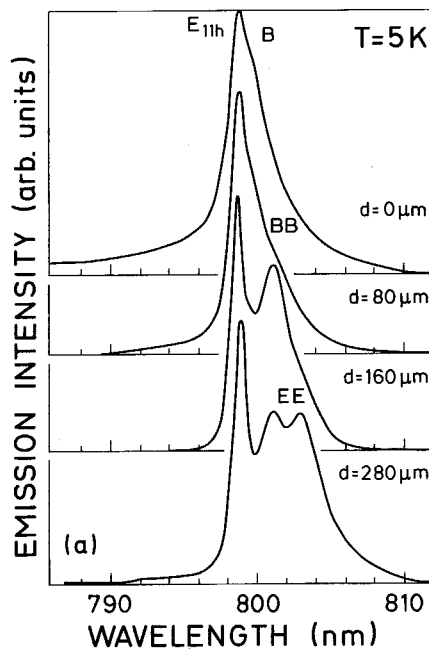

Figure 30. Spatially resolved luminescence from a GaAs/Al$_{0.36}$Ga$_{0.64}$As QW multiple quantum well structure ($L_z = 10.6$ nm $L_b = 15.3$ nm), recorded under picosecond excitation at an excitation intensity of the order of $0.5\,\mathrm{MW\,cm^{-2}}$.

longest value reported up to now in GaAs quantum wells is 400 ps (Kusano, Segawa, Aoyagi, Namba and Okamoto 1989)]. This leads to the establishment of a dense exciton gas in the time interval between two following pump pulses, which gives rise to different radiative recombination processes detectable in a time-integrated experiment depending on the actual exciton and electron density.

The attribution of the observed luminescence bands of figure 30 is made on the basis of the temperature and intensity dependences, spectral positions and decay times of the emission. In figure 31 we show the luminescence decay times of the E_{11h}, B, BB and EE bands measured by spatially resolving the luminescence 280 μm far away from the spot centre. The B band exhibits a lifetime two times shorter than the exciton lifetime, while both the BB and the EE luminescences are characterized by a very short time constant, of the order of 600 and 250 ps, respectively. According to the energy position and to the recombination time the B band is ascribed to biexciton recombination. As shown in figure 30, such biexciton emission is clearly observed near the centre of the excited spot. For larger spatial displacements the BB and EE band become dominant. The shortening of the lifetime indicates that they are due to fast scattering processes between quasi-particles. The BB band lies approximately one biexciton binding energy below the B band, and exhibits a superlinear intensity dependence and a temperature dependence similar to the GaAs band gap (see figure 32). In analogy to the case of II–VI semiconductors (Kuroda and Shionoya 1974), conservation of energy and momentum in the inelastic biexciton scattering results in the creation of free excitons and a photon of energy $\hbar\omega = E_{11h} - 2E_b^{BIEX}$. This interpretation is consistent with the short recombination time of the BB band (figure 31). We therefore conclude that the BB emission is due to inelastic biexciton collisions resulting in the formation of free excitons and electron–hole pairs.

The origin of the EE band requires a more detailed discussion. The line arises 7·5 meV below the E_{11h} band and shifts to the red faster than the GaAs band gap with increasing temperature, as shown in figure 32. The deviation from the expected
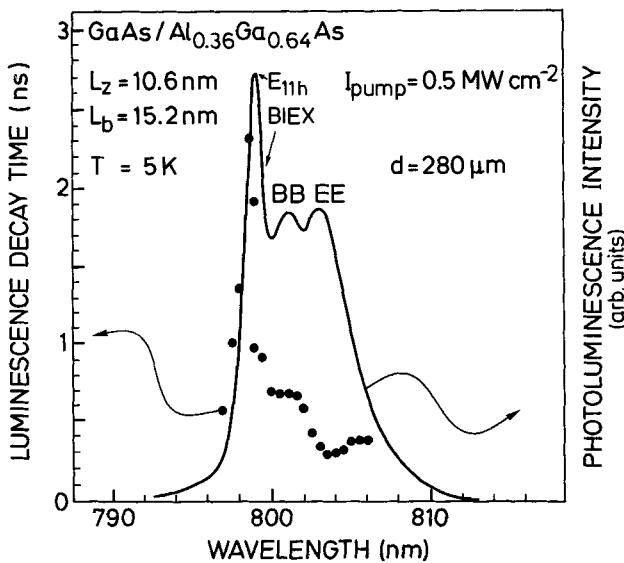

Figure 31.   Decay times of different radiative recombination channels observed in the spatially resolved luminescence spectrum of figure 30 at $d = 280\,\mu m$.

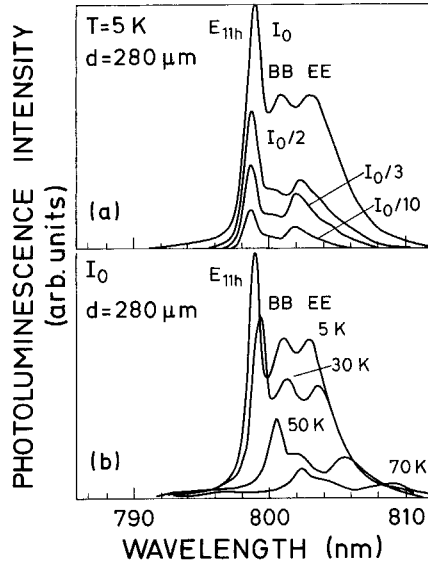Figure 32. Intensity dependence and temperature dependence of the E_{11h}, BB and EE luminescence lines in the $d=280\,\mu m$ spectrum of figure 30.

temperature dependence of the gap is almost linear in the range 20–120 K, and closely resembles the spectral behaviour of the luminescence emitted by inelastic exciton–electron scattering process, resulting in the ionization of the exciton and in the diffusion of a hot electron (Benoit a la Guillame, Debever and Salvan 1969, Fisher and Bille 1974). Energy and momentum conservation account for the observed temperature dependence and spectral position of the EE band. The characteristic emission of the exciton-electron scattering process occurs at

$$\hbar\omega \simeq E_{11h} - \left(\frac{M}{m_e}\right)\frac{\hbar^2 k^2}{2M}, \tag{5.1}$$

where $m_{e,h}$ is the electron (hole) mass and $M = m_e + m_h$ is the total exciton mass. Assuming a Boltzman distribution for the excitons involved in the scattering processes, the exciton–electron emission peaks at

$$\hbar\omega \simeq E_{11h} - \frac{1}{2}\left(\frac{M}{m_e}\right)K_B T, \tag{5.2}$$

which linearly deviates from the expected temperature dependence of the band gap. For GaAs quantum wells the result is $\hbar\omega \simeq E_{11h} - 3k_B T$, in surprisingly good agreement with the measured $\hbar\omega \simeq E_{11h} - 2k_B T$ dependence. Other inelastic exciton scattering mechanisms, like exciton–exciton scattering, cannot be invoked to explain our findings. In fact, momentum and energy conservation for this collision process would lead to the characteristic emission peaked at

$$\hbar\omega \simeq E_{11h} - E_b + \frac{\hbar^2 k^2}{2M}, \tag{5.3}$$

where E_b is the exciton binding energy equal to 9·5 meV in a 10 nm GaAs quantum wells, which does not fit with the observed position of the EE band.
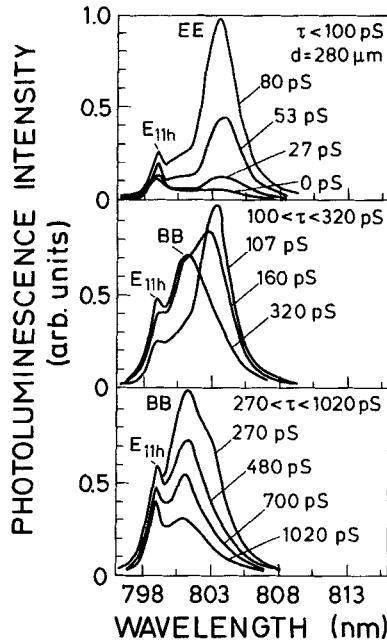
Figure 33. Time evolution of the spatially resolved luminescence (collected 280 μm away from the excited spot centre) induced by inelastic excitonic and biexcitonic collisions at 5 K. The EE and BB band indicate exciton–electron and biexciton–biexciton scattering processes, respectively.

An overview of the time dynamics of the interacting excitonic states in GaAs quantum wells is shown in figure 33. At early times ($\tau < 100$ ps) the EE band arises following the pump pulse, while a weaker emission is observed at the E_{11h} line. Within the first 320 ps the EE band disappears, while the BB band grows and becomes dominant. At longer delays the BB band reduces in intensity, and after about 1 ns the E_{11h} band is the main emission line with a broad low energy shoulder in the BB emission range. The observed time evolution confirms the interpretation given before. Exciton–electron scattering processes are very fast and follow the time evolution of the pulse. This indicates that the radiative recombination process responsible for the EE band involves excitons and electrons photogenerated in the transient of the pump pulse and quickly expanding along the crystal surface. In the 300 ps following the pump pulse the EE scattering process disappears and a mixed exciton–biexciton gas is formed. The emission spectra of figure 33 are indeed very similar to the ones obtained at lower pump intensities, when the photogenerated particle density is not high enough to generate exciton–electron scattering and only the E_{11h} and BB bands are present. In this transient phase the biexciton–biexciton scattering seems to be the most efficient radiative recombination process. For longer times the interaction among excitons looses its importance and the excitonic character of the spontaneous emission is recovered. The described experiments clearly show that the luminescence originating from inelastic collision processes between excitons can be directly observed in spatially resolved luminescence measurements. This method allows the different regions of the crystal surface to be probed, where the actual density of quasi-particles is changing in time owing to the lateral particle expansion, and hence to investigate these otherwise competing decay mechanisms selectively.

Before concluding we recall that the effects of the elastic exciton–exciton and exciton–electron collisions on the broadening of the excitonic luminescence in quantum wells have been studied theoretically by Feng and Spector (1988). The predicted broadening is of the order of several meV and is expected to increase with increasing density of the interacting quasi-particles. To our knowledge experiments to study this broadening effects have not yet been performed.

6. Electron–hole plasma emission

In the previous sections we have discussed the radiative recombination processes in quantum wells and superlattices induced by optical excitation in the transparency region or in the absorption continuum as a function of the photogenerated carrier density. In the examined density ranges ($n < 10^{11}$ cm^{-2}) all the emission processes are based on excitonic transitions, either spontaneous or induced by collisional events. Now, following the scheme of figure 1, we will extensively discuss the optical properties of quantum wells at very high photogeneration rates. Under these conditions excitons are screened. The breakdown of the Coulomb bound states results in the formation of a dense electron–hole plasma (EHP), which strongly affects the optical properties of crystals. Many-body interactions in the dense EHP renormalize the electron–hole pair self-energy, thus changing the ground level of the crystal. All radiative recombination processes are governed by free-carrier optical transitions, and the conditions for optical amplification of the luminescence can be reached if population inversion is maintained by optical or electrical carrier injection.

Optical spectroscopy is used to investigate the electron–hole plasma state in quantum wells and to obtain information on the carrier energetics and energy gap in the presence of the dense Fermi gas. We discuss the main theoretical and experimental aspects of the quasi two-dimensional electron–hole plasma in quantum wells. The effect of the reduced dimensionality on the screening of the Coulomb interaction and on the band gap renormalization will be outlined, with particular attention to the application of these concepts to the interpretation of the optical spectra.

6.1. *Theoretical treatment of the electron–hole plasma in quantum wells*

The EHP phase in a semiconductor is established when the electron–hole (e–h) pair density exceeds a critical density n_M (Mott threshold). This threshold corresponds to the e–h pair density at which the Debye–Hückel screening length (K_D) becomes comparable to the exciton Bohr radius (a_0)

$$K_D^2 a_0^2 \simeq 1, \tag{6.1}$$

where

$$K_D^2 = \frac{8\pi n_{3D} e^2}{\varepsilon_0 k_B T}.$$

In equation (6.1) n_{3D} is the carrier density (in cm^{-3}), ε_0 the static dielectric constant of the crystal and $k_B T$ the carrier thermal energy. At the Mott threshold the weakening of the Coulomb interaction due to free carrier screening leads to the exciton ionization and strongly affects the optical properties of the material. The theoretical description of the ground level properties of the dense electron–hole system in semiconductors is very complex. However, use of the quasi-equilibrium approximation simplifies the treatment of the problem (Haug and Koch 1989). It is assumed that electrons and holes are

distributed in their respective bands in quasi-thermal equilibrium, according to the Fermi–Dirac distribution functions

$$f_{i,k} = \frac{1}{\exp\left(\dfrac{E_{i,k} - \mu_i}{k_B T}\right) + 1},$$ (6.2)

where μ_i is the quasichemical potential which depends on the carrier density of the species i ($i = e$ for electrons and $i = h$ for holes). In two dimensions the density dependence of the chemical potential can easily be computed from the expression

$$n_i = \frac{\pi}{S} \sum_k f_{i,k},$$ (6.3)

which gives

$$\mu_i(T, n) = k_B T \ln\left[\exp\left(\frac{F_i(n)}{k_B T}\right) - 1\right],$$ (6.4)

where F_i is the electron (hole) Fermi energy

$$F_{e,h}(n) = \frac{\hbar^2 k_F^2}{2m_{e,h}} = \frac{\hbar^2 \pi n}{m_{e,h}},$$ (6.5)

$k_F = (2\pi n)^{1/2}$ being the 2D Fermi momentum. At very low temperature the quasi-chemical potential reduces to

$$\mu(n) = F_e(n) + F_h(n).$$ (6.6)

The quasi-equilibrium approximation in most cases is well justified and is usually applied to the interpretation of the optical spectra measured in stationary condition experiments (under ns excitation). Recent femtosecond experiments have clearly demonstrated that intraband carrier relaxation due to Coulomb scattering occurs on a time scale of 100 fs (Kessler and Ippen 1987, Shah 1989), while carrier cooling in the dense EHP phase has a more complex density dependence and occurs on a time scale of the order of several tens of ps (Shah 1986, Leo, Rühle and Ploog 1988, Lobentanzer, Stolz, Nagle and Ploog 1989).

Another important effect of the plasma state is the screening of the Coulomb potential. In two-dimensional systems the screened potential is usually expressed as

$$V_s(q, \omega) = \frac{V_q}{\varepsilon(q, \omega)},$$ (6.7)

where

$$V_q = \frac{2\pi e^2}{\varepsilon_0 q},$$ (6.8)

is the unscreened Coulomb potential and $\varepsilon(q, \omega)$ is the longitudinal dielectric function. In highly excited semiconductors the description of the screening is complicated by the presence of interacting exciton states. The screening efficiency depends on the e–h pair density and, therefore, on the exciton density too. On the other hand, the exciton density decreases when the strength of the screening increases. A quantitative treatment of this effect requires a self-consistent model which has not yet been established (Haug

and Schmitt-Rink 1985). A reliable physical approximation generally used to treat the screening is the random phase approximation (RPA), in which particles in the EHP are assumed to be perturbed by an average external field. Within RPA the density dependent dielectric function is given by the Lindhard formula (Haug and Koch 1989)

$$\varepsilon(\boldsymbol{q}, \omega) = 1 - V_q \frac{1}{V} \sum_{i=\mathrm{e,h};\,\boldsymbol{k}} \frac{f_{i,\boldsymbol{k}} - f_{i,\boldsymbol{k}+\boldsymbol{q}}}{\hbar\omega + \mathrm{i}\delta - E_{i,\boldsymbol{k}+\boldsymbol{q}} + E_{i,\boldsymbol{k}}}, \tag{6.9}$$

where E indicates the carrier energies. Equation (6.9) is usually numerically calculated, but a much simpler solution can be obtained by neglecting the frequency dependence of the longitudinal dielectric constant. A further simplification is made by replacing the multiple poles of equation (6.9) with a single pole at the frequency of the collective plasma oscillation

$$\omega_{\mathrm{pl}}^2 = \frac{2\pi e^2 n q}{\varepsilon_0 m}. \tag{6.10}$$

This is the so called static single plasmon pole approximation (SSPA) which is widely used to calculate the single-particle self-energy in the EHP (Schmitt-Rink and Ell 1985, Ell, Blank, Benner and Haug 1989, Haug and Koch 1989). Within SSPA the screening dielectric constant becomes

$$\frac{1}{\varepsilon(q)} = \left[1 - \frac{\omega_{\mathrm{pl}}^2}{\omega_q^2} \right], \tag{6.11}$$

where

$$\omega_q^2 = \omega_{\mathrm{pl}}^2 \left(1 + \frac{q}{\sigma} \right) + \frac{C}{4} \left(\frac{\hbar q^2}{2m} \right)^2, \tag{6.12}$$

is the dispersion of the plasmon mode. In this equation C is a numerical constant, σ is the inverse screening length and $m = m_{\mathrm{e}} m_{\mathrm{h}} / (m_{\mathrm{e}} + m_{\mathrm{h}})$. It is important to note that although the problem is treated on an equal basis for both 2D and 3D semiconductors, the screening of the Coulomb interaction due to free carriers is less efficient in low dimensional systems than in bulk materials (Schmitt-Rink *et al.* 1985a, b). In quantum wells the decrease of the Coulomb interaction due to excitonic screening is found to be three times more efficient than the corresponding free-carrier screening (Haug and Schmitt-Rink 1985).

The competition between free-carrier and exciton screening has been experimentally investigated by fs time resolved pump-and-probe absorption spectroscopy (Peyghambarian and Gibbs 1985, Knox, Fork, Downer, Miller, Chemla, Shank, Gossard and Wiegmann 1985, Hulin, Mysyrowicz, Antonetti, Migus, Masselink, Morkoc, Gibbs and Peyghambarian 1986). These experiments have shown that screening of the Coulomb interaction due to excitons is most efficient in bleaching the exciton resonance within the first 800 fs after the excitation (Hulin *et al.* 1986). After this ultra-short transient, the exciton oscillator strength recovers the original value and the screening mechanism is then dominated by free-carriers on a much longer time scale and with a reduced efficiency. In addition, it was found that exciton screening causes a renormalization of the exciton energy in the first 10 ps after the excitation, leading to a transient blue shift of the exciton resonance. This phenomenon has been ascribed to the filling of the exciton phase-space similar to the band filling by free-carriers. However, under stationary conditions (times longer than several hundred ps) the free-carrier

screening becomes the dominant effect responsible for the exciton ionization, and the quasi-equilibrium approximation can be successfully applied to the free-carrier population.

Once the effective electron–hole interaction is known, it is possible to evaluate how this interaction affects the free e–h pair energy and, in turn, the optical properties of the crystal. The two basic mechanisms leading to the renormalization of the particle self-energies are the correlation and the exchange interactions. Both effects depend critically on the carrier density in the EHP and result in a net decrease of the carrier's self-energy. Qualitatively, this reflects the energy lost by carriers of the same species in avoiding each other under the effect of Coulomb repulsion (correlation) and exchange. The impact of these effects on the energy bands and on the optical properties of the crystal is schematized in figure 34. The band gap of the crystal (E_g) shrinks proportional to the density of the EHP $(E'_g(n))$, while electrons and holes fill the respective bands up to the Fermi levels $(F_e(n)$ and $F_h(n))$, following a quasi-equilibrium Fermi distribution. As a consequence, the EHP luminescence red-shifts and broadens with increasing carrier density, reflecting the shrinkage of the gap and the increase of the chemical potential (right-hand side of figure 34). Actually in semiconductors equation (6.6) is scaled with respect to the renormalized band gap as $\mu(n) = F_e(n) + F_h(n) + E'_g(n)$. In this way one can directly compare the low and high energy tails of the luminescence with the expected positions of the renormalized band gap edge and on the chemical potential,
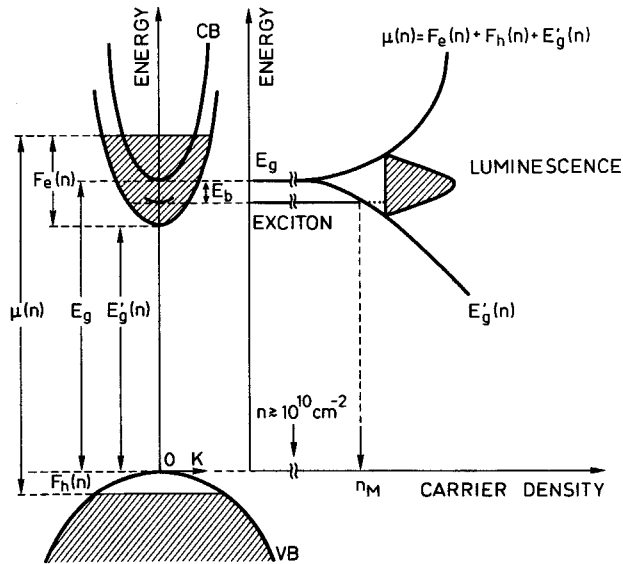

Figure 34.   Illustration of changes of the electronic states induced by the dense electron–hole plasma in semiconductors. E_g is the unperturbed gap of the crystal while $E'_g(n)$ is the density dependent renormalized gap. E_b is the exciton binding energy, $F_{e,h}(n)$ are the electron (hole) quasi Fermi levels and $\mu(n)$ is the total chemical potential of the EHP. For clarity the total band gap renormalization has been indicated by the down-shift of the conduction band only. The carrier density dependence of $\mu(n)$ and $E'_g(n)$ are depicted on the right-hand side of the figure. The splitting between the two curves defines the bandwidth of the EHP luminescence. The density axis scale starts around $10^{10} \, \mathrm{cm}^{-1}$, below this density neither the gap nor the exciton states are significantly perturbed by the carrier population. The density n_M indicates the critical density at which the BGR merges to the exciton state.

whilst the emission linewidths corresponds to the total quasi-Fermi level of the EHP $(F_e(n) + F_h(e))$. It should be mentioned that the exchange and correlation energies have k-dependences equal and opposite, respectively (Vashista and Kalia 1982), thus cancelling the k-dependence of the total band gap renormalization. The gap shrinkage is therefore described as a rigid shift of the band which considerably simplifies the calculations. As schematically shown on the right-hand side of figure 34, over a certain critical density n_M the reduced band gap merges to the exciton level whose energy does not renormalize due to its charge neutrality. Under these conditions the exciton binding energy vanishes and excitons are not stable in the EHP anymore (Schmitt-Rink and Ell 1985). Similarly, Kleinman (1985) has assumed that the exciton stability is lost when the total quasi-Fermi level of the EHP overcomes the exciton binding energy. In both cases the critical density n_M for the exciton stability is found to be in the range of $10^{10}-10^{11}$ cm^{-2}. In this density range excitonic features are bleached in the absorption spectra (see, for example, the experiments reported by Levenson, Abram, Raj, Dolique, Oudar and Alexandre 1988 and Weber, Klingshirn, Chemla, Miller, Cunningham and Ell 1988). Nevertheless, some excitonic emission is expected to persist in the luminescence spectra even at carrier densities larger than n_M due to the effect of the excitonic enhancement (Kleinman 1985, Schmitt-Rink, Ell and Haug 1985b).

It is very important to evaluate the relevant energy parameters depicted in figure 34, quantitatively, in order to calculate the optical spectra. The quantitative estimate of the band gap renormalization is considerably more difficult than the evaluation of the chemical potential made by means of equations (6.4)–(6.6). Much theoretical work has been done on the density dependence of the band gap renormalization in quantum wells (Bauer and Ando 1986, Schmitt-Rink and Ell 1985, Bisti and Silin 1986, Kleinman 1986, Ell *et al.* 1989, Haug and Koch 1989, Hawrylak 1989, Das Sarma, Jalabert and Eric Yang 1989 and 1990). In the quasi-static approximation of Haug and Koch (1989) the band gap renormalization is given by

$$\Delta E_g \simeq [V_s(r=0) - V(r=0)] - \frac{1}{V} \sum_q V_s(q)(f_{e,q} + f_{h,q}). \qquad (6.13)$$

The first term represents the correlation energy term (Coulomb hole), the second the screened exchange contribution which also reduces the band gap. As discussed before, the quantities appearing in equation (6.13) are calculated within the SSP approximation neglecting the frequency dependence of the dielectric constant (quasi-static approximation). The main results of these calculations are the approximated $n^{1/3}$ density dependence and the well width dependence of the BGR. In particular, for a 10 nm GaAs quantum well the calculated band gap renormalization is well approximated by the relation (Schmitt-Rink *et al.* 1989)

$$\Delta E \simeq 3 \cdot 6 \times 10^{-3} n^{1/3}. \qquad (6.14)$$

The density dependence of the chemical potential and of the band gap renormalization for a 10 nm GaAs quantum well are shown in figure 35. The curves calculated by equations (6.6) and (6.14) evidence the carrier density dependence of both the chemical potential and the BGR. The variation of these parameters affects the line shape of the EHP luminescence, as schematically indicated on the right-hand side of figure 34. The increase of the carrier density results in an enhancement of the chemical potential, i.e. in a broadening of the luminescence linewidth and in a blue shift of the high energy tail. The low energy edge of the emission spectrum correspondingly shifts to the red, due to the carrier induced band gap reduction.
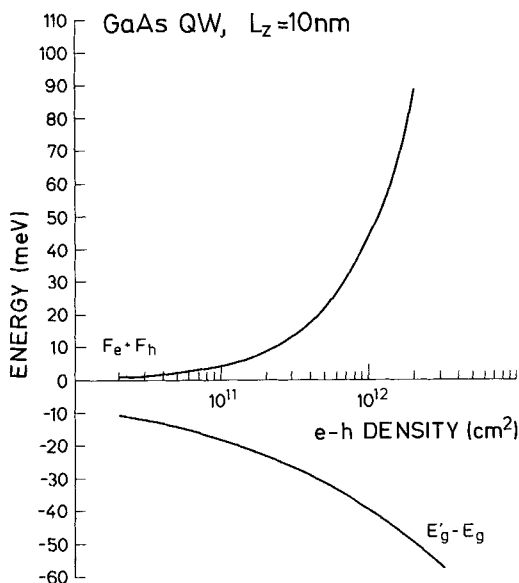
Figure 35.   Calculated band gap renormalization $(E'_g - E_g)$ and chemical potential $[\mu(n) = F_e(n) + F_h(n)]$ at low temperature for a 10 nm wide GaAs quantum well. The curves are obtained from equations (6.14) and (6.15), respectively.

The general trend of the chemical potential and of the BGR shown in figure 35, give only a qualitative indication for the calculation of the optical spectra. In actual experimental spectra there are several homogeneous and inhomogeneous broadening mechanisms due to inter-carrier scattering, lifetime broadenings, interface roughness and crystal potential fluctuations, which prevent the quantitative description of the electronic properties of the EHP. In addition, Das Sarma et al. (1990) have recently discussed the limited accuracy of the single plasmon pole approximation by performing an improved calculation of the BGR which takes into account the full RPA dielectric function and the dynamical electron–phonon interaction. The results of Das Sarma et al. (1990), though confirming the well width dependence of the BGR and the validity of the quasi-static approximation, are about 20% larger than those calculated in the SSP approximation for the same well width. Furthermore, they demonstrate that the well width dependence of the BGR can be almost eliminated provided the interparticle distance is scaled in units of effective quasi two-dimensional Bohr radius. A systematic comparison of these different theoretical models with the results of recent experiments is presented in the next section. We point out that the great efforts made for the theoretical calculations of the optical spectra of highly excited quantum wells has provided a valuable means to understand the physics of the radiative recombination processes in the EHP. This is very important for the design and the operation of semiconductor lasers and opto-electronic devices based on the EHP induced optical non-linearity.

6.2. Many-body effects in the spontaneous luminescence of semiconductor quantum wells
    Following the theoretical outline of the previous section, we now discuss some optical spectroscopy experiments on the quasi-two-dimensional EHP in quantum wells. In most cases the ground level properties of the EHP have been investigated by

high-excitation intensity luminescence experiments under stationary conditions for GaAs quantum wells (Xu, Kreismanis and Tang 1983, Le, Lax, Vojak and Calawa 1985, Borestain, Fekete, Vofsi, Sarfaty and Arza 1986, Tränkle, Leier, Forchel, Haug, Ell and Weimann 1987, Cingolani *et al.* 1988c, Bongiovanni and Staehli 1989, Lach, Lehr, Forchel, Ploog and Weimann 1990) and in $Ga_xIn_{1-x}As$ quantum wells (Alavi, Temkin, Wagner and Cho 1982, Tränkle, Lach, Forchel, Scholz, Ell, Haug, Weimann, Griffiths, Kroemer and Subbanna 1987b, Hunt and Jessop 1988, Fortin, Hua, Roth, Charlebois, Fafard and Lacelle 1989). Further, picosecond time resolved spectroscopy has been used to study the EHP luminescence (Tanaka, Kuno, Yamamoto, Kobayashi, Mizuta, Kukimoto and Saito 1984, Göbel, Höger, Kuhl, Polland and Ploog 1985, Cingolani, Kalt and Ploog 1990d) and the carrier dynamics (Leo *et al.* 1988, Lobentanzer *et al.* 1989, Levenson, Dolique, Oudar and Abram 1990). Typical spontaneous luminescence spectra of a 10 period $GaAs/Al_{0.32}Ga_{0.68}As$ multiple quantum well with $L_z = 12$ nm and $L_b = 13$ nm are shown in figure 36 for different photogeneration rates. The luminescence is excited by a N_2 laser pumped dye laser operating at 600 nm with 10 Hz repetition frequency and a pulse timewidth of 5 ns. The emission spectra reveal the progressive filling up to the third electron sub-band as the excitation intensity is increased. The carrier density can be roughly estimated from the
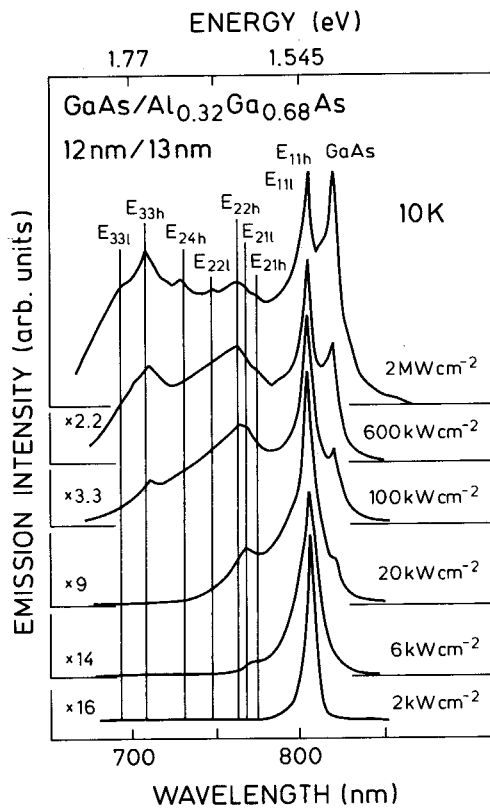

Figure 36. Spontaneous emission spectra obtained from a highly photoexcited $GaAs/Al_xGa_{1-x}As$ multiple quantum well structure (sample 6115 of figure 13) at 10 K and at different excitation intensities. The spectra have been magnified by the indicated factors to be compared.

linewidth of the luminescence spectrum, taking into account the density of states per unit energy of the occupied conduction and valence sub-bands. For the spectrum recorded at the maximum excitation intensity we measure a band filling of about 250 meV corresponding to a carrier density of the order of 10^{13} cm^{-2}. A broadening on the low energy side of the luminescence is clearly observed, indicating a large band gap renormalization. However, quantitative information on this parameter cannot be obtained easily since the luminescence tail merges the bulk GaAs buffer emission (GaAs band). The presence of some forbidden $\Delta n \neq 0$ transitions in the spectra of figure 36 indicates that intercarrier scattering relaxes the selection rules for the recombination, thus adding further recombination channels to the luminescence. In addition, the broadening and the slope of the high energy tail of the luminescence manifest a high carrier temperature of the EHP, indicating that at stationary conditions the quasi-equilibrium distribution is thermalized but still hot.

A possible way to quantitatively estimate the carrier density, the band gap renormalization and the carrier temperature is to theoretically analyse the line-shape of the spontaneous luminescence. This has been attempted by several groups by modelling the line-shape with different spectral functions (Fekete *et al.* 1985, Tränkle *et al.* 1987, Cingolani, Ferrara, Lugara, Moro, Chen, Bassani, Massies and Turco 1988d, Bongiovanni and Staehli 1989, Kulakovski *et al.* 1989, Colocci *et al.* 1989). The general expression for the spectral intensity of the EHP emission $I(\hbar\omega)$ is

$$I(\hbar\omega) \approx \sum_{e,h} \int \int f_e(E_e) f_h(E_h) D_e(E_e, \Gamma_e) D_h(E_h, \Gamma_h) \, dE_e \, dE_h, \qquad (6.15)$$

where the summation is over all the occupied electron and hole sub-bands. In equation (6.15) $D_{e,h}$ is the broadened two-dimensional electron (hole) density of states. In this model the carriers are distributed in different sub-bands according to the Fermi distribution functions $f_e(E_e)$ and $f_h(E_h)$, with common quasi Fermi levels (equations (6.4) and (6.5)) and carrier temperature. The carrier temperature is usually assumed to be equal for electrons and holes and is not necessarily coincident with the lattice temperature. The energy bands are assumed to be parabolic. A phenomenological collisional broadening parameter Γ (Landsberg, Abrahams and Osinski 1985) is introduced in order to avoid the abrupt low energy tail due to the step-like density of states used in the calculation. In general the calculated spectra assuming the carrier density, the band gap renormalization, the carrier temperature and the phenomenological broadening as free parameters reproduce the experimental curves well, whether k-conservation is taken into account (Tränkle *et al.* 1987) or neglected (Cingolani *et al.* 1988d).

A comparison between the experimental and the theoretical EHP line-shapes is shown in figure 37 for a spatially homogeneous electron–hole plasma photogenerated in mesa-etched Ga$_x$In$_{1-x}$As/InP quantum wells (Kulakowskii *et al.* 1989). Lach *et al.* (1990) have recently used this procedure to study the well width dependence of the BGR and to identify the transition from 3D to 2D BGR in GaAs quantum wells (the cross-over thickness has been found to be between 10 and 20 nm). However, this rather complex spectral analysis does not give a very accurate quantitative determination of the BGR. This is shown in figure 38, where we compare a selection of recent experimental data with the full RPA calculation of Das Sarma *et al.* (1990) and the SSPA calculations of Schmitt-Rink *et al.* (1989) for well widths ranging from 8 to 13 nm. As discussed before, the theories differ by about 20%, while the BGR values deduced
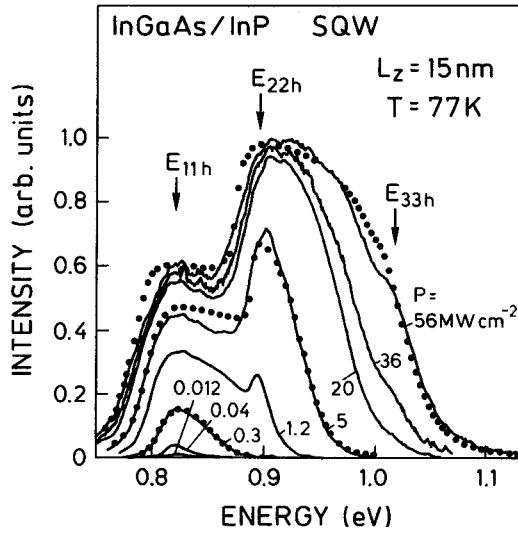
Figure 37. Electron–hole plasma spontaneous emission (solid lines) from $Ga_xIn_{1-x}As/InP$ quantum wells mesa-etched into small structures of about 50 µm size, and theoretically calculated emission line-shapes (dots) at different excitation intensities (after Kulakowskii *et al.* 1989).
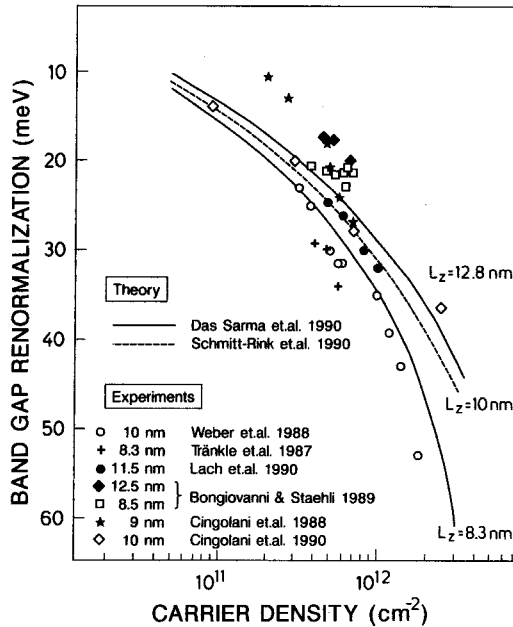

Figure 38. Theoretical (curves) and experimental (symbols) BGR values versus the carrier density in GaAs quantum wells for $8 < L_z < 13$ nm, as reported by different groups. With the exception of the data by Weber *et al.* (1988) and Cingolani *et al.* (1990), the experimental BGR values have been obtained by the line-shape fitting of the EHP spontaneous emission (see text).

from the line-shape fitting are quite scattered. The accuracy of the results does not improve even in more sophisticated models (Bongiovanni and Staehli 1989). The inclusion in the line-shape model of the single particle spectral broadening functions and of the 2D mean interaction potential for the shift of the plasma frequency (within SSPA), at the cost of considerable computational complications, does not give quantitative results in agreement with the most recent theories. A better quantitative agreement between theory and experiment is found for the BGR values measured by pump and probe absorption (Weber *et al.* 1989) and by time resolved spectroscopy (Cingolani *et al.* 1990d). In all these cases the $n^{1/3}$ density dependence of the BGR describes the trend of the experimental data reasonably well.

Before proceeding in the discussion we want to focus our attention on the sharp peaks superimposed to the EHP luminescence around the main excitonic transitions shown in figure 36. These structures are present up to the highest excitation intensities, well above the critical density for the exciton ionization, and can hence not be attributed to excitonic effects in the luminescence. Actually, they originate from the superposition of free-carrier and exciton luminescence emitted from different regions of the crystal surface, where the carrier densities are very different. This effect can be demonstrated by spatially resolving the luminescence through the excited spot on the crystal surface (Cingolani, R., Ploog, Cingolani, A., Moro and Ferrara 1990e) as already discussed in section 4.2. A typical result is shown in figure 39 where we compare the EHP luminescence collected from the whole excited spot (having about 200 μm diameter) with the luminescence spatially filtered through a 50 μm pinhole centred in the excitation region. The excitonic luminescence is found to decrease dramatically,
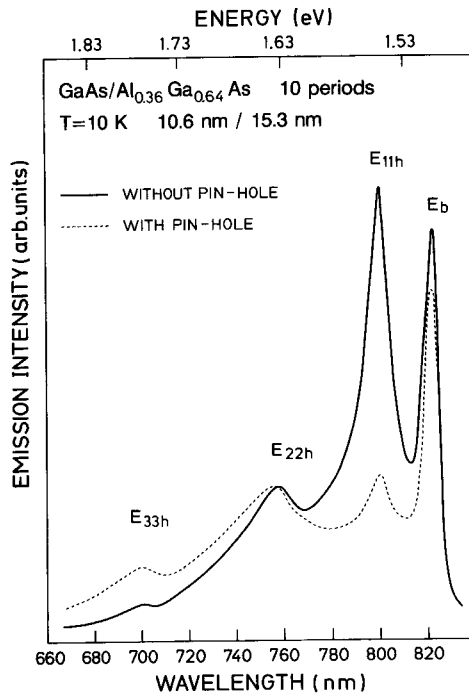

Figure 39. Spontaneous EHP emission from a 10-period GaAs/Al$_{0.36}$Ga$_{0.64}$As multiple quantum well structure with $L_z = 10.6$ nm, collected from the whole excited spot (solid line) and from the central region of the spot by a 50 μm pinhole (dashed line).

while the free-carrier luminescence does not change. This indicates that the photogenerated EHP is spatially inhomogeneous and quickly expands along the quantum well surface. Kulakowskii *et al.* (1989) have limited the effect of the strong EHP expansion by studying $Ga_xIn_{1-x}As/InP$ quantum well samples mesa etched into small squared structures with side lengths of about 20 μm. In this way they have been able to study the luminescence of a perfectly homogeneous EHP in single quantum wells with L_z ranging between 8 and 15 nm (see figure 37). The spatial expansion of the EHP in GaAs quantum wells has also been studied by Tsen and Morkoc (1986) and Tsen, Sankey, Halama, Sen and Moroc (1989) by spatially and time resolved Raman spectroscopy. The authors demonstrated that the EHP expansion is thermodiffusive and that carriers have an average speed of the order of Fermi velocity (about 10^7 cm s^{-1}). Therefore, due to the fast diffusion process, a spatial and temporal distribution of carriers is produced along the crystal surface (Held, Kuhn and Mahler 1990) where excitons and carriers at different densities can coexist, strongly affecting the EHP line-shape.

It is interesting to note that the carrier temperatures usually deduced from the line-shape analysis of these stationary conditions experiments can easily exceed 100 K. This reveals that a considerable excess energy is still available for the EHP carriers, especially in photogeneration experiments in which the optical excitation is above the barrier gap.

Before concluding this section we want to point out the relations between the crystal band structure and the EHP radiative recombination processes. In crystals with indirect or multivalley band structures the exchange and correlation energies are affected by the existence of different minima in the conduction or valence bands (Vashista and Kalia 1982). As schematically shown in figure 40, the presence of an indirect gap at energy quasi-resonant to the direct gap causes the simultaneous band filling of different bands with strong alterations of the EHP luminescence spectra. This has been studied in detail in some bulk semiconductors like GaSe (Cingolani, Ferrara and Lugara 1987) where the indirect energy gap is about 25 meV lower in energy than the Γ point gap, and in the ternary alloy $Al_xGa_{1-x}As$ close to the direct–indirect crossover ($x \simeq 0.4$) (Bohnert, Kalt, Smirl, Norwood, Bogges and D'Haenens 1988, Kalt,
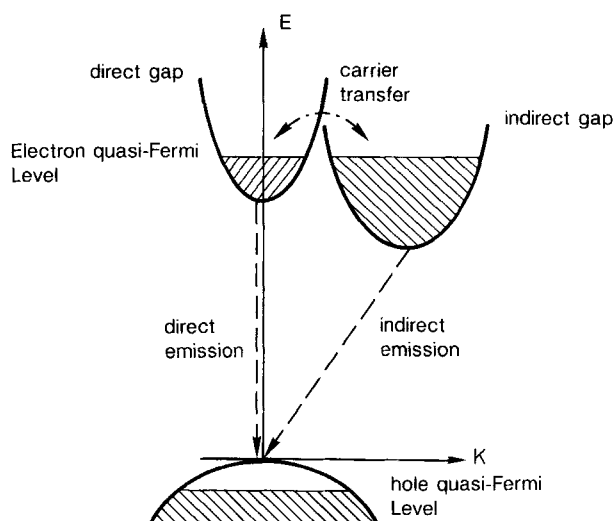

Figure 40.   Schematic electron–hole plasma band filling in indirect-gap semiconductors.

Bohnert, Smirl and Bogges 1988). The basic result of these studies is that, despite the small matrix element of the indirect transitions, radiative recombination from the indirect EHP can occur if the two gaps are not widely separated in the energy space. In this case the indirect EHP can even exhibit stimulated emission (Cingolani *et al.* 1987, Kalt *et al.* 1989).

On the set of GaAs/AlAs ultra-short-period superlattices (USPS) described in section 2.1 we have performed a systematic spectroscopic investigation of the EHP luminescence near the type I–type II cross-over, in order to verify whether both the direct and real space indirect EHP luminescence could be observed (Cingolani *et al.* 1989). The results of these experiments are shown in figure 41. For fully type II USPS ($m = n = 2$ monolayers), both the low- and high-excitation intensity photoluminescence spectra (LEI–PL and HEI–PL, respectively) peak at the same energy, corresponding to the type II emission established in the cw experiments (see section 2.1). When increasing the number of monolayers, the USPS approaches the type I–type II cross-over. For the $m = n = 10$ monolayer USPS the two gaps are separated by about 60 meV (see figure 21). In this case the HEI–PL spectra exhibit the type II emission, coincident with the LEI–PL, only at the lowest excitation intensities. At higher photogeneration rates a sharp emission line (Γ) arises on the high energy side of the type II luminescence, at energy coincident with the type I transition measured in PLE. This behaviour clearly reflects the progressive increase of the EHP chemical potential, which reaches the onset of the higher energy direct gap, as depicted in figure 40. In this situation two radiative recombination proccess can be observed due to the simultaneous population of carriers at the GaAs Γ-point and at the AlAs X point. Above the direct indirect cross-over ($m = n = 15$) the LEI–PL and HEI–PL spectra coincide at the energy of the type I transition, as expected for direct-gap USPS. Nevertheless, at large enough carrier density a shoulder on the high energy side of the direct EHP emission is observed, indicating the population of the higher-energy X point of the AlAs. These phenomena
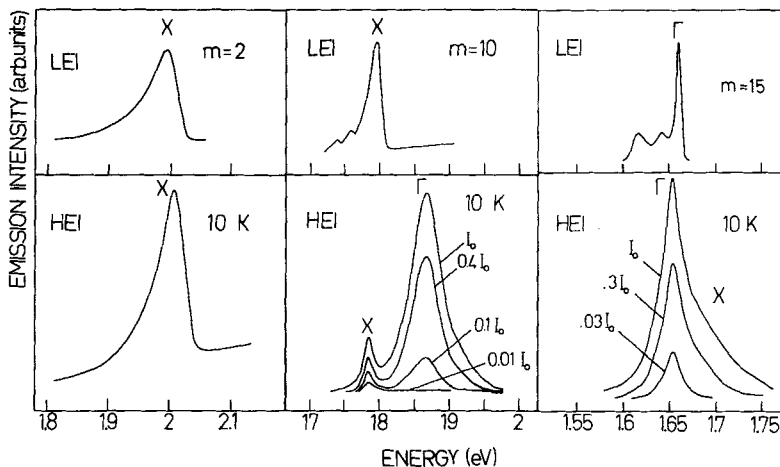

Figure 41.   High-excitation intensity luminescence (HEI–PL) and normal continuous wave luminescence (LEI–PL) spectra measured in a set of symmetric ultra-short period $(GaAs)_m/(AlAs)_m$ superlattices with type II band alignment ($m = 2$), around the type I–type II cross-over ($m = 10$) and with type I alignment ($m = 15$). The electron–hole plasma emission from both the direct (Γ) and the type II gap (X) can be clearly resolved at different excitation intensities ($I_0 \simeq 300 \, kW \, cm^{-2}$).

have been successfully used to study the size induced type I–type II transitions in these USPS (see figure 21), giving a critical monolayer thickness in perfect agreement with the one deduced from PLE measurements.

Carrier lifetimes longer than 100 ns measured by Dawson, Moore, Foxon, t'Hoff and van Hal (1989) in type II USPS indicate that electron–hole liquid condensation may occur at high density of carriers in these artificially layered materials. Our time-resolved measurements of the type II EHP luminescence in GaAs/AlAs USPS near the cross-over evidence a time decay of the emission which is similar to the one measured for the electron–hole liquid droplets in Ge. This is shown in figure 42 for a $(GaAs)_{10}/(AlAs)_{10}$ USPS under high excitation intensity (about $2\,MW\,cm^{-2}$) (Cingolani *et al.* 1989c). The type II luminescence at carrier densities of the order of $10^{13}\,cm^{-2}$ persists after delays as long as 1 μs without appreciable changes in the line-shape, as expected for a constant free-carrier density state in the superlattice (Kleinman 1986). Furthermore the time decay of the luminescence exhibits two distinct decay constants. At earlier times the luminescence decays with a rather long transient, while at longer delays it recovers the decay times measured in the low intensity excitation experiments. Similar behaviour in Ge electron–hole droplets have been interpreted as due to the coexistence of a mixed constant density electron–hole liquid phase in
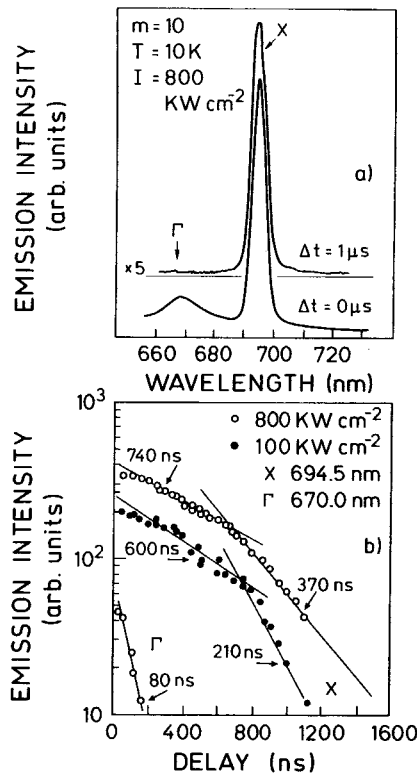

Figure 42. Time resolved luminescence from a type II $(GaAs)_{10}/(AlAs)_{10}$ ultrashort-period superlattice under high photogeneration rate (*a*). No appreciable changes in the luminescence line-shape can be observed 1 μs after the excitation. In (*b*) the temporal decay of the luminescence peak is depicted for different excitation intensities. Two distinct decay times can be observed over the investigated time interval.

saturated vapour pressure equilibrium with a dense exciton gas. In this case, increasing the photogeneration rate results in the increase of the electron–hole liquid volume and hence in a longer decay transient for the luminescence. After a sufficiently long time equilibrium between the two-phases is lost, due to the 'evaporation' of the liquid, and the luminescence recovers the shorter decay time of the excitonic process. However, the conclusive confirmation of this phase transition as well as the theoretically predicted inverse band gap renormalization in type II USPS (Hawrylak 1989) needs additional experimental investigation.

6.3. *Stimulated emission and optical gain spectroscopy*

We now discuss the optical properties of semiconductor quantum wells near the density threshold for stimulated emission. The aim of most of the spectroscopic studies performed in the last 15 years on photoexcited quantum wells was to realize semiconductor laser sources based on quantum size effect. Since the pioneering work of Van der Ziel (1975) on the stimulated emission of GaAs/AlAs multilayer heterostructures, there has been a great improvement of the performance of quantum well lasers. The impressive development of the control of crystal growth on an atomic scale [mainly molecular beam epitaxy (MBE) and metal-organic chemical vapour deposition (MOCVD)] made 'band-gap engineering' possible in different material systems. As a consequence, laser emission in quantum wells is now almost continuously tunable in the range of 600 nm–1·6 μm, by suitably controlling the configurational parameters of different III–V semiconductor heterostructures.

The laser emission in quantum wells has been described in great detail, both the fundamental and the application aspects, in several review papers in the last few years (Holonyak, Kolbas, Dupuis and Dapkus 1980, Tsang 1984, Chiu and Yariv 1985, Landsberg *et al.* 1985, Arakawa and Yariv 1986, Weisbuch and Nagle 1987, Zielinsky, Schweizer, Hausser, Stuber, Pilkuhn and Weimann 1987). The discussion will therefore be limited to a few fundamental aspects of the optical amplification of luminescence and the optical gain processes in quantum wells in order to gain a better insight into the fundamental properties of the confined electron–hole plasma. In particular, we will discuss how the accuracy of the information obtained from the spectral analysis of the spontaneous luminescence can be improved by studying stimulated emission and optical gain in photoexcited multiple quantum wells.

The characteristic EHP luminescence critically depends on the configuration of the photoexcited heterostructure. Experimental studies on separate confinement and graded index confinement heterostructures have revealed the important role played by carrier trapping and confinement in the active region of the multiple quantum well laser heterostructure, either for continuous wave or gain switched lasing (Blood, Fletcher and Woodbridge 1985, Nagle, Hersee, Krakowski, Weil and Weisbuch 1986, Feldmann, Peter, Göbel, Leo, Polland, Ploog, Fujiwara and Nakayama 1987, Sogawa and Arakawa 1990). In addition, optical confinement of the luminescence was found to strongly affect the spectral properties of the EHP emission (Blood 1989, Holonyak, Nam, Plano, Wesely and Hsieh 1989, Cingolani *et al.* 1990e). To understand details of this effect, we have recently performed a systematic investigation of the EHP spontaneous and stimulated emission in a set of identical GaAs/Al$_{0·36}$Ga$_{0·64}$As multiple quantum wells ($L_z = 10·6$ nm and $L_b = 15·3$ nm) as a function of the number of periods ($10 < p < 200$). Our results demonstrate that optical confinement of the luminescence in the quantum well strongly affects the luminescence line-shape at high

carrier densities (Cingolani *et al.* 1990e). Heterostructures comprising 100 or more quantum wells exhibit a strong increase of the luminescence efficiency, saturation of the spontaneous emission and optical amplification of the luminescence. The stimulated luminescence arises at energy below the fundamental E_{11h} transition, and it red-shifts with increasing excitation intensity. The luminescence efficiency is further improved in multiple quantum well heterostructures grown on a thick $Al_xGa_{1-x}As$ cladding layer acting as optical confiner. Conversely, samples consisting of few quantum wells only exhibit the usual band filling luminescence spectra developing on the high energy side of the E_{11h} line, as widely reported in the literature (Borestain *et al.* 1986, Tränkle *et al.* 1987, Cingolani *et al.* 1988c). This difference becomes clear in figure 43, where we compare the EHP luminescence of two multiple quantum well heterostructures with different optical confinement. The luminescence spectra are measured under identical experimental conditions on the two samples (A and B) belonging to the above described set. Sample A consists of 25 periods grown on a 1 μm thick $Al_{0.36}Ga_{0.64}As$ cladding layer, while the 25 periods, sample B, are grown as usual on a GaAs buffer. The optically confined sample exhibits a sharp stimulated emission (S-band) arising about 10 meV below the E_{11h} line. The intensity dependence of the S-emission is shown in figure 44. The sharp stimulated emission line shifts to the red with increasing excitation intensity, grows superlinear with the excitation intensity and becomes dominant at very high pumping rates. It is important to note that the excitonic feature in the spectra of figures 43 and 44 arises from the spatial inhomogeneity of the EHP, as discussed in the previous section, and saturates at high carrier density. The emission intensity is strongly improved in small optical cavities realized by cleaving the sample into small pieces along the [011] directions. In small rectangular cavities of about 2 mm × 100 μm size, the threshold excitation intensity for stimulated emission is lowered by about one order of magnitude as compared to the large area sample, and the stimulated emission is observed up to room temperature with an optical gain as high as $600\,cm^{-1}$ at 300 K.

The differences in the manifestation of the EHP luminescence in heterostructures with a different degree of optical confinement can be explained on the basis of the
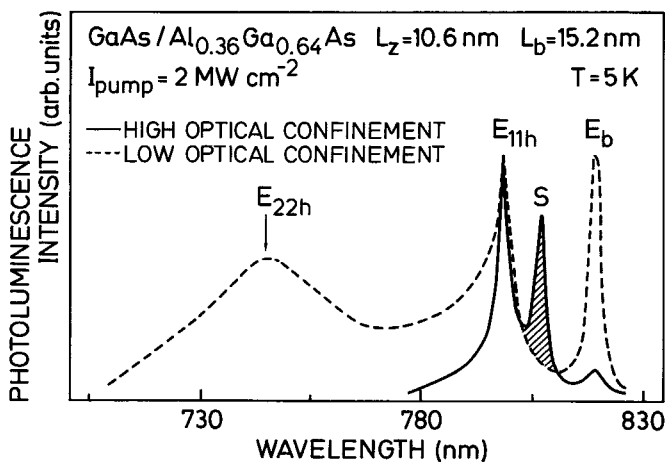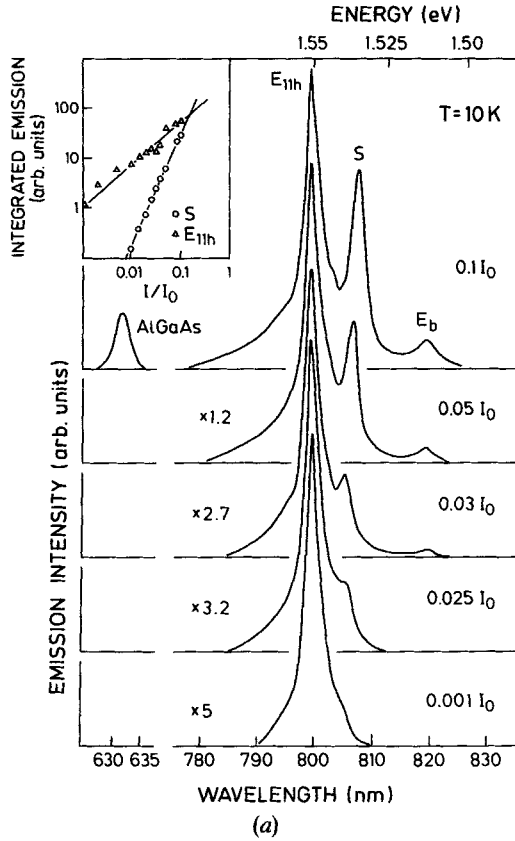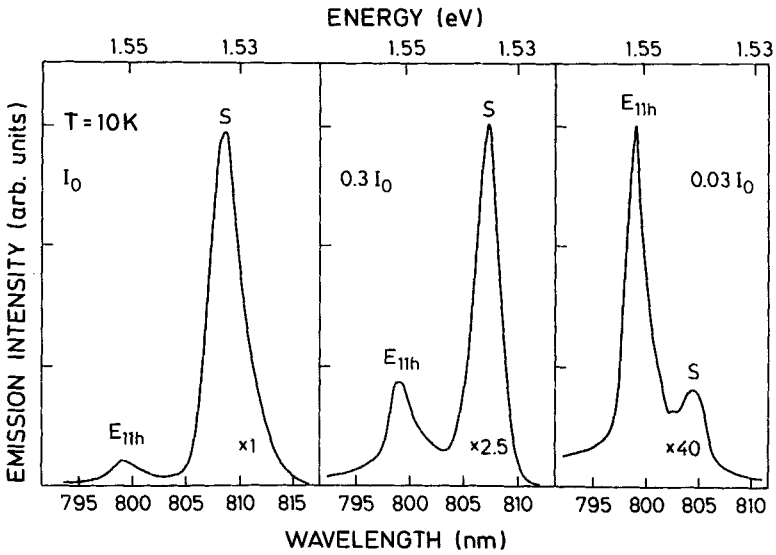

Figure 43. Electron–hole plasma luminescence measured under comparable experimental conditions in two identical GaAs/$Al_xGa_{1-x}As$ multiple quantum well structures with different degree of optical confinement of the luminescence. The sample with high optical confinement is grown on a thick $Al_{0.35}Ga_{0.63}As$ cladding layer (see text).

Figure 44.   (a) Intensity dependence of the EHP luminescence in the optically confined sample of figure 43 for $10^{-3}I_0 < I < 10^{-1}I_0$ and (b) for $0.03I_0 < I < I_0$. The inset shows the integrated emission intensity of the S and E_{11h} bands versus the excitation intensity $(I_0 \approx 1\,\mathrm{MW\,cm^{-2}})$.

photon mode distribution in the optical cavity of a non-directional laser structure (Lasher and Stern 1964). The number of quanta $M(E)$ in a single mode of radiation of energy E inside the active layer is

$$M(E) = \frac{R_{sp}(E)}{[N(E)/\tau] - R_{st}(E)},$$ (6.16)

where $R_{sp}(E)$ and $R_{st}(E)$ are the rates of spontaneous and stimulated emission at the energy E, respectively, $N(E)$ is the number of modes per unit volume and unit energy interval and τ is a term representing the photon losses in a mode of energy E due to self-absorption, transmission and scattering of the luminescence (Q-factor of the mode). For modes with high losses (small Q-factor), R_{st} can hardly approach $N(E)/\tau$. Therefore, the denominator of equation (6.16) is large, resulting in a small number of quanta in the given mode. This situation is usually achieved when the spontaneous luminescence of the quantum well can be absorbed by the underlying GaAs buffer layer due to the poor optical confinement of the structure. On the contrary, for modes with low losses (high Q-factor) even a small $R_{st}(E)$ rate can approach $N(E)/\tau$, resulting in a vanishing denominator for equation (6.16), i.e. in a very large number of photons in the low loss mode. Under this condition a sharp stimulated emission line appears in the luminescence spectrum of the crystal. In a phenomenological explanation this means that all the radiative recombination processes in the crystal occur through the lasing channel owing to the large Q-value of the corresponding fraction of modes. The limit for the existence of a large amount of stimulated emission is given by the condition

$$\frac{N(E)}{\tau} = R_{st}(E).$$ (6.17)

Using the well-known relation between the rate of spontaneous and stimulated emission (Lasher and Stern 1964) the condition of equation (6.17) becomes

$$R_{st}(E) = R_{sp}(E)\left[1 - \exp\frac{E - \mu(n)}{k_B T}\right] = \frac{N(E)}{\tau},$$ (6.18)

where $\mu(n) = F_e(n) + F_h(n) + E_g'(n)$. Equations (6.17) and (6.18) establish an upper limit for the steady-state quasi Fermi levels of the EHP, thus giving a saturation of the spontaneous emission. Under these conditions any increase of the radiative recombination rate occurs through the stimulated emission channel. The discussed mechanism explains the spectral properties of the EHP luminescence shown in figure 43. Multiple quantum well structures in which optical losses in the active layer are large do not show optical amplification, and the EHP spontaneous luminescence exhibits the characteristic band filling behaviour. This is the case for sample B with thin active layers, in which self-absorption of the spontaneous luminescence occurs in the GaAs buffer layer and part of the photogenerated carriers are lost in the underlying substrate. On the contrary, thick multiple quantum well heterostructure epilayers provide an improved optical confinement of the emitted luminescence, which reduces the modal losses in the cavity, thus resulting in the observed sharp emission band. In multiple quantum well samples with a large number of wells ($p > 100$), the effective penetration depth of the exciting radiation usually only involves the first few ten periods. Therefore, the underlying slabs act as an optical confinement layer providing a negative refractive

index discontinuity of the order of 5‰, which is largely sufficient to confine the luminescence in the active layer. The optical confinement is even more efficient in multiple quantum well heterostructures grown on a 1 μm thick cladding layer.

The enhancement of the stimulated emission efficiency through the effect of the optical confinement on the modal distribution in the quantum well is confirmed by the time evolution of the S-band. In figure 45 we show the high-excitation intensity time-resolved luminescence obtained from the samples of figure 43 (Cingolani *et al.* 1990d). The radiative recombination of the EHP in the optically confined sample (sample A) occurs through the extremely fast stimulated emission channel, having a decay time of $\tau_A \simeq 30$ ps. This short luminescence decay time indicates a very large R_{st} rate for the S-emission, while the narrow linewidth clearly evidences the saturation of the spontaneous emission. On the contrary, sample B exhibits the usualy broad band filling luminescence with a decay time of $\tau_B \simeq 600$ ps. Our results are in agreement with the optical gain studies of Göbel *et al.* (1985), who first observed a shortening of the decay time of the quantum well luminescence over the stimulated emission threshold.

The measurement of the temporal evolution of the optically amplified EHP luminescence provides a unique means to detect the transient band-gap renormaliz-ation in quantum wells (Cingolani *et al.* 1990d). Since the stimulated emission occurs at the edge of the renormalized band gap where self-absorption losses are reduced, the time evolution of the spectral position of the S-band can be used to probe the band gap
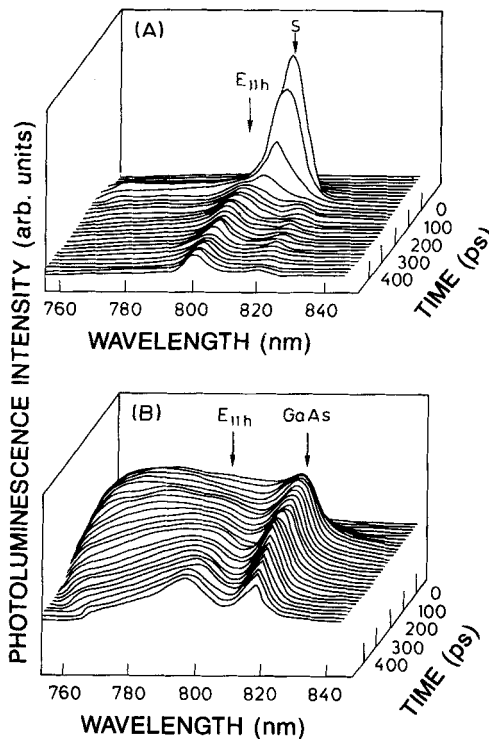

Figure 45. Temporal evolution of the stimulated emission (S-band) from the optically confined GaAs/Al$_x$Ga$_{1-x}$As multiple quantum well structure of figure 43 (sample A) and of the band filling luminescence from the unconfined GaAs heterostructure (sample B). The GaAs emission arises from the bulk GaAs buffer. The temperature is 4 K and the excitation intensity is $I_0/40$ ($I_0 \simeq 180$ MW cm^{-2}).

edge energy at different carrier densities and at different delays after the formation of the EHP. Assuming that the carrier density decreases exponentially as

$$n(t) \approx \exp(-t/\tau), \tag{6.19}$$

the band gap renormalization should in fact diminish following the $n^{1/3}$ power-law (see section 5.1), i.e.

$$\Delta E \approx n(t)^{1/3} \simeq \exp(-t/(3\tau)). \tag{6.20}$$

The time evolution of the S-band is shown in figure 46 for three different photogeneration rates. Below the stimulated emission threshold no S-emission is observed. Above a critical excitation intensity, the S-band appears. At early times the S-band is red-shifted with respect to the exciton line by several tens of meV, depending on the initial photogenerated carrier density, i.e. on the pump intensity. For longer times the S-band blue-shifts and finally merges with the E_{11h} band. This behaviour clearly reflects the decrease of the carrier density recombining at the S-band energy. The ΔE_g values at different delay times can be derived from the splitting between the S-band peak and the energy position of the $n = 1$ electron to heavy-hole interband transition, as obtained from absorption measurements, and located at 1·562 eV in sample A. This is shown in figure 47. The transient BGR occurs within 150 ps after the excitation, exemplifying a fast change in the absorption edge of the excited crystal. The time dependence of the band gap renormalization is in excellent agreement with the theoretical dependence given by equation (6.20) (dashed lines in figure 47). This finding demonstrates that the transient BGR follows the time dynamics of the carrier population. It is worth noting that this transient renormalization of the energy gap is expected to be the basis of the increasing absorption bistability of many semiconductors, as theoretically predicted by Schmitt-Rink, Ell, Koch, Schmidt and Haug (1984). This result is particularly interesting in view of the important applications in fast photonic switching devices based on this non-linear effect.
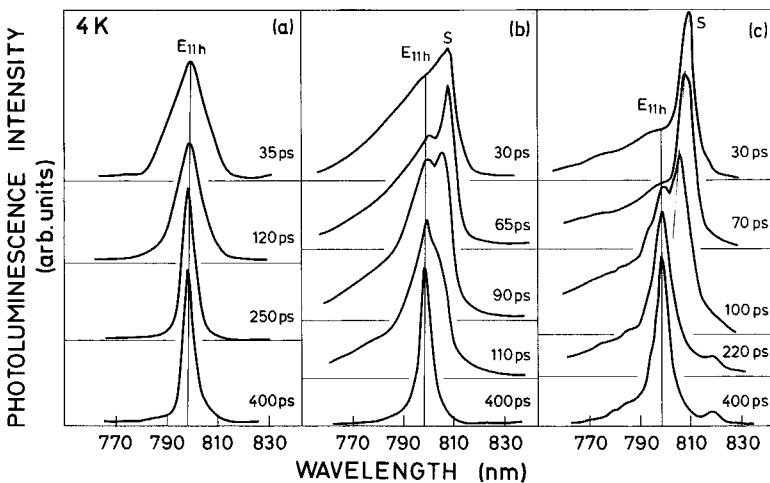

Figure 46. Time evolution of the S-band peak position at different excitation intensities and at 4 K: (*a*) below the stimulation threshold ($I = I_0/400$), (*b*) at $I_0/100$ and (*c*) at $I_0/40$. The lines are guides for the eye indicating the E_{11h} exciton and the S-band shift.
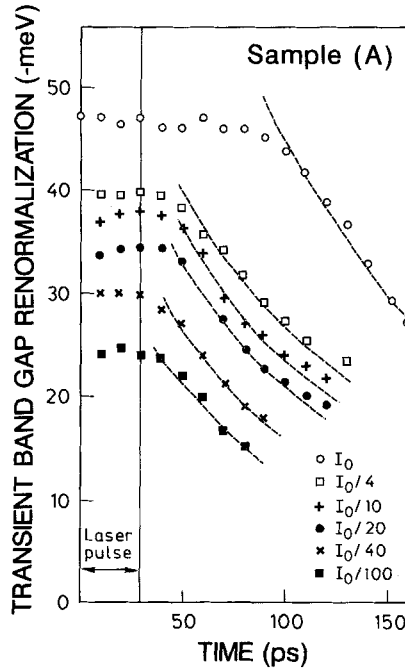
Figure 47.   Transient band gap renormalization versus time at different photogeneration rates. The vertical line defines the end of the exciting pulse. The dashed curves are the exponential regression with the expected $\exp(-t/3\tau)$ decay rate, equation (6.20), corresponding to the $\Delta E_g \simeq n^{1/3}$ power law.

From the results discussed we can also obtain a quantitative measure of the net band gap renormalization at fixed delay times Δt, i.e. at density $n(\Delta t)$, thus measuring the density dependence of the BGR. To do that we need to evaluate the initial photogenerated carrier density in the crystal. Neglecting non-linear absorption processes the carrier density is

$$n(t=0) \simeq \frac{\tau I}{\hbar \omega} (\exp(-\alpha m L_z) - 1), \qquad (6.21)$$

where $\hbar\omega$ is the exciting photon energy (2·42 eV), α the absorption coefficient ($\alpha \simeq 10^5 \, \mathrm{cm}^{-1}$ at $\hbar\omega = 2\cdot41$ eV), m the number of GaAs wells and I the excitation intensity. The short carrier lifetime in the optically confined sample results in an initial photogenerated carrier density reduced by a factor of τ_A/τ_B compared to sample B under identical excitation conditions. In addition, the carrier density scales linearly with excitation intensity. This allows us to estimate the actual photogeneration rate in sample A by scaling the carrier density obtained by the line shape fitting of the luminescence of sample B with carrier lifetime and excitation intensity. The spectral position of the S-band, i.e. of the renormalized band gap edge at different delay times, can thus be related to the instantaneous carrier density in the crystal given by

$$n(\Delta t) \simeq n(t=0) \exp(-\Delta t/\tau). \qquad (6.22)$$

This is shown in figure 38, for a delay time $\Delta t = 70$ ps. The experimental points are in fair agreement with the theory, indicating the reliability of this new method to measure the BGR directly from the luminescence spectra of highly excited quantum wells.

Optical gain spectroscopy is another important technique to obtain information on the chemical potential and BGR induced by the EHP. The optical gain of the EHP can be measured directly from the transmission spectrum of the crystal under simultaneous optical pumping, as reported by Weber *et al.* (1988). In their experiment a stationary condition pump and probe absorption set-up has been used to monitor the changes in the absorption spectrum as a function of the injected carrier density. At high enough carrier densities population inversion occurs and a broad negative absorption band appears at an energy lower than the unperturbed crystal gap in the transmission spectrum. The bandwidth of the negative absorption spectrum grows with the total quasi-Fermi level of the EHP, while the low- and high-energy cross-overs follow the density-induced shift of the band gap and chemical potential, respectively (see figure 34). The BGR values measured with this method agree well with theoretical predictions and describe the band gap shrinkage over a wide carrier density range, as shown in figure 38. Similar measurements have also been adopted to study the carrier dynamics and the renormalization of higher energy sub-bands in $GaAs/Al_xGa_{1-x}As$ quantum wells under ps excitation (Levenson *et al.* 1988) or with sub-picosecond resolution (Shank, Fork, Yen, Shah, Greene, Gossard and Weisbuch 1983).

The pump and probe transmission method provides a direct means to measure the BGR in quantum wells. It may sometimes require the removal of the non-transparent substrate by etching, and the presence of interference fringes in the spectra due to the absorption in the multilayer may lead to complications. Another experimental method to measure the optical gain relies on the exponential dependence of the luminescence on the length of a stripe-shaped excitation region (Shaklee, Nahory and Leheny 1973). In figure 48 we show the optical gain spectra obtained from sample A at different photogeneration rates by means of this variable stripe length method. Neglecting broadening effects due to particle damping, $E'_g(n)$ and $\mu(n)$ can be deduced by the low- and high-energy cross-overs, while the carrier density is related to the spectral bandwidth by equations (6.5) and (6.6). It should be mentioned that an inhomogeneous broadening of the optical gain spectra can change these parameters (Kucharska and Robbins 1990). Nevertheless, the optical gain spectra shown in figure 48 clearly evidence the carrier density dependence of the EHP energy parameters. A more accurate determination of these parameters can be obtained by the line-shape fitting of the gain curve, which proceeds on the same basis as for the spontaneous luminescence. This is shown in figure 49 for a small rectangular $(2\,mm \times 150\,\mu m)$ optical cavity cleaved from sample A and excited by the 600 nm line of a pulsed dye laser at an excitation intensity of $2\,MW\,cm^{-2}$. The optical gain peaks at the S-band emission energy and exhibits a maximum value of about $8000\,cm^{-1}$. The spectrum is fitted by using the statistical model of Zielinsky *et al.* (1987). The calculated curve well reproduces the experimental data. The obtained BGR is in good agreement with the expected value at the carrier density deduced from the chemical potential of the EHP, and it compares well with the results of the pump and probe and time resolved experiments.

Before concluding we want to point out that the increased luminescence efficiency of optically confined quantum well samples strongly affects the optical gain capability of the heterostructure. The comparison of the optical gain spectra of identical samples consisting of a different number of periods demonstrates that heterostructures with a higher degree of optical confinement exhibit a maximum gain about one order of magnitude larger than the reference sample, and the optical amplification of the luminescence persists up to room temperature. In addition, the decrease of the optical
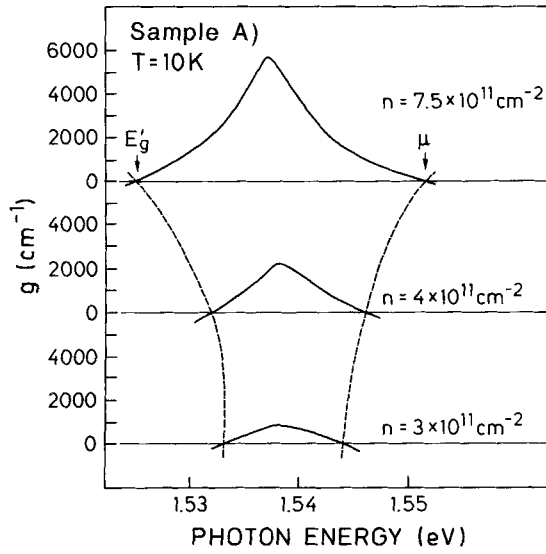
Figure 48.   Optical gain spectra at 10 K and at different carrier densities from the optically confined sample A. The carrier density is estimated from the linewidth according to equation (6.5) neglecting the broadening, and is therefore overestimated. The broken lines are guides for the eye indicating the density dependent shift of the renormalized band gap ($E'_g(n)$) and chemical potential ($\mu(n)$).
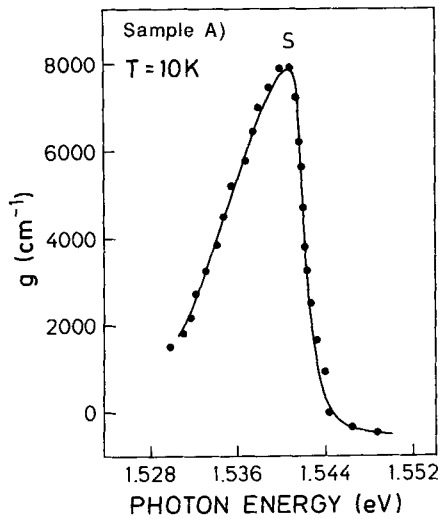

Figure 49.   Theoretical (continuous line) and experimental (dots) optical gain spectrum of a small optical cavity cleaved from the optically confined sample A.
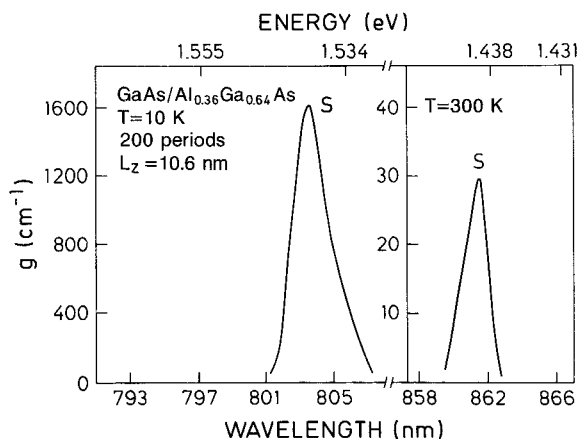
Figure 50.	Optical gain spectra obtained from a $GaAs/Al_{0.36}Ga_{0.64}As$ multiple quantum well structure consisting of 200 periods ($L_z = 10.6$ nm) at 10 and 300 K. The spectrum is taken under pulsed ns excitation at 600 nm and with a power density of $2\,MW\,cm^{-2}$.

gain threshold allows the useful range of carrier densities to be extended in which these EHP stimulated emission processes can be studied. This is shown in figure 50 for a 200 period $GaAs/Al_xGa_{1-x}As$ multiple quantum well structure which exhibits clear room temperature optical gain. Conversely, the identical multiple quantum well sample consisting of only 10 periods does not show any optical amplification. From these data we conclude that a suitable configuration of the investigated heterostructure allows one to study the electron–hole plasma properties in a wide temperature and carrier density range, thus providing more information on the thermodynamics of the EHP in quantum wells.

6.4. *The one-component plasma in quantum wells*

In the previous section we have discussed the radiative recombination processes of the two-component electron–hole plasma confined in quantum wells. We now turn to the very interesting case of the one-component confined plasma, i.e. of a degenerate Fermi gas consisting of a single species of particles (electrons or holes). Modulation doped quantum wells are a unique system for the study of this otherwise ideal many-body state. In recent years, MBE technology has allowed the fabrication of modulation doped quantum wells of high crystalline quality, where a suitable sheet of dopant atoms has intentionally been inserted in the barrier layer (Gossard 1985). In order to reach the electrostatic equilibrium condition the system undergoes a charge redistribution which results in the transfer of the excess carriers into the potential well and in the respective bending of the confining potential. The key feature of these heterostructures is the possibility of having a confined electron or hole plasma of controlled density under stationary conditions by choosing the density and the type of dopant atoms deposited in the barrier properly. This property is of great importance for the fundamental study of the electronic and optical properties of the Fermi gas and has opened up new fields for advanced opto-electronic applications (high mobility transistors and fast optoelectronic modulators).

Modulation doped quantum wells are ideal systems to study the free electron optical transitions investigated under very low excitation intensities. This provides complementary insight into the effect of the many-body interactions on the optical
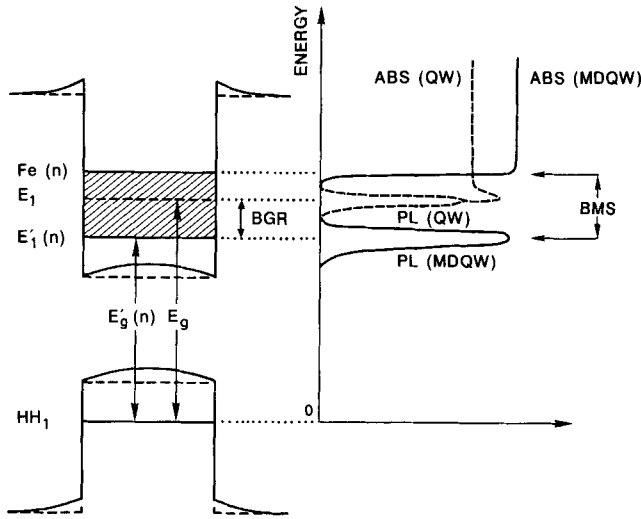
Figure 51.   Schematics of the electronic states in a n-type modulation doped quantum well (left-hand side) and changes in the optical properties induced by the free-carrier plasma. The electron plasma renormalizes the energy of the sub-band to the value $E'_1(n)$ and raises the quasi-Fermi level to $F_e(n)$, while the internal electric field bends the potential profile of the quantum well. As a consequence absorption (ABS) and emission (PL) processes occur above the Fermi-level and at the renormalized band gap edge $E'_g(n)$ (continuous lines on the right-hand side), respectively, resulting in the Burstein–Moss shift (BMS) of the optical spectra. In the corresponding undoped well (dashed lines) the absorption and the luminescence spectra coincide at the energy of the unperturbed gap E_g.

properties usually performed within the limit of intense perturbation, as discussed. The peculiar optical properties of modulation doped quantum wells have been widely studied in recent years either in the GaAs/Al$_x$Ga$_{1-x}$As or in the Ga$_x$In$_{1-x}$As/Al$_y$In$_{1-y}$As material systems (Pinczuk, Shah, Miller, Gossard and Wiegmann 1984, Penna, Shah, Pinczuk and Cho 1984, Meynadier, Orgonasi, Delalande, Brum, Bastard, Voos, Weimann and Schlapp 1986, Lee, Iwasa and Miura 1987, Livescu, Miller, Chemla, Ramaswamy, Chang, Sauer, Gossard and English 1988, Cingolani, Stolz and Ploog 1989b). The changes on the electronic properties induced by the presence of the one-component plasma and their impact on the optical properties of the modulation doped quantum well are qualitatively schematized in figure 51 for an n-type heterostructure. The one-component plasma forms in the lowest electron sub-band (E_1) and generates a band bending in the confining potential. The sub-band energy renormalizes to the value $E'_1(n)$ depending on the actual carrier density, while the quasi-Fermi level extends up to $F_e(n)$. Due to the Pauli exclusion principle, absorption transitions in the modulation doped quantum well can only involve states above the quasi-Fermi level, thus causing a blue shift of the absorption edge compared to the equivalent undoped well (right-hand side of figure 51). The amount of this shift is proportional to the band filling and corresponds to the Burstein–Moss shift (BMS) usually observed in doped bulk semiconductors. On the other hand, radiative recombination processes are expected to occur at the bottom of the sub-band $E'_1(n)$. Therefore the luminescence red-shifts, compared to the undoped well, due to the band gap renormalization. In the following we discuss the experimental results obtained on a set of high quality n-type modulation doped Ga$_{0.53}$In$_{0.47}$As/Al$_{0.52}$In$_{0.48}$As multiple quantum wells of different periods and doping density.
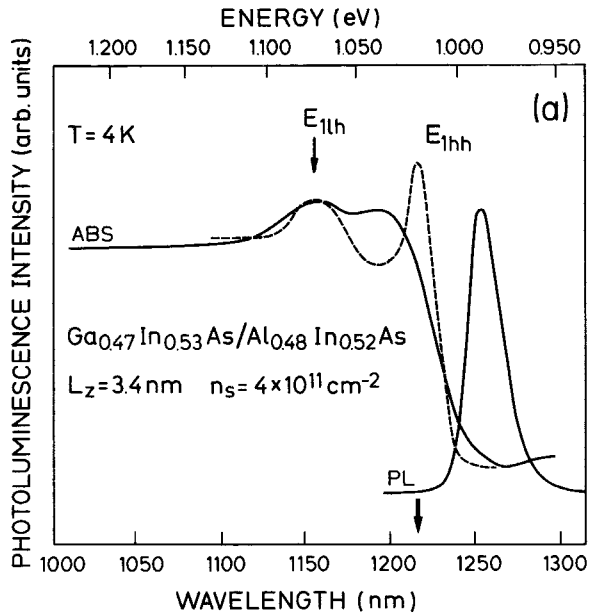
Figure 52. Absorption spectra (ABS) of a modulation doped a $Ga_xIn_{1-x}As/Al_yIn_{1-y}As$ multiple quantum well (continuous line) and an undoped multiple quantum well (dashed line) with identical structural parameters. The sheet electron density per well is $n_s = 4 \times 10^{11}\,cm^{-2}$. The PL line indicates the photoluminescence from the modulation doped quantum well. The vertical arrows indicate the energy position of the heavy-hole (E_{11h}) and light-hole (E_{11l}) excitons in the undoped well.

In figure 52 we show the comparison of the absorption spectra of two identical $Ga_{0.48}In_{0.52}As/Al_{0.47}In_{0.53}As$ samples, one of which is undoped and the other is modulation doped with a sheet electron density of $4 \times 10^{11}\,cm^{-2}$. Several features are noteworthy: first, the heavy-hole exciton peak is absent in the absorption spectrum of the modulation doped sample due to the screening of the Coulomb interaction. Second, neither the absorption edge nor the luminescence lie at the energy of the excitonic transition measured in the undoped sample. The absorption edge in the modulation doped quantum well is blue-shifted with respect to the exciton peak of the undoped sample while the luminescence is displaced towards low energies. In addition, the observed Burstein–Moss shift of 40 meV is much larger than the Stokes shift measured in the undoped sample (about 10 meV) and clearly reflects the Fermi level extension expected for the carrier density of the investigated sample. The observed features exemplify the specific recombination and absorption processes of the one-component plasma. It is worth noting that the coincidence in the energy position of the light-hole peak in both the doped and the undoped quantum wells guarantees that the two samples have identical configurational parameters and that the alloy potential fluctuations in both heterostructures do not appreciably affect the comparison of the optical spectra.

The energy position of the luminescence deserves a more detailed discussion, since it reflects the band gap renormalization in the quantum well. First it is important to note that the observed luminescence arises from free-carrier recombination as no excitons are present in the modulation doping quantum wells. The plasma luminescence is
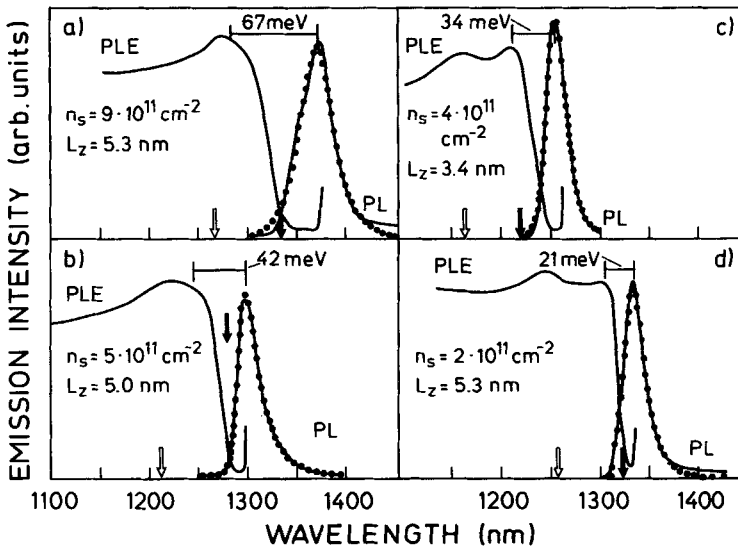
Figure 53. Low temperature photoluminescence excitation (PLE) and luminescence (PL) for a set of modulation doped $Ga_{0.47}In_{0.53}As/Al_{0.48}In_{0.52}As$ multiple quantum well structures with different sheet electron densities. The dotted curves are the theoretical luminescence line-shapes calculated by means of equation (6.23). The vertical arrows indicate the energy position of the light-hole (white arrow) and heavy-hole (black arrow) exciton transitions in the corresponding undoped samples.

therefore easily observed in modulation doped samples under very low power cw excitation. This opens the possibility to study the one-component plasma energetics as a function of the carrier density in quantum wells with different modulation doping densities, as shown in figure 53, where the absorption and PL spectra of several n-type modulation doped $Ga_{0.47}In_{0.53}As/Al_{0.48}In_{0.52}As$ multiple quantum wells are compared. The BMS between the PL and the absorption edge increases according to the well known relation $\Delta E = F_e(n)(1 + m_e/m_h)$, provided the in-plane heavy-hole mass is used in the calculations (Livescu *et al.* 1988). More quantitative information on the luminescence can be obtained by a line shape fit of the free-carrier luminescence. Using a simple k-conserving recombination model, where electrons are described by a quasi-equilibrium Fermi function and holes are distributed according to a Boltzmann statistic (Cingolani *et al.* 1989b, Munnix, Bimberg, Mars, Miller, Larkins and Harris 1989), we obtain

$$I(\hbar\omega) \approx D_e(E, \Gamma) \frac{\exp\left(\dfrac{-m_e}{m_e + m_h} \dfrac{\hbar\omega - E'_g(n)}{k_B T}\right)}{\exp\left(\dfrac{[m_h/(m_e + m_h)][\hbar\omega - E'_g(n)] - F_e(n)}{k_B T}\right) + 1}. \qquad (6.23)$$

The free parameters are the carrier temperature, the density dependent renormalized gap $E'_g(n)$, the carrier density, and the broadening parameter of the 2D density of states (Γ). The theoretically calculated curves well reproduce the experimental luminescence spectra (figure 53). The BGR data obtained from the best fit of the experimental free-carrier luminescence spectra are displayed in figure 54, as a function of the electron gas density, together with the Burstein–Moss shift. The obtained values compare well with
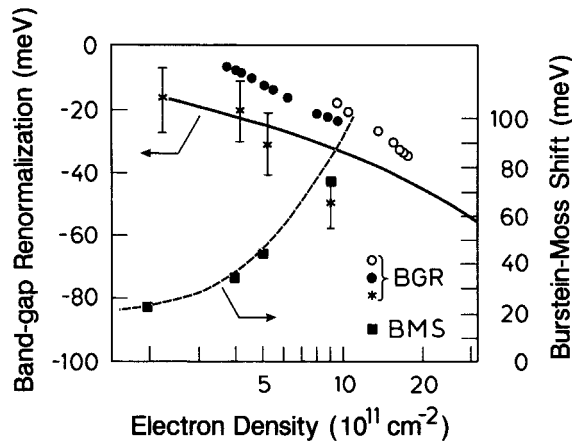
Figure 54. Band gap renormalization (BGR) and Burstein–Moss shift (BMS) obtained from the fitting of the luminescence line-shapes of the modulation doped $Ga_xIn_{1-x}As/Al_yIn_{1-y}As$ multiple quantum well samples of figures 52 and 53. The experimental BGR points represented by open and black dots have been obtained from the luminescence spectra of the modulation doped quantum well sample of figure 62 (see text). The solid curves are the theoretical BGR density dependences calculated by Das Sarma *et al.* (1990) for the one-component electron–hole plasma in $Ga_xIn_{1-x}As$ assuming an electron to heavy-hole density ratio equal to 0·1. The dashed curve is the calculated Burstein–Moss shift assuming an in-plane heavy-hole mass of $0·6 m_0$.

the theoretical model of Das Sarma *et al.* (1990) for the band gap renormalization, taking into account that the total BGR reduces in the one-component plasma compared to the normal EHP by a factor of about 2, depending on the ratio of the electron and hole densities. It should be mentioned that the large error bar in the BGR values are mostly given by the accuracy in the determination of the ternary alloy gap, whose value changes by about 11 meV for an In fluctuation of 1%. This gap variation affects the absolute value of BGR which is given by $\Delta E_g = E_g - E'_g(n)$. The band gap reduction in modulation doped quantum wells has also been studied by photoluminescence and photoluminescence excitation (Kleinman and Miller, 1985, Delalande, Bastard, Organasi, Brum, Liu, Voos, Weimann and Schlapp 1987) and by differential absorption spectroscopy (Bar Joseph, Kuo, Klingshirn, Livescu, Chang, Miller and Chemla 1987) in gated modulation doped quantum wells where the doping density can be varied continuously by applying an external electric field.

In the statistical model of equation (6.23) we have assumed vertical transitions to satisfy the k-conservation rule in the photoemission processes, i.e. all radiative recombination processes involve electrons in the Fermi gas and photogenerated holes with the same momentum. Since in low-intensity photoluminescence experiments the photogenerated low-density hole gas rapidly thermalizes to the top of the valence subband, the k-conservation for optical transitions in modulation doped quantum wells can only be achieved if recombination processes occur at $k = 0$. The k-selection rule breaks-down in the presence of interface defects or impurities which localize the holes. This localization leads to a momentum spread of holes which can then recombine with electrons having large k vectors. Therefore, hole localization due to interface roughness or defects will result in an asymmetric broadening of the high-energy side of the luminescence due to the recombination of high-energy electrons in the Fermi sea (see
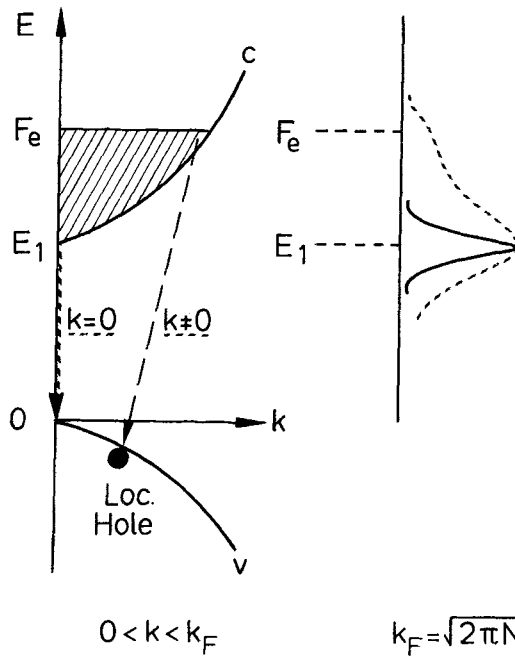
Figure 55.   Effect of the hole localization on the luminescence spectra of modulation doped
quantum wells. The localization causes a spread in the **k** vector of the holes. Non-vertical
transitions involving electrons at the Fermi edge are thus possible, resulting in the high
energy emission around F_e.

figure 55). This feature has been observed in the PL spectra of modulation doped
$Ga_xIn_{1-x}As/InP$ quantum wells and has been ascribed to the absorption enhancement
caused by the increase of electron correlation at the Fermi edge (Skolnick, Rorison,
Nash, Mowbray, Tapster, Bass and Pitt 1987). This unique spectral feature, also named
Fermi edge singularity (FES), has been theoretically calculated in the frame of a
complex many-body formalism taking into account the effect of the multiple e–h
scattering and the static screening in the Bethe Salpeter equation on the Fermi gas
luminescence (Skolnick *et al.* 1987, Ruckenstein and Schmitt-Rink 1987, Livescu *et al.*
1988, J. W. Wu 1989a, b). The measured and calculated line shapes of the FES in the
free-carrier luminescence of the modulation doped quantum wells are shown in
figure 56.

Unlike the excitonic and free-carrier emission, the sharp Fermi edge singularity
disappears from the PL spectra by slightly increasing the temperature or the excitation
intensity. The striking observation of FES in the PL spectra of modulation doped
quantum wells indicates a high degree of localization of holes responsible for these k-
non-conserving radiative recombination processes. However, in the modulation doped
$Ga_xIn_{1-x}As/Al_yIn_{1-y}As$ multiple quantum well structures used for our study we have
not observed any enhancement of the luminescence at the Fermi edge (see figure 53).
This implies that in our samples alloy fluctuations or other extrinsic effects causing
important localization phenomena do not exist. In these high quality samples we were
able to observe a weak Fermi edge singularity only in the absorption spectra (Cingolani
et al. 1989b). In figure 57 where we dipict the PLE spectra of the 3·4 nm multiple
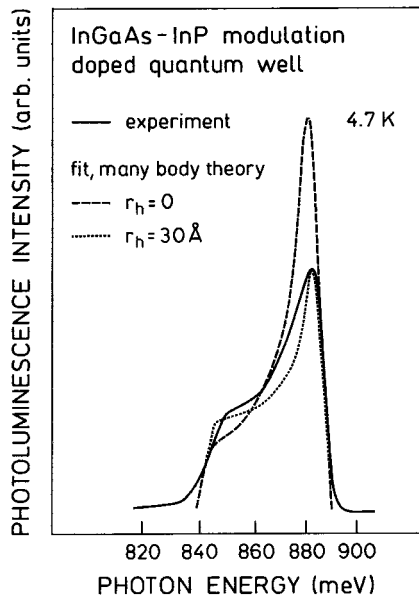
Figure 56. Fermi edge singularity in the luminescence spectrum of a modulation doped $Ga_xIn_{1-x}As/InP$ quantum well structure at 4·7 K (solid line). The dashed and the dotted lines are the theoretical spectra calculated assuming a localized hole with in-plane radius $r_h = 0$ and $r_h = 30$ Å, respectively (after Skolnick *et al.* 1987).
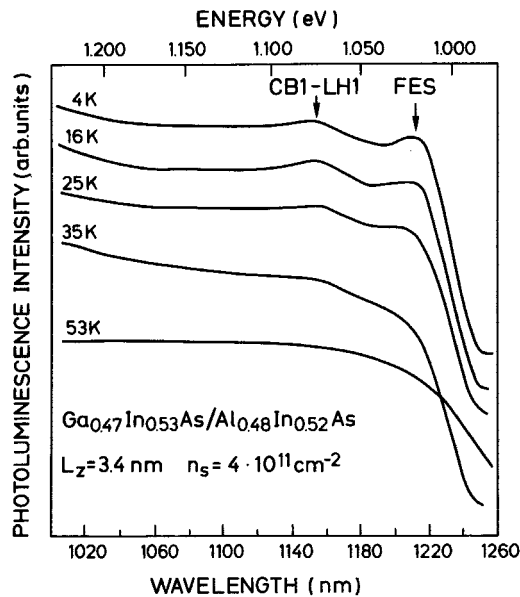
Figure 57. Temperature dependence of the Fermi edge singularity (FES) in the photoluminescence excitation spectra of a *n*-type modulation doped $Ga_xIn_{1-x}As/Al_yIn_{1-y}As$ quantum well structure. Unlike the light-hole to conduction band transition (CB1–LH1), the FES feature disappears around 30 K.
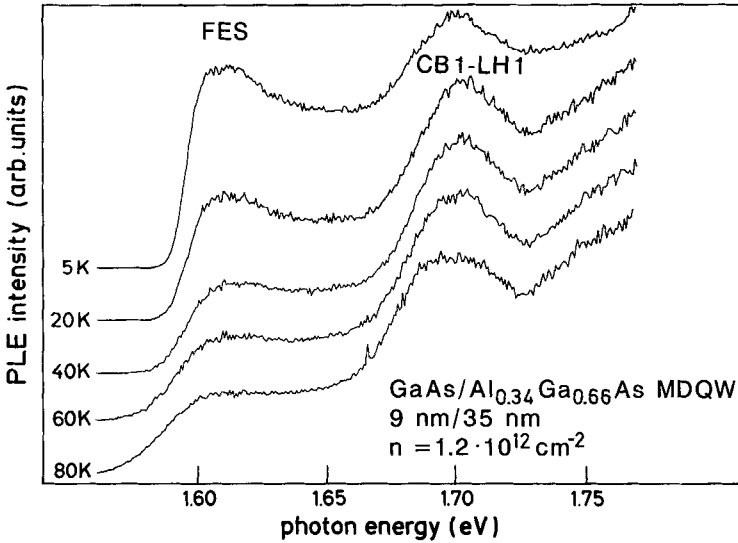
Figure 58.   As in figure 58 but for a $GaAs/Al_xGa_{1-x}As$ heterostructure.

quantum well sample measured in the temperature range 5–53 K. The most interesting feature is a peak close to the Burstein–Moss edge which rapidly disappears by increasing the temperature. This peak cannot be related to excitonic effects, as already discussed. Instead, it is related to the absorption enhancement due to the FES in the 2D plasma. Similar observations have also been reported for modulation doped $GaAs/Al_xGa_{1-x}As$ quantum wells (Livescu et al. 1988, Lee et al. 1987, Kalt, Leo, Cingolani and Ploog 1989b). This absorption enhancement is a characteristic feature of the many-body interactions in the dense electron gas recombining with the photogenerated holes. In fact, the FES is due to the increase of the multiple electron scattering processes only for those electrons close to the Fermi level, which can be scattered into empty states. Conversely, electrons well below the Fermi level have no free final states for the scattering processes, owing to the Pauli exclusion principle, and they do not contribute to the increase of the electron-correlation at the Fermi edge. With increasing temperature the electrons gain energy and the Fermi level spreads in energy. Therefore, the strength of the electron correlation decreases dramatically, resulting in the thermal quenching of the Fermi edge singularity. This is clearly shown in the temperature dependence of the FES of modulation doped $Ga_xIn_{1-x}As/Al_yIn_{1-y}As$ and $GaAs/Al_xGa_{1-x}As$ quantum wells shown in figures 57 and 58. A similar behaviour is also observed when increasing the excitation intensity (Livescu et al. 1988, Kalt et al. 1989b) as shown in figure 59. This behaviour reflects the decrease of the electron correlation due to the increase of phase space occupation and exchange effects (Livescu et al. 1988).

The enhancement of the absorption at the Fermi edge is described by a modified interband density of states

$$D(\hbar\omega) \simeq D_0(\hbar\omega)\rho(\hbar\omega), \tag{6.24}$$

where $D_0(\hbar\omega) = (1 - f_e)$ is the single particle density of states, and $\rho(\hbar\omega)$ is the correlation enhancement due to the multiple Coulomb scattering. Assuming that the radiative recombination efficiency does not change in the narrow investigated spectral range (i.e.
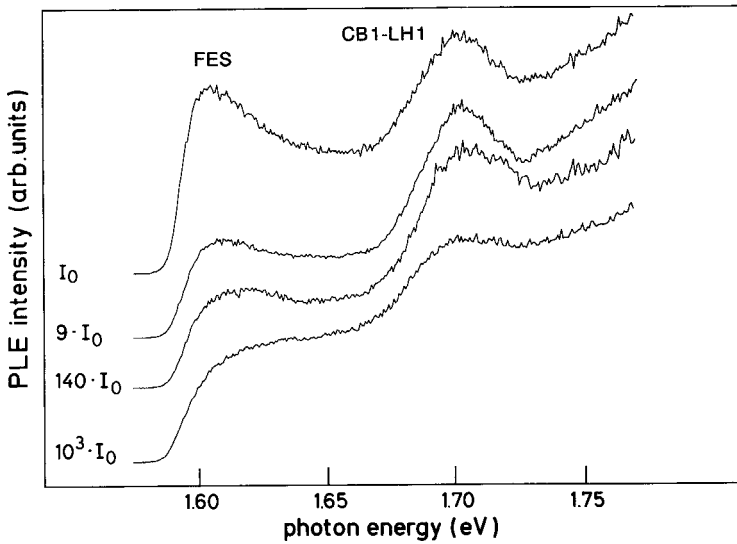
Figure 59. Intensity dependence of the Fermi edge singularity in the photoluminescence excitation spectra of the modulation doped $GaAs/Al_xGa_{1-x}As$ sample of figure 57.

that the PLE is proportional to the absorption) the $D(\hbar\omega)$ factor in equation (6.24) is directly given by the experimental PLE line shape. The single particle density of states without many-body correction $D_0(\hbar\omega)$ is determined by fitting the tails of the experimental PLE curves to the expression $(1-f_e)$. In this way the correlation enhancement can be derived from the experimental curves (Kalt *et al.* 1989b, Cingolani, Stolz, Zhang and Ploog 1989d) according to

$$\rho(\hbar\omega) \simeq \frac{D(\hbar\omega)}{D_0(\hbar\omega)}. \qquad (6.25)$$

This procedure is accurate since excitonic absorption does not contribute to the tail of the PLE spectrum in the investigated samples (see figure 57). The results of these calculations are shown in figures 60 and 61 for the modulation doped $Ga_{0.47}In_{0.53}As/Al_{0.48}Ga_{0.52}As$ and $GaAs/Al_xGa_{1-x}As$ multiple quantum wells investigated in figures 57 and 58, respectively. The curves represent the deviation from the unity ratio in equation (6.25), i.e. the deviation form the single particle interband density of states due to the correlation enhancement in the absorption. The obtained curves peak at the Burstein– Moss edge and their integrated areas scale roughly as $1/k_BT$. The correlation enhancement drops dramatically with increasing temperature and disappears around 50 K in good agreement with theoretical expectations (Livescu *et al.* 1988, Wu 1989a). It is interesting to note that the FES feature is much more pronounced in $GaAs/Al_xGa_{1-x}As$ than in the $Ga_{0.47}In_{0.53}As/Al_{0.48}In_{0.52}As$ materials system. The is probably due to the intrinsic fluctuation of the crystal potential of the ternary alloy heterostructure which somehow affects the long-range correlation in the one carrier plasma. We emphasize that the FES is a peculiar property of the modulation doped heterostructures containing a degenerate electron or hole gas, and it can be considered as a unique counterpart of the excitonic enhancement in degenerate semiconductors and metals proposed by Mahan (1967).
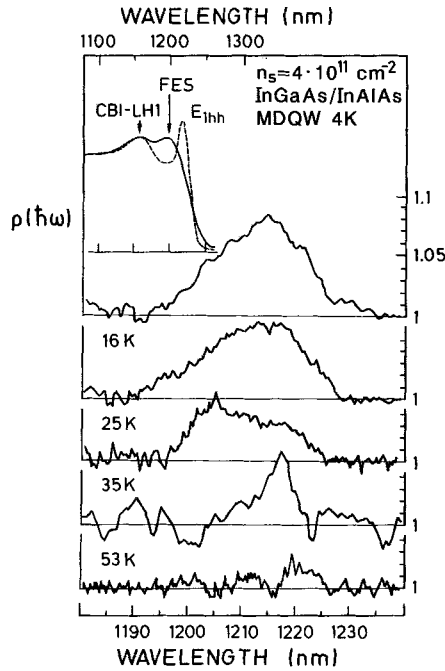
WAVELENGTH (nm)

1100   1200   1300

$\rho(\hbar\omega)$

FES

CBI-LH1 | E_{1hh}

$n_s = 4 \cdot 10^{11}$ cm^{-2}
InGaAs/InAlAs
MDQW 4K

1.1

1.05

1

16 K

1

25 K

1

35 K

1

53 K

1

1190 1200 1210 1220 1230
WAVELENGTH (nm)

Figure 60.   Temperature dependent correlation enhancement at the FES energy in the modulation doped Ga$_x$In$_{1-x}$As/Al$_y$In$_{1-y}$As heterostructure of figure 57. The curves are obtained from the experimental PLE spectra as discussed in the text, equation (6.25).
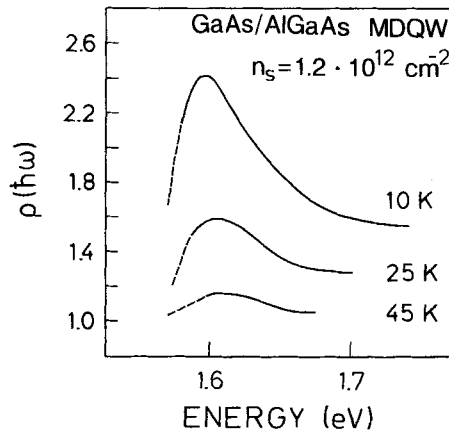
$\rho(\hbar\omega)$

2.6

2.2

1.8

1.4

1.0

GaAs/AlGaAs MDQW
$n_s = 1.2 \cdot 10^{12}$ cm^{-2}

10 K

25 K

45 K

1.6   1.7
ENERGY (eV)

Figure 61.   The same as in figure 60 but for the GaAs/Al$_x$Ga$_{1-x}$As heterostructure of figure 58. The $\rho(\hbar\omega)$ curves have been suitably smoothened.

On the basis of the described results we conclude that the correlation enhancement at the Fermi edge considerably changes the optical spectra of modulation doped quantum wells. Unlike the intrinsic FES in the absorption line-shape, the appearance of this spectral feature in the luminescence needs some extrinsic localization process which releases the *k*-conservation in the recombination between electrons at large *k* vectors and holes at *k* = 0. As discussed before, this process results in the broadening of the electron-plasma luminescence around the chemical potential energy. Conversely,

samples with negligible localization exhibit a k-conserving free-carrier emission with symmetrical line shape and a linewidth considerably narrower than the total quasi-Fermi level of the plasma. This finding raises the interesting question whether a suitable control of the hole-localization process in the modulation doped quantum wells can be used to force electrons of any momentum $(0 < k < k_F)$ to recombine with localized holes. In this case the real step-like dispersion of the electron gas density of states should be directly observable in luminescence. A striking demonstration of this effect is given in figure 62, where we show the intensity dependence of the pure 2D electron gas recombination as a function of the excitation intensity in n-type modulation doped $Ga_{0.47}In_{0.53}As/Al_{0.48}In_{0.52}As$ quantum wells (Zhang, Cingolani and Ploog 1990). The basic idea to achieve this perfectly two-dimensional Fermi gas luminescence is the controlled doping of the well layer with a suitable concentration of Be acceptors (about $3 \times 10^{16}\,cm^{-3}$). Under continuous-wave photoexcitation the electron plasma generated by modulation doping can only recombine with holes localized at the Be acceptor sites. To a first approximation, we can assume that all the radiative recombination processes in this spectra do not fulfill the k-conservation rule. As a consequence, optical transitions in the plasma involve all electrons with energy $0 < E < F_e(n)$. The resulting flat and squared line-shape of the emission spectrum essentially reflects the occupation of the first sub-band up to the quasi-Fermi level. The
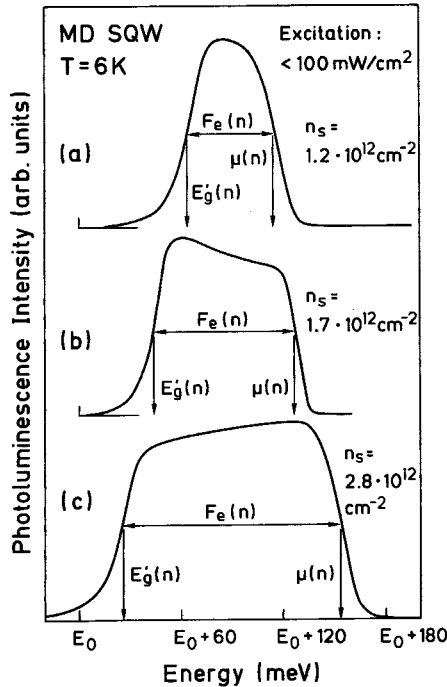

Figure 62. Electron–plasma luminescence spectra obtained fron a set of n-type modulation doped $Ga_xIn_{1-x}As/Al_yIn_{1-y}As$ quantum wells with different sheet electron densities. k-Selection rules are relaxed by the controlled insertion of Be acceptors in the well providing efficient hole localization. The width and the energy positions of the tails at half maximum are arbitrarily chosen to evaluate the quasi-Fermi level $[F_e(n)]$, the renormalized band gap $[E'_g(n)]$ and the chemical potential $[\mu(n)]$, respectively. The spectra are shifted in energy for a better comparison.

linewidth of the 2D plasma increases with the doping density, i.e. it follows the quasi-Fermi level increase, in different samples. In addition, the abrupt tails of the luminescence allow the edges of the renormalized band gap and the chemical potential to be measured with good accuracy, as shown in figure 62.

Up to now we have mainly addressed the optical properties of the one-component electron plasma, when holes have been introduced by low intensity photoexcitation to probe the radiative recombination processes. Dramatic changes occur when the photogeneration rate is increased in such a way that the hole population is no longer negligible with respect to the electron density. Under these conditions a transition from one-component to two-components electron–hole plasma is expected. This effect has been observed in cathodoluminescence (Munnix et al. 1989) and in optical gain experiments (Cingolani, Stolz, Ploog, Ferrara and Moro 1989e) performed in modulation doped GaAs and $Ga_{0.47}In_{0.53}As$ quantum wells. In figure 63 we show the edge luminescence taken from an 8·2 nm $Ga_{0.47}In_{0.53}As/Al_{0.48}In_{0.52}As$ multiple quantum well heterostructure collected at different lengths l of the excitation region on the sample surface (the power density was of the order of 1 MW cm^{-2}). At short stripe
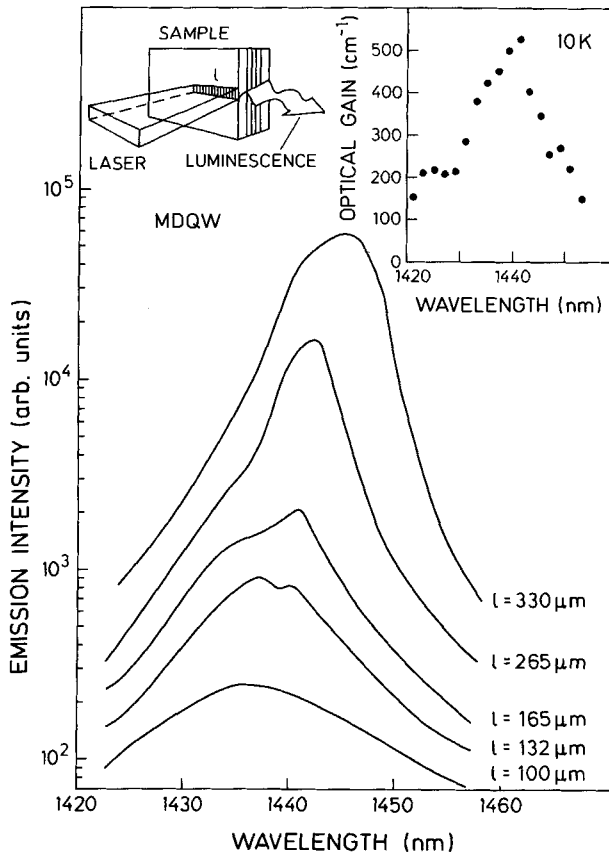
Figure 63. One-component and two-component plasma luminescence spectra measured in a modulation doped $Ga_{0.47}In_{0.53}As/Ga_{0.48}In_{0.52}As$ multiple quantum well structure with $L_z = 8·4$ nm and $n_s = 4 \times 10^{11} cm^{-2}$, at different lengths of the excited region on the crystal surface. The right-hand side inset shows the resulting optical gain spectrum at low temperature. The excitation configuration is depicted in the left corner.

lengths ($l < 130\,\mu\text{m}$) the emitted luminescence coincides with the one-component plasma free-carrier emission measured under low intensity excitation. By increasing the length of the excited region, optical amplification of the luminescence occurs and a superlinear emission arises in the low energy tail of the one-component plasma emission. A similar behaviour is observed in backscattering geometry, but at higher excitation intensities. The unsaturated optical gain spectrum obtained from these curves is shown in the inset of figure 61. The gain curve peaks at the energy position of the superlinear emission and has a maximum value of about $500\,\text{cm}^{-1}$ at low temperature. The presence of the stimulated emission clearly indicates that a photo-induced change from one-component to two-components plasma has occurred in the modulation doped quantum well. At low carrier densities the luminescence is dominated by the one-component plasma recombination. When increasing the photogeneration rate, the normal two-component EHP sets in and stimulated emission can easily be achieved because the original large excess of electrons favours the population inversion. It is worth noting that, based on this idea, ultra-high-speed laser diodes have been successfully fabricated from modulation doped quantum wells with modulation frequencies as high as $30\,\text{GHz}$ (Mishima, Tanque and Uomi 1989).

7. Conclusions

In this review paper we have attempted to provide a unified and comprehensive description of the radiative recombination processes occurring in III–V semiconductor quantum wells and superlattices under different excitation regimes. The change from the dilute exciton gas via the interacting excitonic states domain to the formation of the dense electron–hole plasma phase have been systematically studied through the modification of the luminescence properties of artificially layered crystals. The resulting scenario provides a lot of information on the electronic and excitonic states in quantum wells and on many-body interactions in quasi-two-dimensional systems. We have identified three distinct photogeneration mechanisms and three quasi-particle density ranges in which the optical response of the crystal is characterized by peculiar radiative recombination processes. In the low density range, the application of resonant photogeneration turns out to be the most powerful tool for the investigation of the electronic states in quantum wells, through the relaxation of different excitonic states. Further, excitation in the transparency region of the crystal provides a unique means to study non-linear processes, like multi-photon absorption, from which information on the optical transition selection rules can be obtained. Finally, the free-carrier generation through photon absorption in the continuum of states allows the formation of different many-body states whose energetic parameters depend on the actual density of carriers and excitons. In these regimes inelastic excitonic scattering and biexciton luminescence as well as electron–hole plasma emission can be selectively investigated by tuning the photogeneration rate and the frequency of the exciting field. This overview on the radiative recombination mechanisms in quantum wells under different excitation conditions, as summarized in figure 2, has evidenced the competition between different interaction processes and the importance, not only for fundamental research, of these effects for a comprehensive description of the optical and electronic properties of semiconductor quantum-wells.

Acknowledgements

References

ALAVI, K., TEMKIN, H., WAGNER, W. R., and CHO, A. Y., 1983, *Appl. Phys. Lett.*, **42**, 254.

ANDREANI, L. C., and PASQUARELLO, A., 1988, *Europhys. Lett.*, **6**, 259.

ANDREANI, L. C., and PASQUARELLO, A., 1989, *Superlatt. Microstruct.*, **5**, 59.

ANDREANI, L. C., BASSANI, F., and PASQUARELLO, A., 1989, *Symmetry in Nature*, Quaderni della Scuola Normale Superiore, **9**, 19.

ARAKAWA, Y., and YARIV, A., 1986, *I.E.E.E. J. Quantum Electron.* QE, **22**, 1887.

BAR JOSEPH, I., KUO, J. M., KLINGSHIRN, C., LIVESCU, G., CHANG, T. Y., MILLER, D. A. B., and CHEMLA, D. S., 1987, *Phys. Rev. Lett.*, **59**, 1357.

BASSANI, F., and PASTORI PARRAVICINI, G., 1975, *Electronic States and Optical Transitions in Solids* (Oxford: Pergamon Press).

BASTARD, G., 1981, *Phys. Rev. B*, **24**, 5693.

BASTARD, G., 1982, *Phys. Rev. B*, **25**, 7584.

BASTARD, G., MENDEZ, E. E., CHANG, L. L., and ESAKI, L., 1982b, *Phys. Rev. B*, **26**, 1974.

BASTARD, G., 1988, *Wave Mechanics Applied to Semiconductor Heterostructures* (France: Les Editions Physique, Les Ulis).

BAUER, G. E. W., and ANDO, T., 1986, *Phys. Rev. B*, **34**, 1300.

BEBBS, H., and WILLIAMS, E. W., 1972, *Semiconductor and Semimetals*, **8**, 181.

BENOIT A LA GUILLAUME, C., DEBEVER, J. M., and SALVAN, F., 1969, *Phys. Rev.*, **177**, 567.

BIMBERG, D., MARS, D., MILLER, J. N., BAUER, R., and OERTEL, D., 1986, *J. Vac. Sci. Technol. B*, **4**, 1014.

BISTI, V. E., and SILIN, A. P., 1986, *Soviet. Phys. Solid St.*, **28**, 1330.

BLOOD, P., FLETCHER, E. D., and WOODBRIDGE, K., 1985, *Appl. Phys. Lett.*, **47**, 193.

BLOOD, P., 1989, *Appl. Phys. Lett.*, **33**, 1.

BOHNERT, K., KALT, H., SMIRL, A. L., NORWOOD, D. P., BOGGES, T. F., and D'HAENENS, I. J., 1988, *Phys. Rev. Lett.*, **60**, 37.

BONGIOVANNI, G., and STAEHLI, J. L., 1989, *Phys. Rev. B*, **39**, 8359.

BORESTAIN, S., FEKETE, D., VOFSI, M., SARFATY, R., and ARZA, R., 1986, *Appl. Phys. Lett.*, **50**, 442.

BRANDT, O., TAPFER, L., CINGOLANI, R., PLOOG, K., HOHENSTEIN, M., and PHILLIPS, F., 1990, *Phys. Rev. B*, **41**, 12599.

BRINKMANN, W. F., RICE, T. M., and BELL, B., 1973, *Phys. Rev. B*, **8**, 1570.

CARDONA, M., CHRISTENSEN, N. E., and FASOL, G., 1988, *Phys. Rev. B*, **38**, 1806.

CATALANO, I. M., CINGOLANI, A., FERRARA, M., and LUGARA', M., 1980, *Opt. Acta*, **27**, 625.

CATALANO, I. M., CINGOLANI, A., and LEPORE, M., 1986, *Phys. Rev. B*, **33**, 7270.

CATALANO, I. M., CINGOLANI, A., CINGOLANI, R., and LEPORE, M., 1988, *Physica scripta*, **37**, 579.

CATALANO, I. M., CINGOLANI, A., CINGOLANI, R., LEPORE, M., and PLOOG, K., 1989a, *Phys. Rev. B*, **40**, 1312.

CATALANO, I. M., CINGOLANI, A., CINGOLANI, R., LEPORE, M., and PLOOG, K., 1989b, *Solid-St. Commun.*, **71**, 217.

CATALANO, I. M., CINGOLANI, A., LEPORE, M., CINGOLANI, R., and PLOOG, K., 1990, *Phys. Rev. B*, **41**, 12937.

CHARBONNEAU, S., STEINER, T., THEWALT, M. L. W., KOTELES, E. S., CHI, J. Y., and ELMAN, B., 1988, *Phys. Rev. B*, **38**, 3583.

CHEMLA, D. S., MILLER, D. A. B., SMITH, P. W., GOSSARD, A. C., and WIEGMANN, W., 1984, *I.E.E.E. J. quant. Electron.* QE, **20**, 265.

CHEMLA, D. S., and MILLER, D. A. B., 1985, *J. opt. Soc. Am. B*, **2**, 1155.

CHEN, Y., CINGOLANI, R., ANDREANI, L. C., BASSANI, and MASSIES, J., 1988, *Nuovo Cim. D*, **10**, 847.

CHIU, L. C., and YARIV, A., 1985, *J. Lumin.*, **30**, 551.

CINGOLANI, R., FERRARA, M., and LUGARA', M., 1987, *Phys. Rev. B*, **36**, 9589.

CINGOLANI, R., CHEN, Y., and PLOOG, K., 1988, *Europhys. Lett.*, **6**, 169.

CINGOLANI, R., CHEN, Y., and PLOOG, K., 1988b, *Phys. Rev. B*, **38**, 13578.

CINGOLANI, R., CHEN, Y., and PLOOG, K., 1988c, *Nuovo Cim. D*, **10**, 529.

CINGOLANI, R., FERRARA, M., LUGARA, M., MORO, C., CHEN, Y., BASSANI, F., MASSIES, J., and TURCO, F., 1988d, *Europhys. Lett.*, **7**, 651.

CINGOLANI, R., BALDASSARRE, L., FERRARA, M., LUGARA', M., and PLOOG, K., 1989, *Phys. Rev. B*, **40**, 6101.

CINGOLANI, R., STOLZ, W., and PLOOG, K., 1989b, *Phys. Rev. B*, **40**, 2950.

CINGOLANI, R., PLOOG, K., BALDASSARRE, L., FERRARA, M., and LUGARA', M., 1989c, *Appl. Phys. A*, **50**, 189.

CINGOLANI, R., STOLZ, W., ZHANG, Y. H., and PLOOG, K., 1989d, *J. Lumin.*, **46**, 147.

CINGOLANI, R., STOLZ, W., PLOOG, K., FERRARA, M., and MORO, C., 1989e, *Solid-st. Commun.*, **72**, 807.

CINGOLANI, R., PLOOG, K., SCAMARCIO, G., and TAPFER, L., 1990, *Opt. quant. Electron.*, **22**, S201.

CINGOLANI, R., BRANDT, O., TAPFER, L., SCAMARCIO, G., LA ROCCA, G. C., and PLOOG, K., 1990b, *Phys. Rev. B*, **42**, 3209.

CINGOLANI, R., PLOOG, K., PETER, G., HAHN, R., GÖBEL, E. O., MORO, C., and CINGOLANI, A., 1990c, *Phys. Rev. B*, **41**, 3272.

CINGOLANI, R., KALT, H., and PLOOG, K., 1990d, *Phys. Rev. B*, **42**, 7655.

CINGOLANI, R., PLOOG, K., CINGOLANI, A., MORO, C., and FERRARA, M., 1990e, *Phys. Rev. B*, **42**, 2893.

COHEN, R. M., and FANG, Z. M., 1989, *J. appl. Phys.*, **65**, 612.

COLOCCI, M., GURIOLI, M., QUERZOLI, R., VINATTIERI, A., and FERMI, F., 1990a, *Nuovo Cim. D*, **12**, 245.

COLOCCI, M., GURIOLI, M., VINATTIERI, A., FERMI, F., DEPARIS, C., MASSIES, J., and NEU, G., 1990b, *Europhys. Lett.*, **12**, 417.

DANAN, G., ETIENNE, B., MOLLOT, F., PLANEL, F., JEAN-LOUIS, A. M., ALEXANDRE, F., JUSSERAND, B., LE ROUX, G., MARZIN, J. Y., SAVARY, H., and SARMAGE, S., 1987, *Phys. Rev. B*, **35**, 6207.

DAS SARMA, S., JALABERT, R., and YANG, S.-R. ERIC, 1989, *Phys. Rev. B*, **39**, 5516.

DAS SARMA, S., JALABERT, R., and YANG, S.-R. ERIC, 1990, *Phys. Rev. B*, **41**, 8288.

DAWSON, P., WILSON, B. A., TU, C. W., and MILLER, R. C., 1986, *Appl. Phys. Lett.*, **48**, 541.

DAWSON, P., MOORE, K. J., DUGGAN, G., RALPH, H. I., and FOXON, C. T., 1986b, *Phys. Rev. B*, **34**, 6007.

DAWSON, P., MOORE, K. J., FOXON, C. T., T'HOFF, G. W., and VAN HAL, R. P. M., 1989, *J. appl. Phys.*, **65**, 3606.

DAWSON, P., 1990, *Opt. quant. Electron.*, **22**, S231.

DELALANDE, C., BASTARD, G., ORGANASI, J., BRUM, J. A., LIU, H. W., VOOS, M., WEIMANN, G., and SCHLAPP, W., 1987, *Phys. Rev. Lett.*, **59**, 2690.

DEVEAUD, B., EMERY, J. Y., CHOMETTE, A., LAMBERT, B., and BAUDET, M., 1984, *Appl. Phys. Lett.*, **45**, 1078.

DEVEAUD, B., DAMEN, T. C., SHAH, J., and TU, C. W., 1987, *Appl. Phys. Lett.*, **51**, 828.

DE MIGUEL, J. L., FUJIWARA, K., BRIONES, F., PLOOG, K., 1986, *Japan J. appl. Phys.*, **25**, L360.

DIGNAM, M. M., and SIPE, J. E., 1990, *Phys. Rev. B*, **41**, 2865.

DINGLE, R., 1975, *Festkörperprobleme XV*, edited by H. J. Queisser (Verlag).

DUGGAN, G., and RALPH, H. I., 1987, *Phys. Rev. B*, **35**, 4152.

DUGGAN, G., RALPH, H. I., DAWSON, P., MOORE, K. J., FOXON, C. T. B., NICHOLAS, R. J., SINGLETON, J., and ROGERS, D. C., 1987, *Phys. Rev. B*, **35**, 7784.

DUY PACH, V., BIVAS, A., HÖNERLAGE, B., and GRÜN, J. B., 1977, *Phys. Stat. Sol.* (b), **84**, 731.

EKENBERG, U., and ALTARELLI, M., 1987, *Phys. Rev. B*, **35**, 7585.

ELL, C., BLANK, R., BENNER, S., and HAUG, H., 1989, *J. opt. Soc. Am. B*, **6**, 2006.

FEKETE, D., BORENSTAIN, S., RON, A., and COHEN, E., 1985, *Superlatt. Microstr.*, **1**, 245.

FELDMANN, J., PETER, G., GÖBEL, E. O., LEO, K., POLLAND, H.-J., PLOOG, K., FUJIWARA, K., and NAKAYAMA, T., 1987, *Appl. Phys. Lett.*, **51**, 226.

FENG, Y. P., and SPECTOR, H. N., 1988, *I.E.E.E. J. quant. Electron.* QE, **24**, 1659.

FISHER, T., and BILLE, J., 1974, *J. Appl. Phys.*, **45**, 3937.

FORTIN, E., HUA, B. Y., ROTH, A. P., CHARLEBOIS, A., FAFARD, S., and LACELLE, C., 1989, *J. Appl. Phys.*, **66**, 4854.

FRÖHLICH, D., WILLE, R., SCHLAPP, W., and WEIMANN, G., 1988, *Phys. Rev. Lett.*, **61**, 1878.

FU, Q., LEE, D., MYSYROWICZ, A., NURMIKKO, A. V., GHUNSHOR, R. L., and KOLODZIEJSKY, L. A., 1988, *Phys. Rev. B*, **37**, 8791.

FUJIWARA, K., TSUKADA, N., and NAKAYAMA, T., 1988, *Appl. Phys. Lett.*, **53**, 675.

FUJIWARA, K., KANAMOTO, K., TSUKADA, N., MIYATAKE, H., and KOYAMA, H., 1989a, *J. Appl. Phys.*, **66**, 1488.

FUJIWARA, K., KANAMOTO, K., and TSUKADA, N., 1989b, *Phys. Rev. B*, **40**, 9698.

GERSHONI, D., TEMKIN, H., PANISH, M. B., and HAMM, R. A., 1989, *Phys. Rev. B*, **39**, 5531.

GIANNOZZO, P., GROSSO, G., and PASTORI PARRAVICINI, G., 1990, *La Rivista del Nuovo Cimento*, **13**, 1.

GIBBS, H. M., TARNG, S. S., JEWELL, J. L., WEINBERGER, D. A., TAI, K., GOSSARD, A. C., McCALL, S. L., PASSNER, A., and WIEGMANN, W., 1982, *Appl. Phys. Lett.*, **41**, 221.

GÖBEL, E. O., SHAKLEE, K. L., and EPWORTH, R., 1975, *Solid-St. Comm.*, **17**, 1185.

GÖBEL, E. O., JUNG, H., KUHL, J., and PLOOG, K., 1983, *Phys. Rev. Lett.*, **51**, 1588.

GÖBEL, E. O., HÖGER, R., KUHL, J., POLLAND, H. J., and PLOOG, K., 1985, *Appl. Phys. Lett.*, **47**, 781.

GOLDSTEIN, L., HORIKOSHI, Y., TARUCHA, S., and OKAMOTO, H., 1983, *Japan J. appl. Phys.*, **22**, 1489.

GOLOVIN, A. A., and RASHBA, E. I., 1973, *JETP Lett.*, **17**, 478.

GOSSARD, A. C., 1985, *Molecular Beam Epitaxy and Heterostructures*, edited by L. L. Chang and K. Ploog, NATO ASI series, **87**, 499.

GREENE, R., BAJAI, K. K., and PHELPS, D. E., 1984, *Phys. Rev. B*, **29**, 1807.

HAJALMARSON, H. P., 1982, *J. Vac. Sci. Techn.*, **21**, 524.

HANAMURA, E., 1975, *J. Phys. soc. Japan*, **38**, 1516.

HANAMURA, E., 1989, *Opt. quant. Electron.*, **21**, 441.

HAUG, H., and SCHMITT-RINK, S., 1985, *J. opt. Soc. Am. B*, **2**, 1135.

HAUG, H., and KOCH, S. W., 1989, *Phys. Rev. A*, **39**, 1887.

HAWRYLAK, P., 1989, *Phys. Rev. B*, **39**, 6264.

HELD, T., KUHN, T., and MAHLER, G., 1990, *Phys. Rev.*, B, **41**, 5144.

HOLONYAK JR. N., NAM, D. W., PLANO, W. E., WESELY, E. J., and HSIEH, K. C., 1989, *Appl. Phys. Lett.*, **54**, 1022.

HOLONYAK JR. N., KOLBAS, R. M., DUPUIS, R. D., and DAPKUS, P. D., 1980, *I.E.E.E. J. quant. Electron.* QE, **16**, 170.

HOLTZ, M., CINGOLANI, R., REIMANN, K., MURALIDHARAN, R., SYASSEN, K., and PLOOG, K., 1989, *Phys. Rev. B*, **41**, 3641.

HÖNERLAGE, B., LEVY, R., GRÜN, J. B., KLINGSHIRN, C., and BOHNERT, K., 1985, *Phys. Rep.*, **124**, 161.

HOU, H. Q., SEGAWA, Y., AOYAGI, Y., NAMBA, S., and ZHOU, J. M., 1990, *Phys. Rev. B*, **42**, 1284.

HUANG-SIK CHO and PRUCNAL, P. R., 1987, *Phys. Rev. B*, **36**, 3237.

HULIN, D., MYSYROWICZ, A., ANTONETTI, A., MIGUS, A., MASSELINK, W. J., MORKOC, H., GIBBS, H. M., and PEYGHAMBARIAN, N., 1986, *Phys. Rev. B*, **33**, 4389.

HUNT, N. E. J., and JESSOP, P. E., 1988, *Superlatt. Microstr.*, **4**, 671.

INOUE, M., and TOYOZAWA, Y., 1965, *J. Phys. soc. Japan*, **20**, 363.

KALT, H., BOHNERT, K., SMIRL, A. L., and BOGGESS, T. F., 1988, *Proc. 19th Int. Conf. Phys. Semicond.*, Warsaw, p. 1377.

KALT, H., SMIRL, A. L., and BOGGESS, T. F., 1989a, *J. appl. Phys.*, **65**, 294.

KALT, H., LEO, K., CINGOLANI, R., and PLOOG, K., 1989b, *Phys. Rev. B*, **40**, 12017.

KELDYSH 1982.

KESSLER, M. P., and IPPEN, E. P., 1987, *Appl. Phys. Lett.*, **51**, 1765.

KLEINMAN, D. A., 1983, *Phys. Rev. B*, **28**, 871.

KLEINMAN, D. A., and MILLER, R. C., 1985, *Phys. Rev. B*, **32**, 2266.

KLEINMAN, D. A., 1985, *Phys. Rev. B*, **32**, 3766.

KLEINMAN, D. A., 1986, *Phys. Rev. B*, **33**, 2540.

KLINGSHIRN, C., and HAUG, H., 1981, *Phys. Rep.*, **70**, 315.

KNOX, W. H., FORK, R. L., DOWNER, M. C., MILLER, D. A. B., CHEMLA, D. S., SHANK, C. V., GOSSARD, A. C., and WIEGMANN, W., 1985, *Phys. Rev. Lett.*, **54**, 1306.

KOHL, M., HEITMANN, D., TARUCHA, S., LEO, K., and PLOOG, K., 1989, *Phys. Rev. B*, **39**, 7736.

KOTELES, E. S., and CHI, J. C., 1988, *Phys. Rev. B*, **37**, 6332.

KOTELES, E. S., OWENS, D. A., BERTOLET, D. C., and LAU, K. M., 1988, *Phys. Rev. B*, **38**, 10139.

KUBOTA, K., MIZUTA, T., NAKAYAMA, M., KATOH, H., and SANO, N., 1984, *Solid-St. Commun.*, **52**, 333.

KUCHARSKA, A., and ROBBINS, D. J., 1990, *I.E.E.E. J. quant. Electron.* QE, **26**, 443.

KULAKOWSKII, V. D., LACH, E., FORCHEL, A., and GRÜTZMACHER, D., 1989, *Phys. Rev.* B, **40**, 8087.

KURODA, H., and SHIONOYA, S., 1974, *J. phys. soc. Japan*, **36**, 476.

KUSANO, J., SEGAWA, Y., AOYAGI, Y., NAMBA, S., and OKAMOTO, H., 1989, *Phys. Rev.* B, **40**, 1685.

LACH, E., LEHR, G., FORCHEL, A., PLOOG, K., and WEIMANN, G., 1990, *Surf. Sci.*, **228**, 168.

LANDSBERG, P. T., ABRAHAMS, M. S., and OSINSKI, M., 1985, *I.E.E.E. J. quant. Electron.* QE, **21**, 24.

LASHER, G., and STERN, F., 1964, *Phys. Rev.* A, **133**, 553.

LAURELLE, F., and ETIENNE, B., 1988, *Solid-St. Commun.*, **65**, 565.

LE, H. Q., LAX, B., VOJAK, B. A., and CALAWA, A. R., 1985, *Phys. Rev.* B, **32**, 1419.

LEE, H. J., JURAVEL, L. Y., WOLLEY, J. C., and SPRING THORPE, A. J., 1980, *Phys. Rev.* B, **21**, 659.

LEE, J., SPECTOR, H. N., and MELMAN, P., 1985, *J. appl. Phys.*, **58**, 1893.

LEE, J. S., IWASA, Y., and MIURA, N., 1987, *Semicond. Sci. Technol.*, **2**, 675.

LEO, K., RÜHLE, W., and PLOOG, K., 1988, *Phys. Rev.* B, **38**, 1947.

LEVENSON, J. A., ABRAM, I., RAJ, R., DOLIQUE, G., OUDAR, J. L., and ALEXANDRE, F., 1988, *Phys. Rev.* B, **38**, 13443.

LEVENSON, J. A., DOLIQUE, G., OUDAR, J. L., and ABRAM, I., 1990, *Phys. Rev.* B, **41**, 3688.

LEVY, R., HÖNERLAGE, B., and GRÜN, J. B., 1988, *Optical Non-linearities and Instabilities in Semiconductors*, edited by H. Haug (Academic Press).

LI, G. H., JIANG, D. S., HAN, H. X., WANG, Z. P., and PLOOG, K., 1989, *Phys. Rev.* B, **40**, 10430.

LIVESCU, G., MILLER, D. A. B., CHEMLA, D. S., RAMASWAMY, M., CHANG, T. Y., SAUER, N., GOSSARD, A. C., and ENGLISH, J. H., 1988, *I.E.E.E. J. quantum. Electron.* QE, **24**, 1677.

LOBENTANZER, H., STOLZ, W., NAGLE, J., and PLOOG, K., 1989, *Phys. Rev.* B, **39**, 5234.

LOUDON, R., 1962, *Proc. Phys. Soc.*, **80**, 852.

LU, Y. T., and SHAM, L. J., 1989, *Phys. Rev.* B, **40**, 5567.

MAAN, J. C., BELLE, G., FASOLINO, A., ALTARELLI, M., and PLOOG, K., 1984, *Phys. Rev.* B, **30**, 2253.

MAAN, J. C., 1987, *Physics and Applications of Quantum Wells and Superlattices*, NATO ASI ser., edited by E. E. Mendez and K. von Klitzing, **170**, 347.

MAHAN, G. D., 1967, *Phys. Rev.*, **153**, 882.

MAHAN, G. D., 1968, *Phys. Rev. Lett.*, **20**, 332.

MARZIN, J. Y., and GERARD, J. M., 1989, *Phys. Rev. Lett.*, **62**, 2172.

MASUMOTO, Y., MATSUURA, M., TARUCHA, S., and OKAMOTO, H., 1985, *Phys. Rev.* B, **32**, 4275.

MATSUURA, M., and SHINOZUKA, Y., 1984, *J. phys. Soc. Japan*, **53**, 3138.

MENENDEZ, J., PINKZUK, A., WERDER, D. J., GOSSARD, A. C., and ENGLISH, J. H., 1986, *Phys. Rev.* B, **33**, 8863.

MEYNADIER, M. H., ORGONASI, J., DELALANDE, C., BRUM, J. A., BASTARD, G., VOOS, M., WEIMANN, G., and SCHLAPP, W., 1986, *Phys. Rev.* B, **34**, 2482.

MEYNADIER, M. H., NAHORY, R. E., WORLOCK, J. M., TAMARGO, M. C., DE MIGUEL, J. L., and STURGE, M. D., 1988, *Phys. Rev. Lett.*, **60**, 1338.

MILLER, D. A. B., CHEMLA, D. S., EILENBERGER, D. J., SMITH, P. W., GOSSARD, A. C., and TSANG, W. T., 1982, *Appl. Phys. Lett.*, **41**, 679.

MILLER, R. C., KLEINMAN, D. A., TSANG, W. T., and GOSSARD, A. C., 1981, *Phys. Rev.* B, **24**, 1134.

MILLER, R. C., KLEINMAN, D. A., GOSSARD, A. C., and MONTENAU, O., 1982, *Phys. Rev.* B, **25**, 6545.

MILLER, R. C., GOSSARD, A. C., SANDERS, G. D., CHANG, Y. C., and SCHULMAN, J. N., 1985a, *Phys. Rev.* B, **32**, 8452.

MILLER, R. C., GOSSARD, A. C., and KLEINMAN, D. A., 1985b, *Phys. Rev.* B, **32**, 5443.

MILLER, R. C., and KLEINMAN, D. A., 1985, *J. Lumin.*, **30**, 520.

MILLER, R. C., TU, C. W., SPUTZ, S. K., and KOPF, R. F., 1986, *Appl. Phys. Lett.*, **49**, 1245.

MISHIMA, T., TANQUE, T., and UOMI, K., 1989, *J. Cryst. Growth*, **95**, 382.

MIYAZAWA, T., TARUCHA, S., OHMORI, Y., SUZUKI, Y., and OKAMOTO, H., 1986, *Japan J. appl. Phys.*, **25**, L200.

MOORE, K. J., DUGGAN, G., DAWSON, P., and FOXON, C. T., 1988, *Phys. Rev.* B, **38**, 5535.

MOORE, K. J., DUGGAN, G., RAUKEMA, A., and WOODBRIDGE, K., 1990a, *Phys. Rev.* B, **42**, 1326.

MOORE, K. J., DUGGAN, G., WOODBRIDGE, K., and ROBERTS, C., 1990b, *Phys. Rev.* B, **41**, 1090.

MOORE, K. J., DUGGAN, G., WOODBRIDGE, K., and ROBERTS, C., 1990c, *Phys. Rev.* B, **41**, 1095.

MORIYA, T., and KUSHIDA, T., 1976, *J. phys. Soc. Japan*, **40**, 1668.

MUNNIX, S., BIMBURG, D., MARS, D. E., MILLER, J. N., LARKINS, E. C., and HARRIS, J. S., 1989, *Superlatt. Microstr.*, **6**, 369.

NAGASAWA, N., KUWATA, M., HANAMURA, E., ITHO, T., and MYSYROWICZ, A., 1989, *Appl. Phys. Lett.*, **55**, 1999.

NAGLE, J., HERSEE, S., KRAKOWSKI, M., WEIL, T., and WEISBUCH, C., 1986, *Appl. Phys. Lett.*, **39**, 1325.

NATHAN, V., GUENTER, A. H., and MITRA, S. S., 1985, *J. Opt. Soc. Am.* B, **2**, 294.

NITHISOONTORN, M., UNTERRAINER, K., MICHAELIS, S., SAWAKI, N., GORNIK, E., and KANO, H., 1989, *Phys. Rev. Lett.*, **62**, 3078.

NITHISOONTORN, M. *et al.*, 1990, *Proc. 20th International Conference Physics of Semiconductors*, Tessaloniki (Greece).

OSSAU, W., JAKEL, B., BANGERT, E., LANDWEHR, G., and WEIMANN, G., 1986, *Surf. Sci.*, **174**, 188.

PASQUARELLO, A., and QUATTROPANI, A., 1988, *Phys. Rev.* B, **38**, 6206.

PASQUARELLO, A., and QUATTROPANI, A., 1990a, *Phys. Rev.* B, **41**, 12728.

PASQUARELLO, A., and QUATTROPANI, A., 1990b, *Proc. 20th International Conference Physics of Semiconductors*, Tessaloniki (Greece).

PENNA, A. F. S., SHAH, J., PINCZUK, A., and CHO, A. Y., 1984, *Appl. Phys. Lett.*, **46**, 184.

PETROU, A., WAYTENA, G., LIU, X., RALSTON, J., and WICKS, G., 1986, *Phys. Rev.* B, **34**, 7436.

PEYGHAMBARIAN, N., and GIBBS, H. M., 1985, *J. Opt. Soc. Am.* B, **2**, 1215.

PINCZUK, A., SHAH, J., MILLER, R. C., GOSSARD, A. C., and WIEGMANN, W., 1984, *Solid-St. Commun.*, **50**, 735.

REYNOLDS, D. C., BAJAJ, K. K., STUTZ, C. E., JONES, R. L., THEIS, W. M., YU, P. W., and EVANS, K. R., 1989, *Phys. Rev.* B, **40**, 3340.

ROGERS, D. C., SINGLETON, J., NICHOLAS, R. J., FOXON, C. T., and WOODBRIDGE, K., 1986, *Phys. Rev.* B, **34**, 4002.

RÖSSLER, U., 1988, *Solid-St. Commun.*, **49**, 943.

RUCKENSTEIN, A. E., and SCHMITT-RINK, S., 1987, *Phys. Rev.* B, **35**, 7551.

SAUER, R., HARRIS, T. D., and TSANG, W. T., 1987, *Appl. Phys. Lett.*, **62**, 3374.

SCAMARCIO, G., CINGOLANI, A., CINGOLANI, R., and PLOOG, K., 1989, *Surf. Sci.*, **223**, 1026.

SCHMITT-RINK, S., ELL, C., KOCH, S. W., SCHMIDT, H. E., and HAUG, H., 1984, *Solid-St. Commun.*, **52**, 123.

SCHMITT-RINK, S., and ELL, C., 1985, *J. Lumin.*, **30**, 585.

SCHMITT-RINK, S., CHEMLA, D. S., and MILLER, D. A. B., 1985a, *Phys. Rev.* B, **32**, 6601.

SCHMITT-RINK, S., ELL, C., and HAUG, H., 1985b, *Phys. Rev.* B, **33**, 1183.

SCHMITT-RINK, S., CHEMLA, D. S., and MILLER, D. A. B., 1989, *Adv. Phys.*, **38**, 89.

SCHUBERT, E. F., GÖBEL, E. O., HORIKISHI, Y., PLOOG, K., and QUEISSER, H. J., 1984, *Phys. Rev.* B, **30**, 813.

SHAH, J., 1986, *I.E.E.E. J. quant. Electron.* QE, **22**, 1728.

SHAH, J., 1989, *Superlatt. Microstruct.*, **6**, 293.

SHAKLEE, K., NAHORY, R. E., and LEHENY, R. F., 1973, *J. Lumin.*, **7**, 284.

SHANK, C. V., FORK, R. L., YEN, R., SHAH, J., GREENE, B. I., GOSSARD, A. C., and WEISBUCH, C., 1983, *Solid-St. Commun.*, **47**, 981.

SHIMIZU, A., 1989, *Phys. Rev.* B, **40**, 1403.

SHINADA, M., and SUGANO, M., 1966, *J. Phys. Soc. Japan*, **21**, 1936.

SHINOZUKA, Y., and MATSUURA, M., 1983, *Phys. Rev.* B, **28**, 4878.

SHIRAISHI, K., and YAMAGUCHI, E., 1990, *Phys. Rev.* B, **42**, 3064.

SKOLNICK, M. S., RORISON, J. M., NASH, K. J., MOWBRAY, D. J., TAPSTER, P. R., BASS, S. J., and PITT, A. D., 1987, *Phys. Rev. Lett.*, **58**, 2130.

SMITH, D. L., and MAILHIOT, C., 1990, *Rev. mod. Phys.*, **62**, 173.

SNOKE, D. W., WOLFE, J. P., and MYSYROWICZ, A., 1990, *Phys. Rev. Lett.*, **64**, 2543.

SOGAWA, T., and ARAKAWA, Y., 1990, *J. Appl. Phys.*, **67**, 2675.

SONG, J. J., JUNG, P. S., YOON, Y. S., CHU, H., CHANG, Y. C., and TU, C. W., 1989, *Phys. Rev.* B, **39**, 5562.

SPECTOR, H. N., 1987, *Phys. Rev.* B, **35**, 5876.

STOLZ, W., MAAN, J. C., ALTARELLI, M., TAPFER, L., and PLOOG, K., 1987, *Phys. Rev.* B, **36**, 4306.

TAI, K., MYSYROWICZ, A., SLUSHER, R. J., and CHO, A. Y., 1989, *Phys. Rev. Lett.*, **62**, 1784.

TANAKA, S., KUNO, M., YAMAMOTO, A., KOBAYASHI, H., MIZUTA, M., KUKIMOTO, H., and SAITO, H., 1984, *Japan J. appl. Phys.*, **23**, L427.

TAPFER, L., STOLZ, W., and PLOOG, K., 1989, *J. Appl. Phys.*, **66**, 3217.

TARUCHA, S., OKAMOTO, H., IWASA, Y., and MIURA, N., 1984, *Solid-St. Commun.*, **52**, 815.

TARUCHA, S., IWAMURA, H., SAKU, T., OKAMOTO, H., IWASA, Y., and MIURA, N., 1986, *Surf. Sci.*, **174**, 194.

TIKHODEEV, S. G., 1985, *Sov. Phys. Usp.*, **28**, 1.

TRÄNKLE, G., LEIER, H., FORCHEL, A., HAUG, H., ELL, C., and WEIMANN, G., 1987, *Phys. Rev. Lett.*, **58**, 419.

TRÄNKLE, G., LACH, E., FORCHEL, A., SCHOLZ, F., ELL, C., HAUG, H., WEIMANN, G., GRIFFITHS, G., KROEMER, H., and SUBBANNA, S., 1987b, *Phys. Rev. B*, **36**, 6712.

TSANG, W. T., 1984, *I.E.E.E. J. quant. Electron.* QE, **20**, 119.

TSEN, K. T., and MORCOC, H., 1986, *Phys. Rev. B*, **34**, 6018.

TSEN, K. T., SANKEY, O. F., HALAMA, G., SEN, SHU-CHEN Y., and MORCOC, H., 1989, *Phys. Rev. B*, **39**, 6276.

UETA, M., KANZAKI, H., KOBAYASHI, K., TOYOZAWA, Y., and HANAMURA, E., 1986, *Excitons*, Springer Verlag series in Solid State Sciences, **60**.

VAN DER ZIEL, J. P., 1975, *Appl. Phys. Lett.*, **26**, 463.

VAN DER ZIEL, J. P., 1976, *Phys. Rev. B*, **16**, 2775.

VAN DER ZIEL, J. P., and GOSSARD, A. C., 1978, *Phys. Rev. B*, **33**, 765.

VASHISTA, P., and KALIA, R. K., 1982, *Phys. Rev. B*, **25**, 6492.

VIÑA, L., COLLINS, R. T., MENDEZ, E. E., and WANG, W. I., 1988, *Phys. Rev. Lett.*, **58**, 832.

VIÑA, L., 1989, *Spectroscopy of the Semiconductor Heterostructures*, edited by G. Fasol, A. Fasolino and P. Lugli, NATO ASI series, **206**, 367.

WEBER, C., KLINGSHIRM, C., CHEMLA, D. S., MILLER, D. A. B., CUNNINGHAM, J. E., and ELL, C., 1988, *Phys. Rev. B*, **38**, 12748.

WEINER, J. S., PEARSON, D. B., MILLER, D. A. B., CHEMLA, D. S., SIVCO, D., and CHO, A. Y., 1986, *Appl. Phys. Lett.*, **49**, 531.

WEISBUCH, C., and NAGLE, J., 1987, *Phys. Scr. T*, **19**, 209.

WEISBUCH, C., 1987, *Physics and Applications of Quantum Wells and Superlattices*, edited by E. E. Mendez and K. von Klitzing, NATO ASI series, **170**, 261.

WHITTAKER, D. M., 1990, *Phys. Rev. B*, **41**, 3238.

WILSON, B. A., 1988, *I.E.E.E. J. quant. Electron.* QE, **24**, 1763.

WU, J. W., 1989a, *Phys. Rev. B*, **39**, 12944.

WU, J. W., 1989b, *Phys. Rev. B*, **39**, 7992.

XIA, J. B., and CHANG, Y. C., 1990, *Phys. Rev. B*, **42**, 1781.

XU, Z. Y., KREISMANIS, V. G., and TANG, C. L., 1984, *Appl. Phys. Lett.*, **44**, 136.

ZHANG, Y. H., CINGOLANI, R., and PLOOG, K., (unpublished).

ZHOU, P., JIANG, H. X., BANNWART, R., SOLIN, S. A., and BAI, G., 1989, *Phys. Rev. B*, **40**, 11862.

ZIELINSKY, E., SCHWEIZER, H., HAUSSER, S., STUBER, R., PILKUHN, M. H., and WEIMANN, G., 1987, *I.E.E.E. J. quant. Electron.* QE, **23**, 969.